Electron Transfer at n-Silicon-Methanol Junctions

Thesis by
Gary A. Shreve

In Partial Fulfillment of the Requirements
for the Degree of Doctor of Philosophy

California Institute of Technology
Pasadena, California

1995

(Submitted December 2, 1994)

To Nancy & Ben
For Patience and Love

Acknowledgments

I want to thank all the people who have made my years here at Cal Tech enjoyable. There are too many of you to name here and, besides, I'd spell your names wrong anyway. A general thanks to the Lewis Group for being a great group to work in, to past and a few present members of the Bercaw group for opening up the wonders of backpacking the Sierras, and to Nate, for his support and dedication to Truth. Finally, to Nancy for her constant confidence and optimism, I wouldn't have made it without you, and to Ben, thanks for the enjoyment of life that you've shared; it's put things in perspective many times. Both of you have allowed this all to happen.

Abstract

One of the first semiconductor systems limited by electron transfer has been explored. Rate constants for electron transfer from n-Si to methyl viologen dichloride ($MVCl_2$) and benzyl viologen dichloride ($BVCl_2$) in LiCl methanol solutions have been measured for the first time. The driving force dependence of k_{et} for electron transfer to $MVCl_2$ from n-Si has been determined. Best fit to the data gave a reorganization energy of 0.9 eV and a maximum rate constant ($k_{et,max}$) for this system of 10^{-15} cm^4-s^{-1}. To our knowledge this is the first experimentally determined value for the maximum rate constant predicted by Marcus theory at a semiconductor/liquid interface. This allowed an upper limit of $k_{et,max}$ no greater than 10^{-14} cm^4-s^{-1} to be determined for this system.

This work describes a search for active corrosion of Si in contact with CH_3OH-ferrocene$^{+/0}$ and CH_3OH-dimethylferrocene$(Me_2Fc)^{+/0}$ solutions through the use of very sensitive electrochemical, chemical, and physical methods. For CH_3OH-1.0 M $LiClO_4$-100 mM Me_2Fc-80 mM Me_2Fc^+ solutions, an upper limit on the active corrosion rate of $6.6x10^{-6}$ nm-s^{-1} has been established through direct experimental measurements; thus, a 400 μm thick Si photoelectrode in contact with the CH_3OH-$Me_2Fc^{+/0}$ electrolyte would require over 1500 years to corrode completely at room temperature. An alternative explanation for scanning electrochemical microscopy data published previously claiming 4 μm-hr^{-1} is presented, based on the documented existence of an inversion layer at the Si/liquid contact, and shown to be consistent with the available data.

Key differences between the conventional and "irreversible" models of semiconductor photoelectrochemistry are identified and discussed within the

framework of experimental observations. Conceptual differences between these two models appear to lie in the treatment of interfacial charge transfer processes for photogenerated charge carriers. It is shown analytically that the two models predict differences in the behavior of the available free energy produced by a photoelectrochemical cell at a fixed incident light intensity and are compared to experimental results for semiconductor/liquid junctions.

Table of Contents:

		Page
Acknowledgments		ii
Abstract		iii
Table of Contents		v
List of Figures and Tables		vi
Summary		1
Chapter 1	Introduction to Photoelectrochemistry	3
Chapter 2	Electron Transfer Rate Constants at Silicon/Methanol Interfaces	13
Chapter 3	Limits on the Active Corrosion Rate of Si Surfaces in Contact with CH_3OH-Ferrocene$^{+/0}$ and CH_3OH-1,1'-Dimethylferrocene$^{+/0}$ Solutions	61
Chapter 4	An Analytical Description of the Consequences of Abandoning the Principles of Detailed Balance and Microscopic Reversibility in Semiconductor Photoelectrochemistry	89

List of Figures and Tables

Chapter One: Page

Figure #1 A schematic representation of the five recombination mechanisms of semiconductor devices. 5

Chapter Two:

Figure #1 A schematic representation of the two pathways that control electron transport through the semiconductor interface. 18

Figure #2 ln J vs. applied potential plot for n-Si in 10/10 mM MV CH_3OH. 24

Figure #3 ln J *vs.* applied potential plot for n-Si in 10/10 mM BV CH_3OH. 27

Figure #4 Bode plots for n-Si in 10/10 mM BV CH_3OH. 29

Figure #5 Mott-Schottky plots for two dopant densities of n-Si in 10/10 mM BV CH_3OH. 35

Figure #6 log k_{et} *vs.* ΔG plot for n-Si in MV CH_3OH solution. 39

Figure #7 Fits of different λ values to log k_{et} *vs.* ΔG plot for n-Si in 10/10 mM MV CH_3OH. 42

Figure #8 Fits of different λ values to log k_{et} *vs.* ΔG plot with the addition of maximum k_{et} from $Me_2Fc^{+/0}$ CH_3OH system. 51

Chapter Three:

Figure #1 Dark J *vs.* applied potential plot for n-Si in CH_3OH 0.10 M Me_2Fc 0.020 M Me_2Fc^+. 68

Figure #2 Dark J *vs.* applied potential plot for p-Si in CH_3OH 0.10 M Me_2Fc 0.020 M Me_2Fc^+. 70

Figure #3 Scanning Electron Micrograph of patterned Si samples used in corrosion experiments. 73

Figure #4 Schematic representation of the process for making oxide posts on Si wafers. 76

Table #1 Collation of the data from the profilometry measurements, the means and standard deviations. 79

Chapter Four:

Figure #1 Schematic representation of the principle of microscopic reversibility at arbitrary energies. 93

Figure #2 Schematic representation of the energetics of a semiconductor/liquid junction. 98

Summary

This thesis deals with three different aspects of semiconductor/liquid junctions. Chapter 1 is a brief introduction to some of the important aspects of semiconductor/liquid junctions. Chapter 2 involves the measurement of bimolecular electron transfer rate constants (k_{et}) to methyl viologen at n-silicon electrodes. These rate constants were measured as a function of the driving force for the reaction ($\Delta G^{\circ\prime}$) for the first time. This allowed the log k_{et} *vs.* $\Delta G^{\circ\prime}$ plot to be fit to a Marcus theory equation and the first experimental values for the reorganization energy (λ) and the maximum rate constant ($k_{et,max}$) at a silicon electrode to be determined. The λ determined (0.9 eV) is much bigger than the λ estimated from the solution self-exchange rate (0.5 eV). More redox couples are needed to understand completely why this might be. The maximum rate constant determined from the fit to the data was 10^{-15} cm^4-s^{-1}. This work has allowed an upper limit of $k_{et,max} \leq 10^{-14}$ cm^4-s^{-1} to be established. This compares to some theoretical estimates of 10^{-17} cm^4-s^{-1}. Again more work is needed to understand whether there is some deficiency in the simple theory or if there are other factors influencing these rates.

Chapter 3 deals with determining the upper limits on the corrosion rate of silicon in $LiClO_4$ CH_3OH, $LiClO_4$-dimethylferrocene-dimethylferricenium CH_3OH, and $LiClO_4$-ferrocene-ferricenium CH_3OH solutions. Silicon samples with blocking posts of oxide were immersed in the above solutions for ~116 days. Scanning electron microscopy of the samples showed no evidence for pitting of the silicon thus only uniform corrosion was expected. The blocking posts were removed, and the resultant corrosion quantified by profilometry of the exposed *vs.* the protected areas of the

samples. The profilometry showed the life time of a 400 μm thick wafer of silicon to be ≥12000 years in $LiClO_4$-CH_3OH, ≥1500 in years $LiClO_4$-dimethylferrocene-dimethylferricenium-CH_3OH, and ≥750 years in $LiClO_4$-ferrocene-ferrocenium-CH_3OH solutions.

Chapter 4 involves an attempt to demonstrate that in order to explain the behavior of semiconductor/liquid junction photoelectrochemical cell, the principles of microscopic reversibility and detailed balance must be implicitly or explicitly invoked. It is shown that a failure to consistently apply microscopic reversibility and detailed balance leads to unrealistic predictions about the effect of light intensity on the photovoltage of semiconductor/liquid junctions, which is not justified by experimental observations of any known system.

Chapter One

Introduction to Photoelectrochemisty

Interest in solar energy conversion with semiconductor/liquid junctions exploded after the publication of Honda and Fujishima's *Nature* paper in 1972 claiming to have split H_2O to form H_2 with TiO_2 using only the energy of light.[1] In the context of the oil crisis of the time, it was touted as a way to produce "unlimited" amounts of fuel from sunlight. No "unlimited" source of fuel has been discovered, but our understanding of these systems has increased dramatically. Most of the work has focused on using the electric fields developed at single crystal or polycrystalline materials immersed in redox solutions to separate charge and collect it.[2-4]

Photoelectrochemical cells provide the most efficient known chemical method of converting solar energy into stored chemical or electrical energy.[2,5-9] Efficiencies of optimized devices can exceed 16%,[10,11] while a variety of semiconductor/liquid junctions have efficiencies of 10%.[12-18] Several of these systems have service lifetimes that project to several years, and in this respect research in this area can be considered to be a success.

There are three basic requirements to harness the energy of light: 1) there must be an absorption of the light with creation of excited particles; 2) there must be charge separation so the particles do not recombine and convert the energy of the light into heat; 3) the particles must be efficiently collected so the concentrations do not build up to the point that recombination becomes significant.[2] Plants perform these three functions in the photocenter of chlorophyll with an array of ordered molecules that directs each excited electron created by light to a reaction center, and then the charge is stored as chemical energy.[19,20]

Semiconductor/liquid junctions also meet the criteria above but with a slightly different mechanism of charge separation. In general, when a semiconductor is placed in solution with a redox active species, charge transfer occurs until the electrochemical potential of the semiconductor (Fermi level) equals the electrochemical potential of the solution. These charges are taken from easily ionized dopants in the semiconductor. This equilibration process sets up an electric field at the interface. The width of this depletion region depends on the difference in the initial contact potentials and on the density of dopants in the semiconductor.[2] That electric field is used by most photoelectrochemical devices to separate the excited electrons from the electron vacancies (holes) left in the valence band by the absorption of light. An interfacial electric field is also the basis for most semiconductor devices in use today.[21]

There are many fundamental features of semiconductor/liquid junctions that are not well understood even after decades of research. Various mechanisms operate in a semiconductor/liquid junction to limit the rate of charge transfer in the system (See Fig. 1). These include bulk recombination, recombination in the depletion region, recombination at the semiconductor surface, tunneling through the depletion region, and direct charge transfer from the conduction band into the acceptor species of the electrolyte, as well as charge transfer through intermediate surface states at the solid/liquid interface.[13,22-26] Usually only one of these mechanisms dominates the charge flow in any system. One of the most interesting mechanisms is the direct charge transfer. Understanding the factors that influence and control this charge transfer from the semiconductor into the solution would impact a wide area of semiconductor applications. Charge transfer rates are important for minimizing unwanted semiconductor

Figure 1 Recombination pathways that can control charge flow in the semiconductor/liquid junction. 1) Bulk region recombination current J_{bk}. 2) Depletion region recombination J_{dr}. 3) Surface state recombination J_{ss}. 4) Tunnelling recombination J_{th}. 5) Direct electron transfer from the conduction band of the semiconductor J_{et}. Only J_{et} is always dependent on the acceptor concentration (A) in solution and only by measuring the direct electron transfer rate constant for this process can Marcus theory be tested for this system.

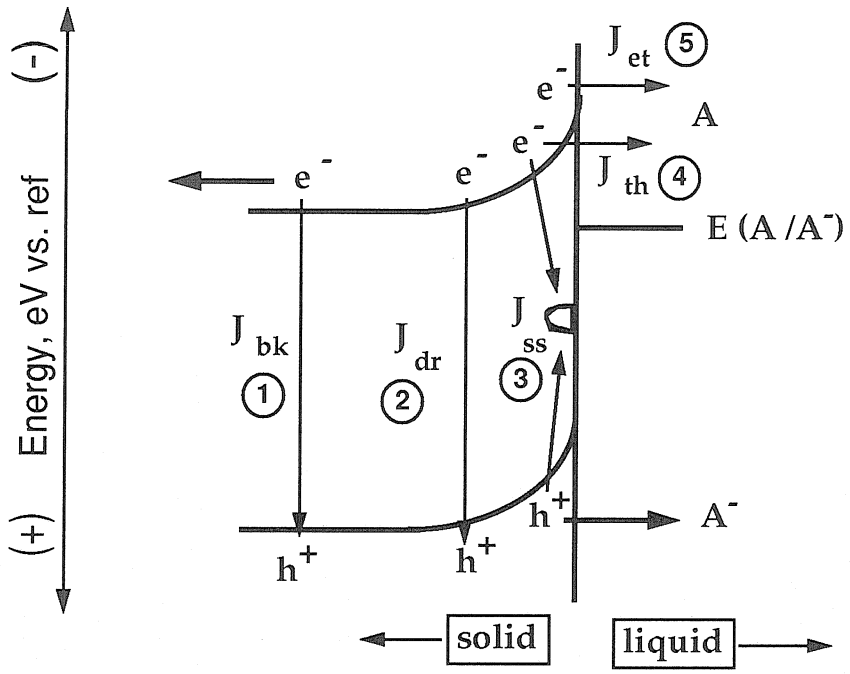
Energy, eV vs. ref
(-)
(+)
J et
5
e-
A
e-
e-
e-
J th
4
E (A /A-)
J bk
1
J dr
2
J ss
3
h+
h+
h+
A-
solid
liquid

photocorrosion processes,[27] for controlling photoinduced semiconductor etching in lithography,[28-30] in porous Si formation,[31,32] for directing multi-electron charge transfer processes at semiconductor photoelectrodes,[2,33] for light-induced dye sensitization energy conversion schemes,[14,34,35] for evaluating the prospects of hot carrier injection at semiconductor photoelectrodes,[36-38] and for design of new chemical sensors.[39,40] Numerous other applications of semiconductor electrochemistry and thus charge transfer, detailed in various reviews and books,[2,4,41-43] also rely on a basic understanding of interfacial charge transfer kinetics at the semiconductor/liquid junction.

The theory for charge transfer at semiconductors was originally published by Brattain and Gerischer.[44-46] Gerischer's model modified homogenous solution Marcus Theory.[47,48] Unfortunately, there have been few experimental tests of this theory for semiconductor interfaces. In fact few systems have been found that even allow the measurement of the rate constants for electron transfer to solution species. Morrison published the change in k_{et} for a variety of very different redox couples on zinc oxide.[49] Unfortunately, these redox couples in water were not all outer sphere electron acceptors and it is unlikely that the electronic overlaps were the same for the acceptors. Thus this system does not allow a valid comparison to Marcus theory.

The requirements for a system to experimentally determine if simple Marcus theory can be applied to semiconductor/liquid junctions are as follows:

1) Use of a one-electron outer sphere redox couple is needed to allow results from similar molecules with different driving forces (ΔG) to be

compared. This implicitly assumes the electronic overlap of such redox couples will be similar.

2) Determination of a first order dependence of the electron transfer rate on the solution acceptor species gives confidence that electron transfer is important in the charge flow of the semiconductor/liquid junction. There are many pathways that can restrict charge flow in semiconductor/liquid junctions;[2] most do not have a dependence on the acceptor concentration except as it affects the solution potential.
3) Some determination of the electron concentration is needed to calculate a bimolecular rate constant, whether from direct or indirect real time measurements of the decay from a light pulse or from steady-state measurement of the energy of the bandedge and calculation from that of a surface electron concentration.

These are the three requirements to measure electron transfer rate constants that can be compared to Marcus theory at semiconductor/liquid junctions. To date few systems have met all of the above requirements, with only a handful of rate constants calculated.[50] Many systems using one-electron outer sphere redox couples have been evaluated, have been found not to be electron transfer limited and thus are not of use for understanding the electron transfer process.[3,51,52]

Ultimately, understanding the charge transfer process will allow some of the following questions to be answered:

1) What are the criteria for obtaining an economical, efficient photoelectrochemical cell?
2) What factors are responsible for the interfacial energetics and how are these factors different for metal/redox *vs.* semiconductor/redox interfaces?

3) Does the Marcus-Gerischer theory of charge transfer[45-48] predict the correct behavior for these systems?

Continued work in this area needs many more examples of "ideal" systems to help understand and answer these questions.

References

(1) Fujishima, A.; Honda, K. *Nature* **1972**, *238*, 37.

(2) Tan, M. X.; Laibinis, P. E.; Nguyen, S. T.; Kesselman, J. M.; Stanton, C. E.; Lewis, N. S. *Prog. Inorg. Chem.* **1994**, *41*, 21.

(3) Koval, C. A.; Howard, J. N. *Chem. Rev.* **1992**, *92*, 411.

(4) Finklea, H. O. *Semiconductor Electrodes*; Elsevier: New York, 1988.

(5) Archer, M. D. *J. Appl. Electrochem.* **1975**, *5*, 17.

(6) Gerischer, H. In *Solar Energy Conversion. Solid-State Physics Aspects*; B. O. Seraphin, Ed.; Springer-Verlag: Berlin, 1979; Vol. 31; pp 115.

(7) *Energy Resources through Photochemistry and Catalysis*; Grätzel, M., Ed.; Academic Press: New York, NY, 1983, pp 573.

(8) Heller, A. *Acc. Chem. Res.* **1981**, *14*, 154.

(9) Memming, R. *Electrochmica Acta*. **1980**, *25*, 77.

(10) Tufts, B. J.; Abrahams, I. L.; Santangelo, P. G.; Ryba, G. N.; Casagrande, L. G.; Lewis, N. S. *Nature* **1987**, *326*, 861.

(11) Licht, S.; Peramunage, D. *Nature* **1990**, *345*, 330.

(12) Parkinson, B. A. *J. Chem. Ed.* **1983**, *60*, 338.

(13) Lewis, N. S. *Acc. Chem. Res.* **1990**, *23*, 176.

(14) O'Regan, B.; Gratzel, M. *Nature* **1991**, *353*, 737.

(15) Hodes, G.; Manassen, J.; Cahen, D. *Nature* **1976**, *261*, 403.

(16) Licht, S.; Tenne, R.; Dagan, G.; Hodes, G.; Manassen, J.; Cahen, D.; Triboulet, R.; Rioux, J.; Levy-Clement, C. *Appl. Phys. Lett.* **1985**, *46*, 608.

(17) Bachmann, K. J.; Menezes, S.; Kotz, R.; Fearheily, M.; Lewerenz, H. J. *Surface Science* **1984**, *138*, 475.

(18) Rajeshwar, K. *J. Appl. Electrochem.* **1985**, *15*, 1.

(19) *The Photosynthetic Reaction Center*; Deisenhofer, J.; Norris Jr., J. R., Ed.; Academic: San Diego, CA, 1993.

(20) Amesz, J. In *Photosynthesis*; Alan R. Liss, Inc.: Stanford, CA, 1988; pp 123.

(21) Sze, S. M. *The Physics of Semiconductor Devices;* 2nd ed.; Wiley: New York, 1981.

(22) Fonash, S. J. *Solar Cell Device Physics*; Academic: New York, 1981.

(23) Lewis, N. S. *Ann. Rev. Mater. Sci.* **1984**, *14*, 95.

(24) Shockley, W.; Read, W. T. *Phys. Rev.* **1952**, *87*, 835.

(25) Rosenbluth, M. L.; Lewis, N. S. *J. Am. Chem. Soc.* **1986**, *108*, 4689.

(26) Lewis, N. S. *J. Electrochem. Soc.* **1984**, *131*, 2496.

(27) Gerischer, H. *Faraday Discuss.* **1980**, *70*, 137.

(28) Kohl, P. A.; Harris, D. B.; Winnick, J. *J. Electrochem. Soc.* **1990**, *137*, 3315.

(29) Kohl, P. A.; Ostermayer, F. W. *Ann. Rev. Mat. Sci.* **1989**, *19*, 379.

(30) Elliott, D. J. *Integrated Circuit Fabrication Technology*; Mc-Graw Hill: New York, 1989.

(31) Wu, W.-T.; McEvoy, A. J.; Grätzel, M. *J. Electroanal. Chem.* **1990**, *291*, 235.

(32) Unagami, T. *J. Electrochem. Soc.* **1980**, *127*, 476.

(33) Gerischer, H. *Pure & Appl. Chem.* **1980**, *52*, 2649.

(34) Nazeeruddin, M. K.; Kay, A.; Rodicio, I.; Humphry-Baker, R.; Muller, E.; Liska, P.; Vlachopoulos, N.; Gratzel, M. *J. Amer. Chem. Soc.* **1993**, *115*, 6382.

(35) Valchopoulos, N.; Liska, P.; Augustynski, J.; Gratzel, M. *J. Amer. Chem. Soc.* **1988**, *110*, 1216.

(36) Rosenwaks, Y.; Thacker, B. R.; Nozik, A. J.; Ellingson, R. J.; Burr, K. C.; Tang, C. L. *J. Phys. Chem.* **1994**, *98*, 2739.

(37) Rosenwaks, Y.; Thacker, B. R.; Ahrenkiel, R. K.; Nozik, A. J. *J. Phys. Chem.* **1992**, *96*, 10096.

(38) Shreve, G. A.; Lewis, N. S. *J. Electrochem. Soc.* **1995**, *142*, 112.

(39) Hafeman, D. G.; Parce, J. W.; McConnell, H. M. *Science* **1988**, *240*, 1182.

(40) de Rooij, N. F.; van de Vlekkert, H. H. In *Chemical Sensor Technology;* N. Yamazoe, Ed.; Kodansha, Ltd.: Tokyo, 1991; Vol. 3; pp 213.

(41) Gregory, R. P. F. *Photosynthesis;* Blackie & Son Ltd.: Glasgow, 1989, pp 160.

(42) Morrison, S. R. *Electrochemistry at Semiconductor and Oxidized Metal Electrodes;* Plenum: New York, 1980.

(43) Wrighton, M. S. *Interfacial Photoprocesses: Energy Conversion and Synthesis;* American Chemical Society: Washington, DC, 1980; Vol. 184, pp 1.

(44) Garrett, C. G. B.; Brattain, W. H. *Phys. Rev.* **1955**, *99*, 376.

(45) Gerischer, H. *Adv. Electrochem. Electrochem. Engr.* **1961**, *1*, 139.

(46) Gerischer, H. *J. Phys. Chem.* **1991**, *95*, 1356.

(47) Marcus, R. A. *J. Chem. Phys.* **1965**, *43*, 679.

(48) Marcus, R. A. *J. Phys. Chem.* **1990**, *94*, 1050.

(49) Morrison, S. R. *Surface Science* **1969**, *15*, 363.

(50) Horrocks, B. R.; Mirkin, M. V.; Bard, A. J. *J. Phys. Chem.* **1994**, *98*, 9106.

(51) Koval, C. A.; Olson, J. B. *J. Phys. Chem.* **1988**, *92*, 6726.

(52) Koval, C. A.; Olson, J. B.; Parkinson, B. A. In *Electrochemical Surface Science: Molecular Phenomena at Electrode Surfaces;* M. P. Soriaga, Ed.; American Chemical Society: Washington, 1988; Vol. 378; pp 438.

Chapter Two

Electron Transfer Rate Constants at Silicon/Methanol Interfaces

Abstract: One of the first semiconductor systems limited by electron transfer to the solution acceptor has been explored. Rate constants for electron transfer from n-Si to methyl viologen dichloride ($MVCl_2$) and benzyl viologen dichloride ($BVCl_2$) in LiCl methanol solutions have been measured for this purpose. Steady-state current-voltage curves and surface electron concentrations calculated from energies determined from frequency independent Mott-Schottky plots were used to determine k_{et}. A slow reaction that changed the conduction bandedge energy has allowed a determination of the driving force dependence of k_{et} for electron transfer to $MVCl_2$ from n-Si. A best fit to the data gave a reorganization energy of 0.9 eV and a maximum rate constant ($k_{et,max}$) for this system of 10^{-15} cm^4-s^{-1}. To our knowledge this is the first experimentally determined value for the maximum rate constant predicted by Marcus Theory at a semiconductor/liquid interface. This allowed an upper limit of $k_{et,max}$ no greater than 10^{-14} cm^4-s^{-1} to be established for this system.

I. INTRODUCTION

One of the outstanding problems in semiconductor electrochemistry involves understanding the interfacial charge transfer kinetics at semiconductor/liquid contacts.[1,2] Such charge transfer rates are important for minimizing unwanted semiconductor photocorrosion processes,[3] for controlling photoinduced semiconductor etching in lithography[4-6] and porous Si formation,[7] for directing multi-electron charge transfer processes at

semiconductor photoelectrodes,[2,8] for light-induced dye sensitization energy conversion schemes,[9-11] for evaluating the prospects of hot carrier injection at semiconductor photoelectrodes,[12-14] and for design of new chemical sensors.[15,16] Numerous other applications of semiconductor electrochemistry, detailed in various reviews and books,[2,17-20] also rely on a basic understanding of interfacial charge transfer kinetics at the semiconductor/liquid junction.

To date, however, there are relatively few measurements of the interfacial charge transfer rate constant from a semiconducting solid into a one-electron, outer sphere, dissolved redox acceptor species.[1,12,19,21-25] In this respect, the understanding of charge transfer processes in semiconductor electrochemistry lags that of charge transfer processes in molecular donor-acceptor systems.[26-29] Such heterogeneous charge transfer kinetic measurements are fundamentally important because they would allow a quantitative comparison with theoretical predictions of electron transfer theories developed by Marcus, Gerischer, and others.[30-35 36]

In its simplest formulation, the rate of charge transfer across a semiconductor/liquid contact is closely related to kinetic expressions that have been developed recently for intermolecular charge transfer between molecular donors and acceptors, where the donors are confined to one liquid phase, the acceptors are confined to another liquid phase, and the two liquids are immiscible.[33] Considering the electron as a donor of radius, r_e, and the acceptor as an ion of radius r_A, and integrating over all possible distances and angles for each donor-acceptor pair yields the overall rate. Assuming a random distribution of donors and acceptors gives the rate constant for charge

transfer (k_{et}) between the electron and the acceptor ion as:

$$k_{et} = \nu_n \kappa_{el} \kappa_n \quad (1)$$

$$\kappa_{el} = 2\pi (r_A + r_e)\beta^{-3} \quad (2)$$

$$\kappa_n = \exp\left[\frac{-\left(\Delta G^{o'} + \lambda\right)^2}{4kt\lambda}\right] \quad (3)$$

with ν_n the frequency factor, κ_{el} the electronic coupling between the donor-acceptor, κ_n the nuclear term containing the free energy ($\Delta G^{o'}$) dependence, β the distance dependence of the electronic overlap, λ the solvent reorganization energy, k the Boltzmann constant, and T the temperature of the reaction. This theory has formed the basis for applications of semiconductor electrochemistry, but has not been rigorously tested to date, despite recent advances in both experimental methods and in theoretical descriptions of the charge transfer process.[1]

Taking representative values for ν_n (10^{13} s^{-1}), β (10^8 cm^{-1}), r_e (10^{-7} cm) r_A ($3x10^{-8}$ cm), and setting $\kappa_n = 1$, gives an order of magnitude estimate for the maximum expected rate constant $k_{et(max)} \approx 10^{-17}$ cm^4-s^{-1}. This estimate contrasts greatly with some reported values of k_{et} as high as 10^{-12} cm^4-s^{-1}.[12] Of concern, of course, is whether the electron transfer process in such systems is adiabatic, how the delocalized electrons in the solid should be theoretically treated in the donor-acceptor interaction, and whether repulsive terms in the electrostatic contributions to the solvent reorganization energy at a semiconductor/liquid contact are operative and important in affecting the rate constants for charge transfer.

To address these issues, kinetic measurements on several well-defined, stable semiconductor surfaces in contact with outer sphere, one-electron redox species need to be performed and compared with theoretical predictions. One simple method for performing such comparisons involves measurement of the steady-state current density-applied voltage (J-V) curves of a forward-biased semiconductor/liquid interface. When interfacial charge transfer between a delocalized electron in the semiconducting solid (the donor) and an acceptor in the solution is controlling the current flow, the rate of the reaction should obey a bimolecular rate law:

$$\text{rate} = \text{current}/q = k_{et}\, n_s\, [A]_s \qquad (4)$$

where q is the charge on an electron, $[A]_s$ is the acceptor concentration in the interface region and n_s is the electron concentration at the surface of the semiconductor. If this rate law is observed, independent determination of n_s then allows extraction of k_{et}.

The problem with this approach is several-fold. First, reliable measurements of n_s are problematic at many semiconductor surfaces of interest, in that the primary method of determining n_s, differential capacitance *vs.* voltage plots, often yields frequency dependent data thwarting an unambiguous calculation of n_s.[2,23,37] Other methods for determining n_s are generally either ambiguous or are not sufficiently quantitative. Secondly, comparison of rates for various different redox species requires that the semiconductor/liquid interface display "ideal" electron transfer limited behavior over a range of redox potentials,[1,38] and such behavior has been observed in few systems to date. Thirdly, careful voltammetric measurements in recent years have shown that many semiconductor/liquid contacts based on nonaqueous solvents with well-defined, one-electron, outer

sphere redox couples (the redox couples that simple Marcus theory applies to) do not obey the rate law of Eq. 4, but instead exhibit a rate that is independent of the acceptor concentration:[21,39]

$$\text{rate} = k'_{et}\, n_s \qquad (5)$$

In this situation, another charge transfer mechanism dominates the overall interfacial carrier flow, so no direct information on the theoretically interesting value of k_{et} can be obtained by measurement of the steady state current.

The rate law obtained in Eq. 5 can be rationalized by considering a stepwise process, in which the charge transfer first occurs to defect sites on the semiconductor surface (traps), and is followed by a subsequent charge transfer step to the acceptor species in the solution (See Fig. 1). The total rate of charge transfer through the two pathways can be expressed as:

$$\text{rate} = k_{et}[A]_s n_s + k_{sol}[A]_s N_t f_t \qquad (6)$$

where k_{sol} = the rate constant for electron transfer from the surface state, N_t = the density of traps on the surface and f_t = the percentage of filled traps (i.e., defects containing electrons). By steady-stating the occupancy of the traps, an expression for f_t can be obtained and substituted into Eq. 6:

$$\text{rate} = k_{et}[A]_s n_s + k_{sol}[A]_s N_t \left[\frac{k_{ss} n_s}{k_{ss} n_s + k_{sol}[A]}\right] \qquad (7)$$

Where k_{ss} = the rate constant for electron transfer from the semiconductor to the surface state. Thus if $k_{sol}[A]_s >> k_{ss} n_s$ and $k_{ss} N_t >> k_{et}[A]_s$, then the measured rate will be independent of $[A]_s$, and will only depend on the density of electrical traps at the solid/liquid interface and n_s. Taking

Figure #1 Two pathways for the electron transfer through a semiconductor interface: k_{et} is the rate constant for the direct electron pathway. k_{ss} is the rate constant for filling surface states, and k_{sol} is the rate constant for transfer from the surface state to the acceptor species (A) in solution. Together these two steps represent a second possible pathway into solution.

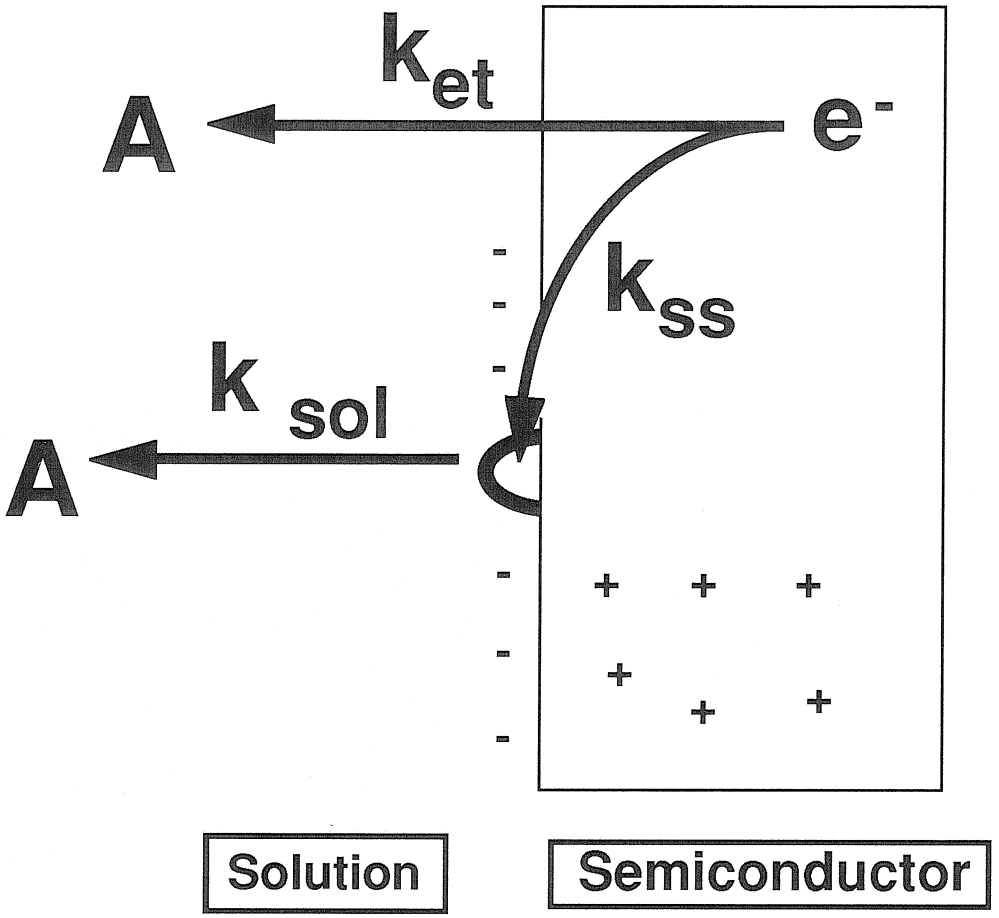
k et
A
e -
k ss
k sol
A
Solution
Semiconductor

$1x10^{-14}$ cm^2 as a typical cross section for capture by a surface trap, a surface state density of $1 \times 10^{14} cm^{-2}$ (one defect for every 10^2 surface atoms), and a thermal velocity of 10^7 $cm\text{-}s^{-1}$ gives an electron capture velocity (S) of 10^7 $cm\text{-}s^{-1}$. With $S = k_{et}[A]_s$, even an acceptor concentration of 0.1 M (6.02×10^{19} cm^{-3}) will not provide enough dissolved acceptors to compete with the surface state trapping route (10^2 *vs.* 10^7 $cm\text{-}s^{-1}$; assuming $k_{et(max)} = 10^{-17}$), so the desired value of k_{et} cannot not be obtained from current measurements of such surface state dominated contacts. Based on similar arguments, Gerischer has recently proposed that this type of mechanism will dominate the current transport at almost all semiconductor/liquid interfaces.[35]

Thus, to evaluate the electron transfer rate constant, k_{et}, requires discovery of stable, ideally-behaving, semiconductor/liquid contacts. These contacts must be sufficiently defect-free to allow the desired rate law of Eq. 4 to be observed experimentally. Reliable determinations of n_s are also required in order to extract k_{et} from the measured value of the current at a specific bias. In this report, we describe such a system, which has been fabricated from n-type Si electrodes in contact with methanol-LiCl solutions of methyl viologen chloride ($MV^{2+/\bullet+}$) or benzyl viologen chloride ($BV^{2+/\bullet+}$). This system has allowed us to obtain some of the first experimental values for charge transfer rate constants at a semiconductor/liquid contact and allows a direct comparison between these rate constants and theoretical predictions.

II. EXPERIMENTAL

Methyl viologen dichloride and benzyl viologen dichloride were obtained from Aldrich Chemical and were dried under vacuum at 60°C before use. $FcBF_4$ was prepared as described previously.[40,41] LiCl (EM Scientific) was dried at ~250°C under vacuum before use. Mg powder (EM Scientific)

and I_2 (EM Scientific) were added to reagent grade methanol (EM Scientific) and the pure liquid was distilled under an ambient pressure of N_2. All experiments were performed in a Plexiglas tank that was continuously purged with N_2(g) and that displayed oxygen concentrations of less than 10 ppm (as monitored by fuming of diethyl zinc).

(100)-oriented, phosphorus doped, n-Si wafers (Silicon Sense; Nashua, NH) used in these experiments were made into electrodes and exposed areas determined by magnified photography as described previously.[40] The sample conductivity was either 4.2 Ω-cm or 0.1 Ω-cm as measured by 4-point probe and the respective donor densities (N_d) were 1.1×10^{15} cm^{-3} and 8.0×10^{16} cm^{-3}, as calculated the data of Thurber *et al.*[42] The electrodes were etched in 48 wt% *aq.* HF (Mallinckrodt, Inc., Paris, KY), rinsed with H_2O, rinsed with methanol, blown dry in a stream of N_2(g), and taken into the N_2-tank. The electrodes were then exposed to 0.20 M of $FcBF_4$ in CH_3OH and rinsed with CH_3OH prior to immersion in the redox couple. J-V data were collected in a 3-electrode one-compartment cell using a Princeton Applied Research (PAR) model 173 potentiostat, a PAR model 175 universal programmer, and a Houston Instruments model 2000 X-Y recorder.

All the reduced forms of the viologens were generated electrochemically by potentiostatic reduction of the dication to the monocation *in situ*. This was done by addition of a separate fritted counter electrode and a CH_3OH-LiCl SCE that had been previously calibrated against a standard SCE (E_{LiCl} = -0.010 V). The desired ratio of oxidized to reduced form of the viologen was monitored both by the redox potential of the cell and by the mass transport limited current at a Pt wire electrode in a stirred cell. For J-V and MottSchottky (M-S) measurements, the CH_3OH SCE was replaced

with a Pt wire since the SCE caused large frequency dispersion in the M-S plots.

Flat band potentials (V_{fb}) were obtained from the Mott-Schottky plots of the differential capacitance of the Silicon/CH_3OH junction.[23] Impedance spectra from +1.0 V to +0.2V in 0.1V steps and currents at -0.1 V and -0.2 V *vs.* the solution potential were obtained using a Schlumberger Model 1260 frequency response analyzer and a Model 1286 potentiostat under computer control. The semiconductor capacitance (C) was calculated from the imaginary part of the impedance spectrum (Z") using the equation $Z''= 1/2\pi fC$, where f = the frequency of the AC signal. The intercept of the line from the plot of C^{-2} *vs.* applied potential (V) gave the flat band potential (V_{fb}).

The potentials (-0.1V and -0.2V) at which currents were measured were corrected for cell resistance (typically ~100 Ω), then concentration overpotentials were calculated from the measured limiting current of the silicon electrode and the solution concentrations.[37] The rate constant (k_{et}) was then determined using Eq. 4 by calculating the surface electron concentration (n_s) at the corrected potential using Eq. 8 and the experimentally determined value of the diode quality factor (a = 1.4). The driving force $\Delta G^{\circ'}$ was determined from $\Delta G^{\circ'} = qV_{fb} - kT - qV_n - qE^{\circ'}$, where V_n = bulk potential of the semiconductor and $E^{\circ'}$ the standard redox potential of the redox couple. All fits were performed using standard least-squares fitting routines.

III. RESULTS

1. I-V Properties of Ferricenium treated n-Si/$MV^{2+/\bullet+}$ and n-Si/$BV^{2+/\bullet+}$ Contacts

Figure 2 displays the ln J-V properties of n-Si in contact with 1.00 M LiCl-CH_3OH with 10/10 mM $MV^{2+/\bullet+}$ and 100/10 mM $MV^{2+/\bullet+}$. The Si was HF etched, immersed in a 0.20 M ferricenium tetrafluoroborate (Fc^+BF_4) CH_3OH solution for 1 min., rinsed with CH_3OH, and then immersed into the $MV^{2+/\bullet+}$ solution. The diode quality factor (a) was 1.4 for this surface, and the current was linearly proportional to the acceptor concentration from at least 0.100 M < $[MV^{2+}]$ < 0.010 mM. Thus, over this range of concentration, the rate law of Eq. 4 accurately described the interfacial electron transfer kinetics of this n-Si/CH_3OH-LiCl-$MV^{2+/\bullet+}$ interface. The equilibrium current density (J_o) obtained from a plot of ln J *vs.* V was 1.7×10^{-6} A-cm^{-2}. The J_o indicates the exchange current for this semiconductor/liquid interface at equilibrium and is related to the ease with which electrons can pass through the junction.

The slope of a ln J *vs.* V plot indicates the extent to which the applied voltage affects the current through changes in the surface concentration of majority carriers. Expressing the surface electron concentration in these n-type samples explicitly as a function of applied bias (V) yields:[43]

$$n_S = n_{SO} e^{-\frac{qV}{akT}} \qquad (8)$$

with n_{so} the equilibrium electron concentration at the surface (i.e., $n_S = n_{so}$ when J=0 and V=0). Eq. 8 indicates that, whenever an interfacial charge transfer reaction is kinetically first-order in n_s, a plot of ln J *vs.* V should yield a straight line with a diode quality factor (a) of unity. This situation is expected for both the rate laws of equations (4) and (5).

Figure #2 ln [current density(J)] *vs.* applied potential (V) for a (100) ferricinium (Fc^+) treated n-Si electrode in two 1.00 M LiCl-CH_3OH solutions: 10/10mM $MV^{2+/\bullet+}$ and 100/10mM $MV^{2+/\bullet+}$. These plots have been corrected for solution resistance and concentration overpotentials. The overlap of the curves shows that the current as a function of V is "ideal" with the solution concentration of acceptor [MV^{2+}]. These plots have a diode quality factor of 1.4 and a saturation current density (J_o) of 1.7×10^{-6} A-cm^{-2}.

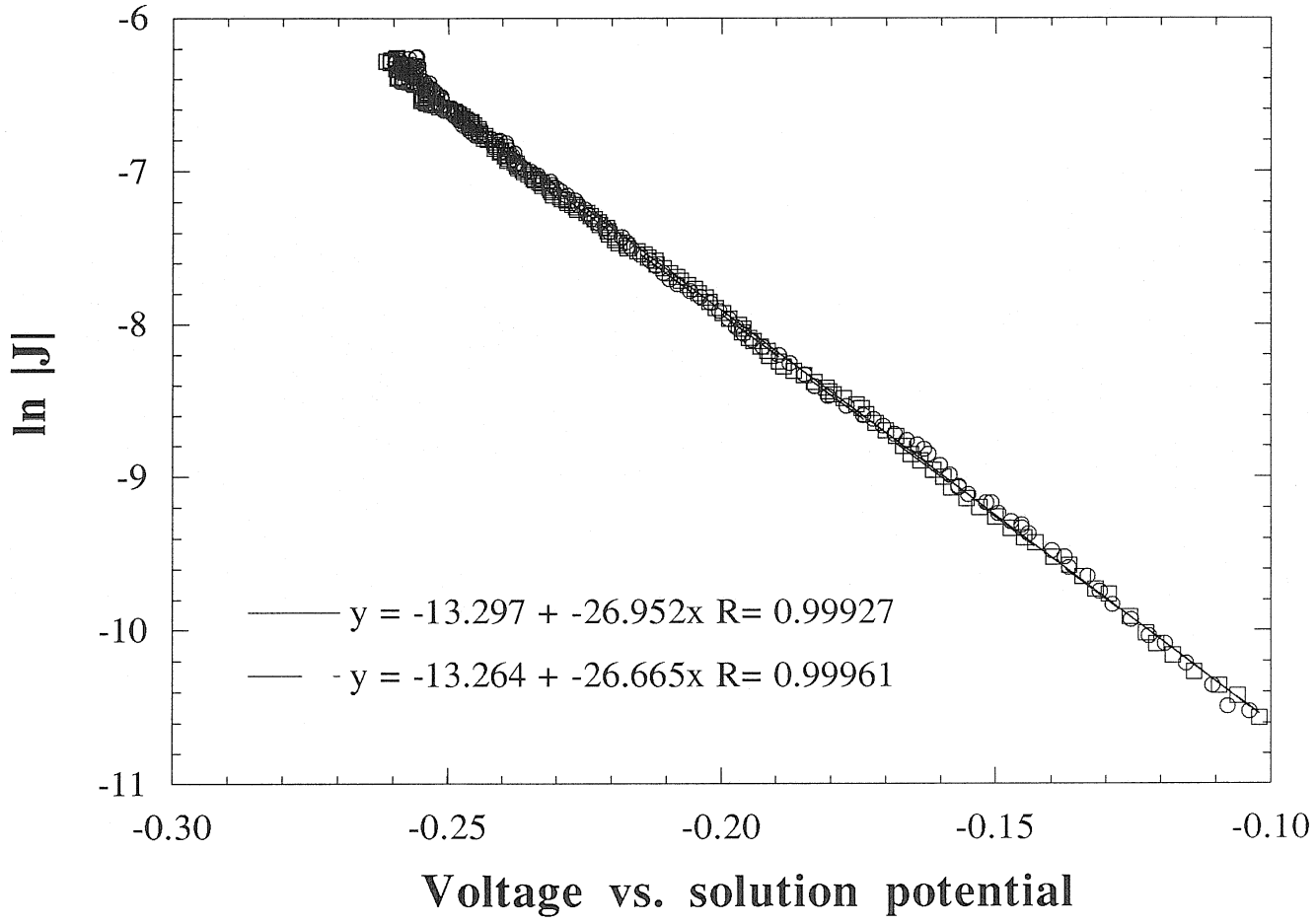
-6
-7
-8
-9
-10
-11
ln |J|
y = -13.297 + -26.952x R= 0.99927
y = -13.264 + -26.665x R= 0.99961
-0.30
-0.25
-0.20
-0.15
-0.10
Voltage vs. solution potential

Initial experiments with HF etched n-Si samples in CH_3OH-$MV^{2+/\bullet+}$ solutions showed that the junction produced a non-rectifying contact. Thus there was little or no electric field present at the interface to control the surface concentration of electrons. These currents are not in a semiconductor limited regime and thus a bimolecular k_{et} cannot be calculated from these curves. This surface was also not suitable for rate constant determinations since the capacitance of the semiconductor in this situation will likely rival the Helmholtz layer and change $\Delta G^{\circ\prime}$ as a potential is applied to the electrode. If the electrode was left in solution (~2-3 hr) or given a one minute treatment in 0.20 M $FcBF_4$-CH_3OH after HF etching, the J-V curves became rectifying in LiCl-CH_3OH. Most importantly, this surface displayed a first order dependence on acceptor concentration.

Figure 3 shows the ln J-V behavior of the n-Si/CH_3OH-1.00 M LiCl-$BV^{2+/\bullet+}$ interface with 10/10 mM $BV^{2+/\bullet+}$ and 100/10 mM $BV^{2+/\bullet+}$. This system also exhibited behavior in accord with the rate law of Eq. 4. It showed a diode quality factor of 1.3 and a first-order dependence of the current on the concentration of $[BV^{2+}]$ from at least 0.100 M<$[BV^{2+}]$<0.010 M. The saturation current density for this system was 3.7×10^{-7} A-cm^{-2}, and was thus somewhat smaller than that for the n-Si/CH_3OH-$MV^{2+/\bullet+}$ contact, as expected for a larger barrier height junction.

2. Mott-Schottky Plots of n-Si/CH_3OH-$MV^{2+/\bullet+}$ and n-Si/CH_3OH-$BV^{2+/\bullet+}$ Contacts

Figures 4(a-d) display, in various forms, the frequency dependence of the impedance for the n-Si/CH_3OH-$BV^{2+/\bullet+}$ contacts over a range of applied biases. In reverse bias (+0.2 to +1.0 V *vs.* solution potential) for 10 kHz<frequency (f) <100 kHz, Bode plots yielded straight lines with slopes of -1

Figure #3 ln J *vs.* applied potential (V) for a (100) ferricinium (Fc^+) treated n-Si electrode in two 1.00 M LiCl-CH_3OH solutions: 10/10 mM $BV^{2+/\bullet+}$ and 100/10 mM $BV^{2+/\bullet+}$. These plots have been corrected for solution resistance and concentration overpotentials. This system also demonstrates the current as a function of V is "ideal" with the solution concentration of acceptor [BV^{2+}]. These plots have a diode quality factor of 1.3 and a J_o of 3.7×10^{-7} A-cm^{-2}.

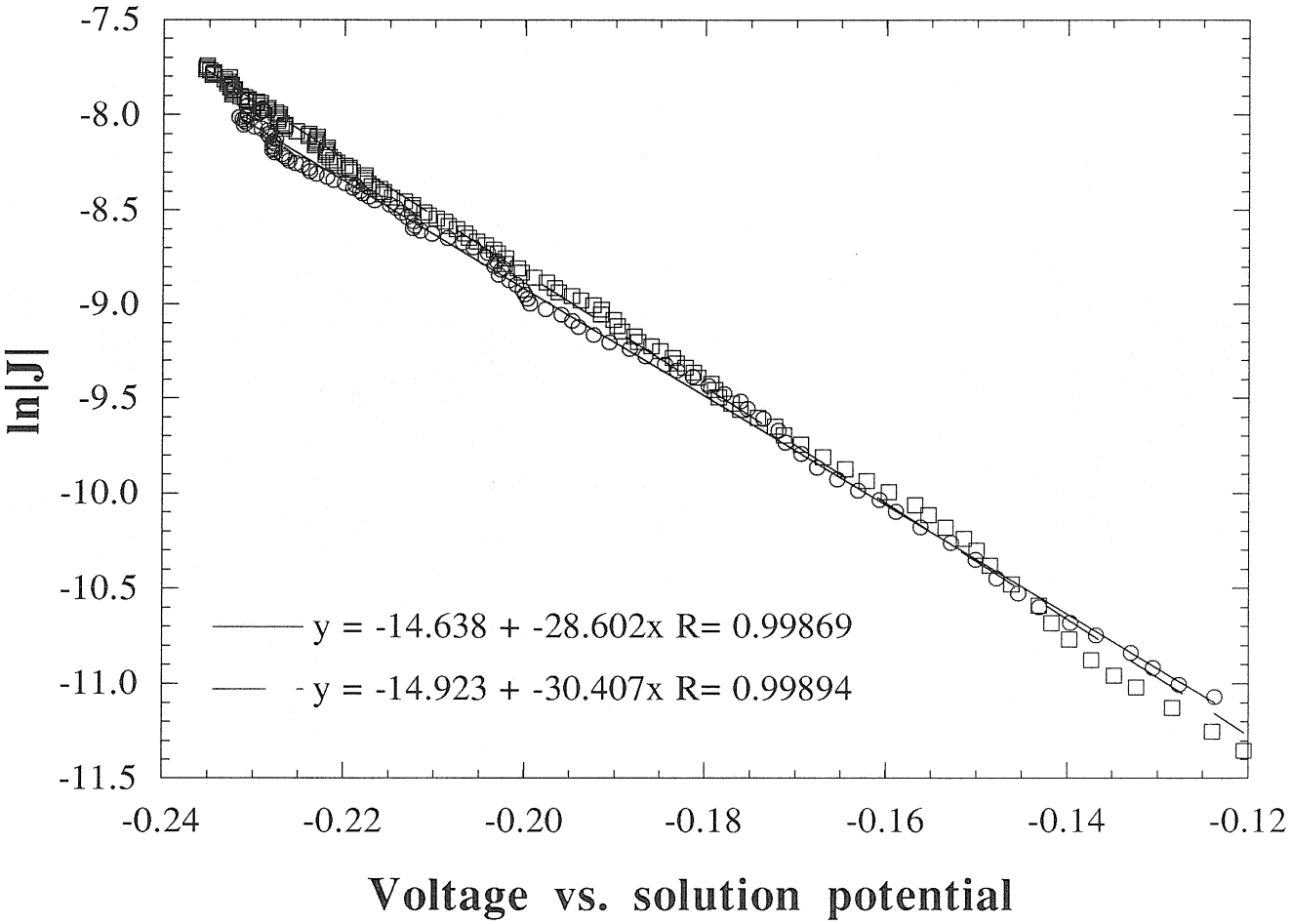
-7.5
-8.0
-8.5
-9.0
-9.5
-10.0
-10.5
-11.0
-11.5
ln|J|
y = -14.638 + -28.602x R= 0.99869
y = -14.923 + -30.407x R= 0.99894
-0.24
-0.22
-0.20
-0.18
-0.16
-0.14
-0.12
Voltage vs. solution potential

Figure #4 Bode plots take in a 10/10 mM $BV^{2+/\bullet+}$ 1.00 M LiCl-CH_3OH solution at 0.2 V and 0.8V *vs.* solution potential. a) log [vector magnitude ($|Z|$)] *vs.* log [frequency(f)] at 0.2V *vs.* solution potential. b) phase angle (ϕ) *vs.* log f at 0.2 V. c) log $|Z|$ *vs.* log (f) at 0.8V. d) ϕ *vs.* log f at 0.8 V. Both a) and c) have slope of -1 from 10 kHz $\leq f \leq$ 100 kHz indicating the change in $|Z|$ is changing with f. Both b) and d) show ϕ's of almost 90° indicating a capacitance dominating the impedance.

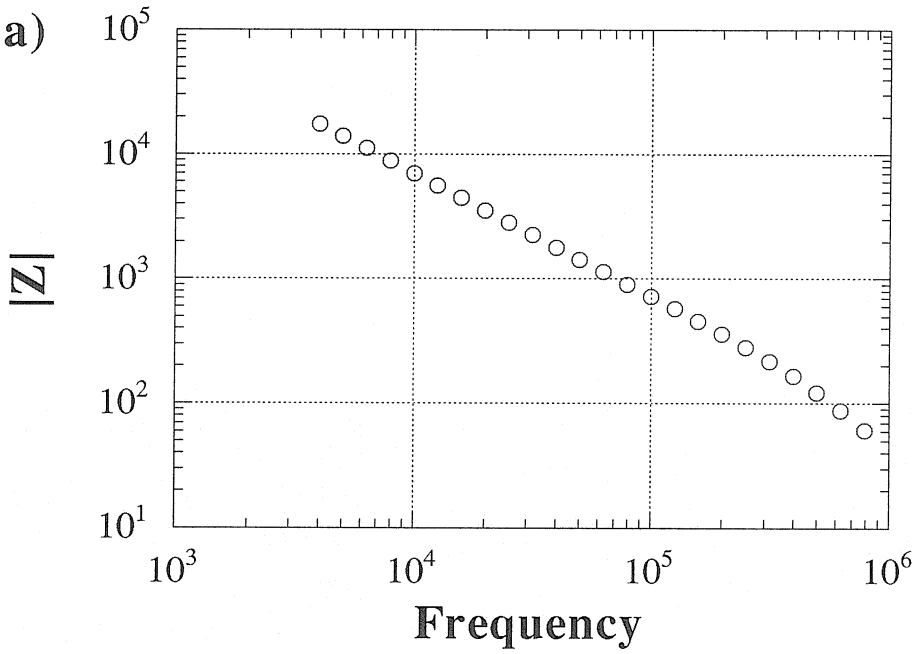
a)
|Z|
10^5
10^4
10^3
10^2
10^1
10^3
10^4
10^5
10^6
Frequency

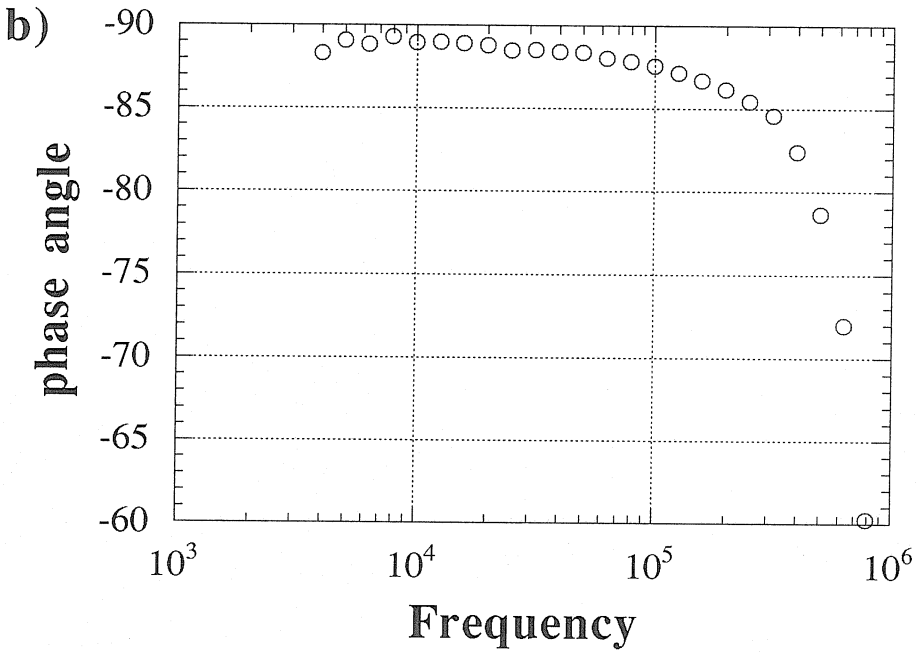
b)
-90
-85
-80
-75
-70
-65
-60
phase angle
10^3
10^4
10^5
10^6
Frequency

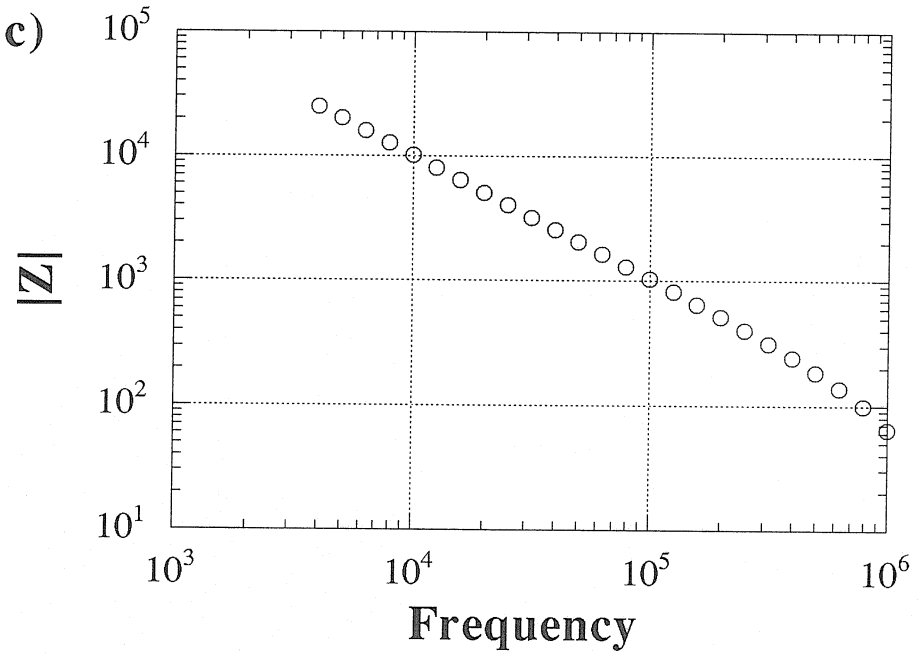
c)
|Z|
10^5
10^4
10^3
10^2
10^1
10^3
10^4
10^5
10^6
Frequency

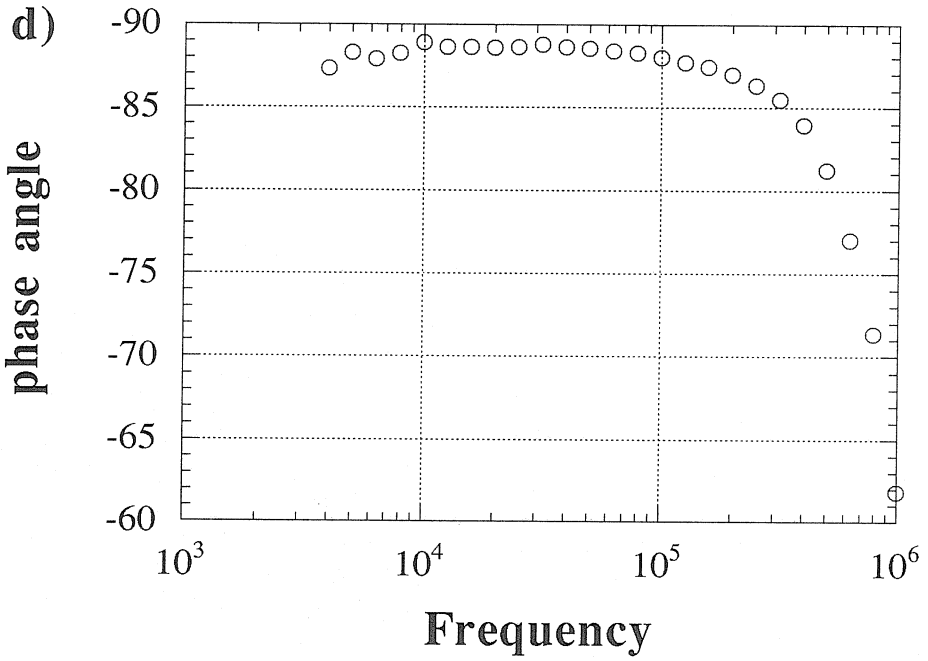
d)
phase angle
-90
-85
-80
-75
-70
-65
-60
10^3
10^4
10^5
10^6
Frequency

and phase angles of ≈ 90° (Figure 4 a-d). These data indicated that a frequency-independent, purely capacitive component dominated the cell impedance over this bias and frequency range.[23] Similar results were obtained using $MV^{2+/\bullet+}$ as the redox couple.

Figure 5 presents these $BV^{2+/\bullet+}$ data in Mott-Schottky form (differential capacitance^{-2} *vs.* V) for two different doping densities of the Si sample. The slopes of such plots were in excellent agreement with the values calculated from the known donor density of the samples; furthermore, the x-intercepts of the $BV^{2+/\bullet+}$ data shifted as predicted from the Mott-Schottky equation with changing doping density ($\Delta V_{predicted}$ = 110 mV; ΔV_{exp} = 116±8 mV). These data therefore allow a reliable assignment of the imaginary component of the measured impedance to the differential capacitance of the semiconductor space charge region. Application of the Mott-Schottky equation:[19]

$$\frac{1}{C^2} = \frac{2}{qN_d\varepsilon_s A_s^2}\left(V_{app} - V_{fb} - \frac{kT}{q}\right) \qquad (9)$$

(where C is the capacitance in F-cm^{-2}, N_d the donor density, ε_s the dielectric of the semiconductor, A_s the surface area of the electrode, V_{fb} the flatband potential, and V_{app} the applied potential) and correcting for the bulk semiconductor potential, V_n, yielded a potential for the bottom of the conduction band, E_{cb}, of -1.05 V *vs.* SCE.

The measurements of E_{cb} for the $MV^{2+/\bullet+}$ system were more complicated. M-S plots had the correct slopes as determined by independent measurements of N_d and A_s (±8%), but the measured E_{cb} shifted negatively with time in solution, with E_{cb} finally coming to a value of about -1.1 V *vs.* SCE. This conduction bandedge energy shift detected by M-S plots is

Figure #5 Mott-Schotky plot of two (100) n-Si electrodes in 10/10mM $BV^{2+/\bullet+}$ 1.00 M LiCl-CH_3OH solution: a) Donor density (N_d) = 1.1×10^{15} cm^{-3}, bulk silicon potential (V_n) = 0.261 V, area = 0.153 cm^{-2}; flat-band potential (V_{fb}) = -0.380±0.005 V *vs.* solution potential, slope = 3.4×10^{17}. b) $N_d = 8.6 \times 10^{16}$ cm^{-3}, V_n = 0.151 V, area = 0.163 cm^{-2}; V_{fb} = -0.496±0.008 V *vs.* solution potential, slope = 7.5×10^{15}. $E_{cb} = V_{fb} - kT/q - V_n$ so a) gives E_{cb} = -0.667±0.005 V *vs.* solution, b) gives E_{cb} = -0.673±0.008 V *vs.* solution. This demonstrates that this silicon methanol junction is following the simple M-S equation (Eq. 9).

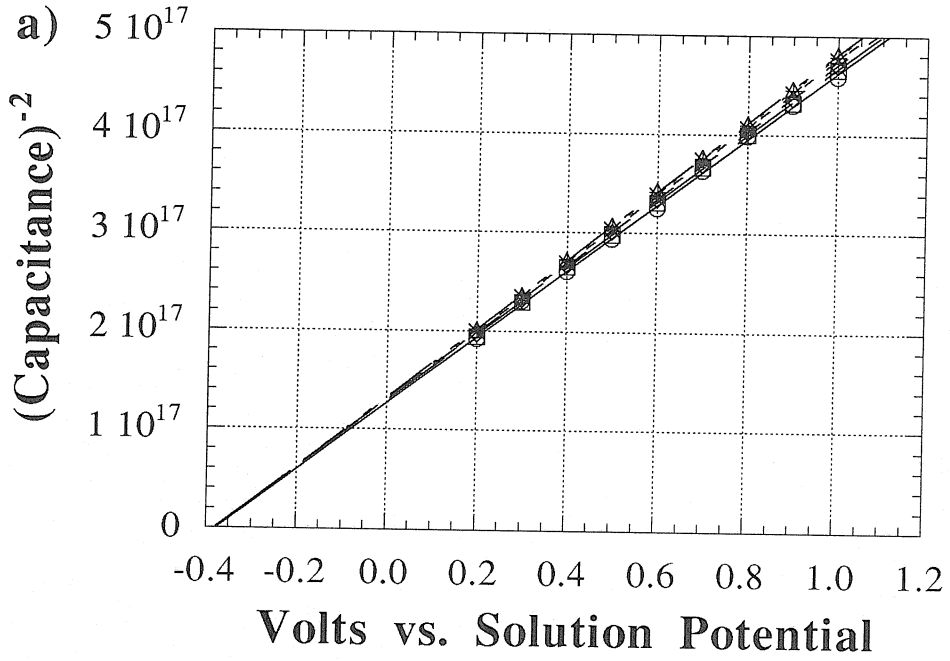
a)
5 10^17
4 10^17
3 10^17
2 10^17
1 10^17
0
(Capacitance)^-2
-0.4
-0.2
0.0
0.2
0.4
0.6
0.8
1.0
1.2
Volts vs. Solution Potential

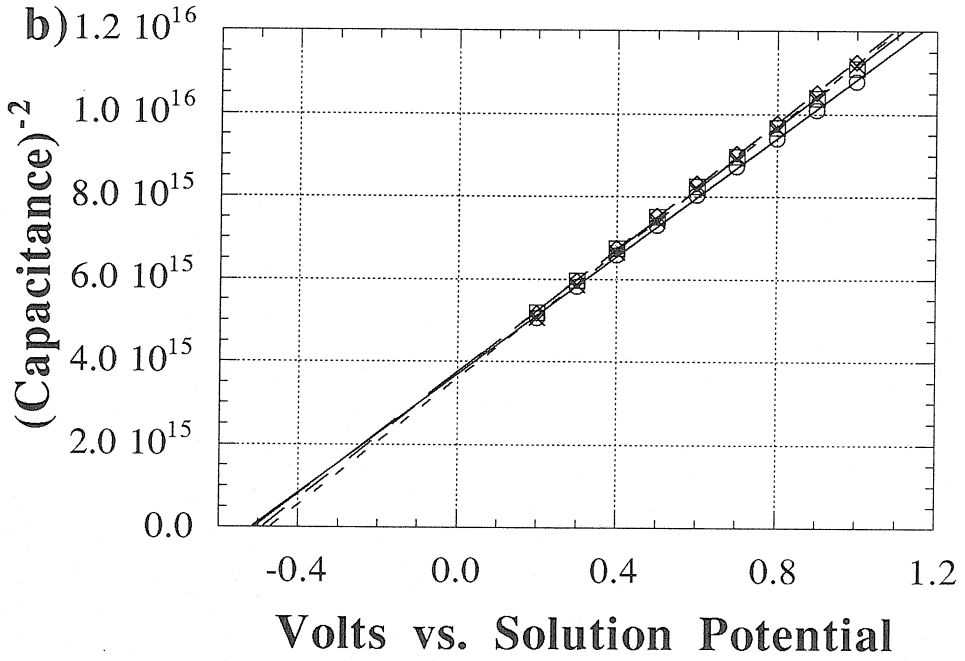
b)
1.2 10^16
1.0 10^16
8.0 10^15
6.0 10^15
4.0 10^15
2.0 10^15
0.0
(Capacitance)^-2
-0.4
0.0
0.4
0.8
1.2
Volts vs. Solution Potential

consistent with previous reports of initial shifts of V_{oc} under illumination for CH_3OH/Si systems.[41] This shift is also induced by exposure of the HF etched Si to an Fc^+-CH_3OH solution. It is known this solution removes the Si-H bond formed on the surface during HF etching,[44] but the exact chemical species remaining on the surface and the mechanism of the bandedge shift are unclear at present.

Since these shifts were slow on the timescale of the M-S measurements, the E_{cb} values could be used to evaluate the driving force dependence of the rate constant for electron transfer into $MV^{2+/\bullet+}$. Figure 6 shows the compilation of many determinations of k_{et} and E_{cb} in a $\Delta G^{\circ\prime}$ *vs.* log k_{et} plot. The data can be fit with Eq. 3, yielding a $k_{et,max}$ of 10^{-15} cm^4-s^{-1}, and λ = 0.9 eV, with a correlation coefficient (R) = 0.76. Given the uncertainty, these data do not prove the applicability of Eq. 3 to this semiconductor liquid system, but these data are consistent with a Marcus region for this silicon-CH_3OH system.

IV. DISCUSSION

The discovery of a system showing an ideal response to a change in concentration of acceptor in solution is important in and of itself, since it demonstrates that it is possible to define systems where electron transfer rate constants can be measured and compared to theory.[1] Some workers previously had argued that these measurements might never be possible from steady-state measurements since crystal faces inherently have surface states, and trapping would always dominate current flow.[35]

There are two pathways that can account for the observed concentration dependence. In the first and most likely, the Si surface is electrically defect free (on the order of $\leq$ 1 defect per 10^6 surface atoms). This

Figure #6 Compilation of the log k_{et} *vs.* $\Delta G^{\circ\prime}$ data calculated in this work ($\Delta G^{\circ\prime} = qE_{cb} - qE^{\circ\prime}$). Error bars are reasonable estimates for the data ($\Delta G^{\circ\prime}$ ±0.01 V; log k_{et} ±0.25). The data was fit to the equation $\log k_{et} = -(\Delta G^{\circ\prime} + \lambda)^2/(4kT\lambda) + C$, where $C = \log (\upsilon_n \kappa_{el}) = \log k_{et,max}$. Best fit was obtained with $\lambda = 0.86$ eV and $C = -14.92$, corresponding to 1.2×10^{-15} $cm^4\text{-}s^{-1}$.

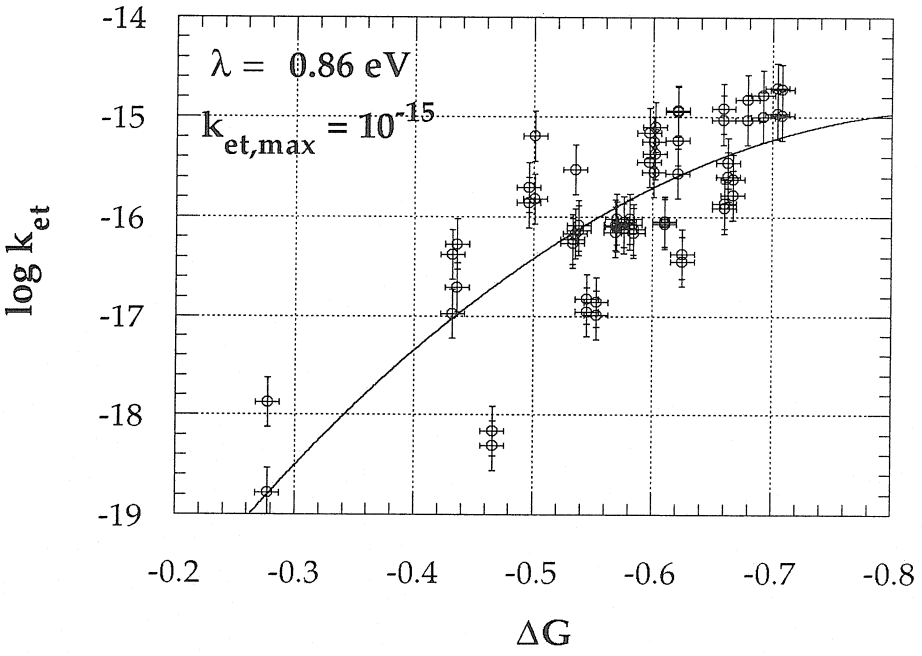
λ = 0.86 eV
k et,max = 10-15
log k et
-14
-15
-16
-17
-18
-19
-0.2
-0.3
-0.4
-0.5
-0.6
-0.7
-0.8
ΔG

would allow the direct electron transfer to an acceptor in solution to dominate the current flow. Alternatively, a mechanism involving surface states (Fig. 1) cannot be ruled out. This would require that electron transfer to solution from the surface state be slow relative to the filling of the traps, that the activity of the traps be sufficient to carry the observed current, and that the traps be in equilibrium with the electrons in the silicon. In order for this mechanism to explain the results, Eq. 7 shows that $k_{sol}[A]_s$ must be on the order of $k_{ss}n_s$, otherwise there would be a dependence of J on $[A]_s$ or n_s, but not both. It is not likely that these products are fortuitously equal, since the rate in this $MV^{2+/\bullet+}$ system is dependent on both n_s and $[A]_s$ over a relatively wide range of potential and concentration. Thus it is not likely that the surface states are involved in the electron transfer process.

The observation of frequency independent Mott-Schottky plots has also been essential to making these determinations of k_{et}. This "ideal" behavior lends confidence to the measured E_{cb}'s for these systems.[23] Knowing E_{cb} allows both $\Delta G^{\circ\prime}$ and n_s to be determined and thus k_{et} to be calculated.

A plot of log k_{et} *vs.* $\Delta G^{\circ\prime}$ is shown in Fig. 6 and spans a range of $\Delta G^{\circ\prime}$ of about 0.4 eV (0.3 to 0.7 eV). Assuming a Marcus relationship holds, and fitting these data to Eq. 3, gives a reorganization energy for the system (λ) of 0.9 eV. The fit is reasonable for values of λ above 0.6 eV if log $k_{et,max}$ is allowed to float (See Fig. 7 a-g). This best fit λ = 0.9 eV is larger than the λ calculated from the self exchange rate constant of $MV^{2+/\bullet+}$ in solution (λ = 0.5 eV; $k_{self} = 1 \times 10^7$ M^{-1}-s^{-1}) using the equation:

$$k_{self} = Z_{sol} e^{-\frac{\lambda}{2kT}} \qquad (10)$$

where $Z_{sol} = 10^{11}$ M^{-1}-s^{-1} (the collision frequency of molecules in solution). Little is known about how λ will change from its value in a homogeneous

Figure #7 Best fit to the log k_{et} *vs.* $\Delta G^{\circ'}$ data calculated in this work ($\Delta G^{\circ'} = E_{cb} - E^{\circ'}$) when λ is fixed and $k_{et,max}$ is varied from 0.5 eV to 1.1 eV. a) Best fit with λ = 0.5 eV was obtained with log $k_{et,max}$ = -15.66, corresponding to 2.2 x 10^{-16} cm^4-s^{-1}. b) Best fit with λ = 0.6 eV was obtained with log $k_{et,max}$ = -15.79, corresponding to 1.6 x 10^{-16} cm^4-s^{-1}. c) Best fit with λ = 0.7 eV was obtained with log $k_{et,max}$ = -15.62, corresponding to 2.4 x 10^{-16} cm^4-s^{-1}. d) Best fit with λ = 0.8 eV was obtained with log $k_{et,max}$ = -15.24, corresponding to 5.8 x 10^{-16} cm^4-s^{-1}. e) Best fit with λ = 0.9 eV was obtained with log $k_{et,max}$ = -14.73, corresponding to 1.9 x 10^{-15} cm^4-s^{-1}. f) Best fit with λ = 1.0 eV was obtained with log $k_{et,max}$ = -14.13, corresponding to 7.5 x 10^{-15} cm^4-s^{-1}. g) Best fit with λ = 1.1 eV was obtained with log $k_{et,max}$ = -13.46, corresponding to 3.5 x 10^{-14} cm^4-s^{-1}.

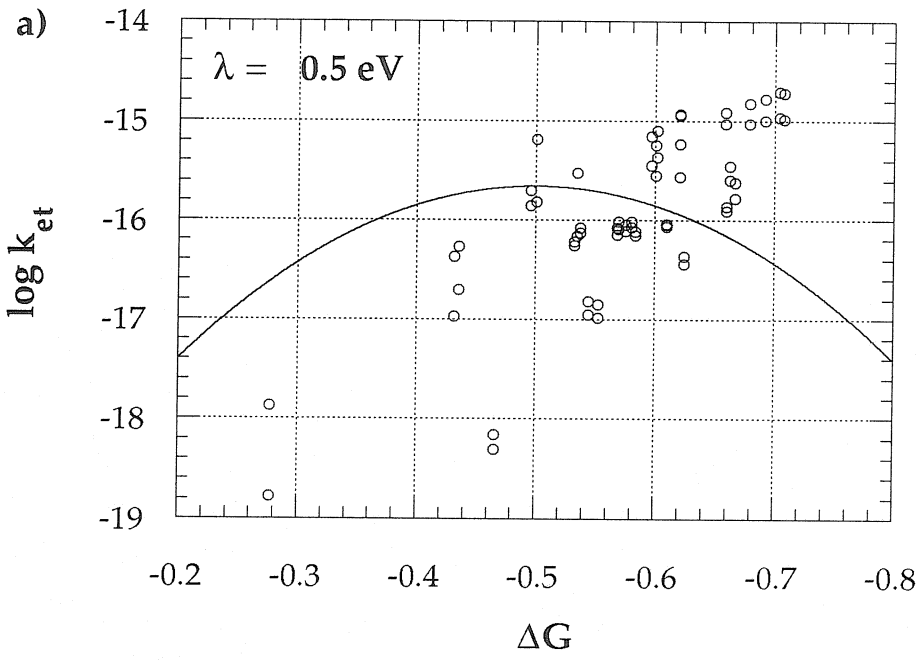
a)
λ = 0.5 eV
log k_et
-14
-15
-16
-17
-18
-19
-0.2
-0.3
-0.4
-0.5
-0.6
-0.7
-0.8
ΔG

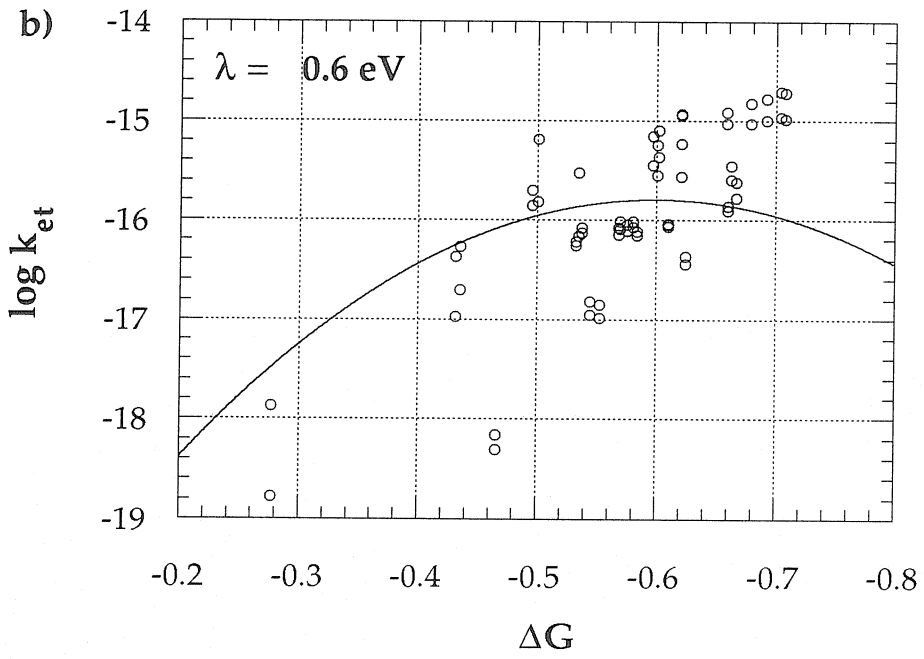
b)
λ = 0.6 eV
log k_et
-14
-15
-16
-17
-18
-19
-0.2
-0.3
-0.4
-0.5
-0.6
-0.7
-0.8
ΔG

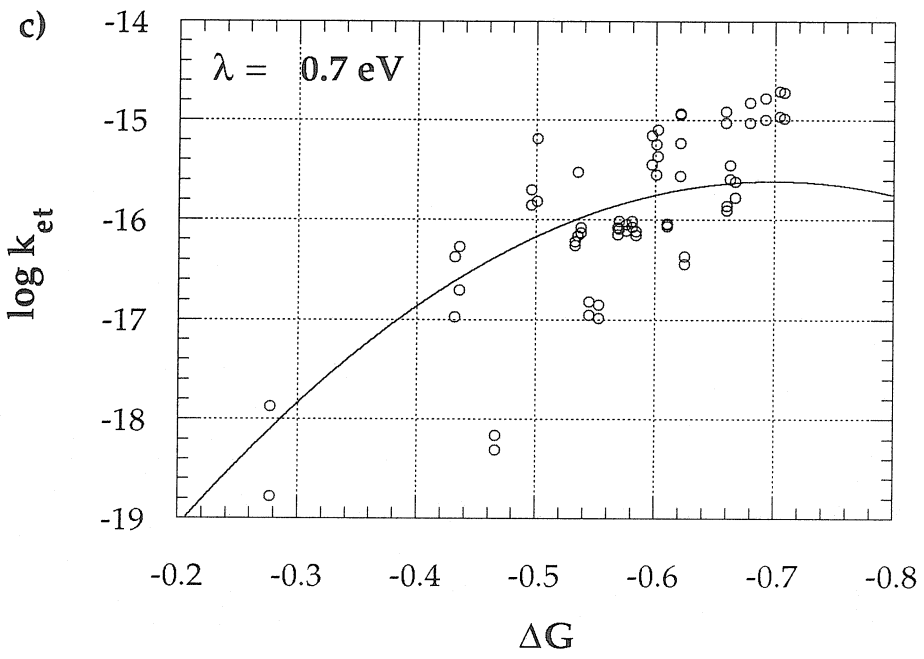
c)
λ = 0.7 eV
-14
-15
-16
-17
-18
-19
log k_et
-0.2
-0.3
-0.4
-0.5
-0.6
-0.7
-0.8
ΔG

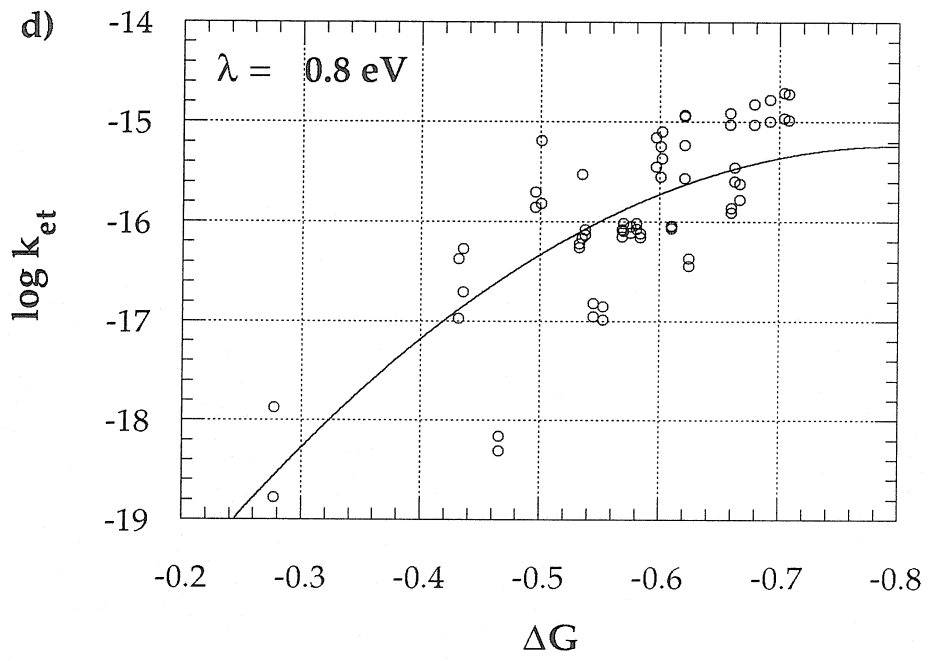
d)
λ = 0.8 eV
log k_et
-14
-15
-16
-17
-18
-19
-0.2
-0.3
-0.4
-0.5
-0.6
-0.7
-0.8
ΔG

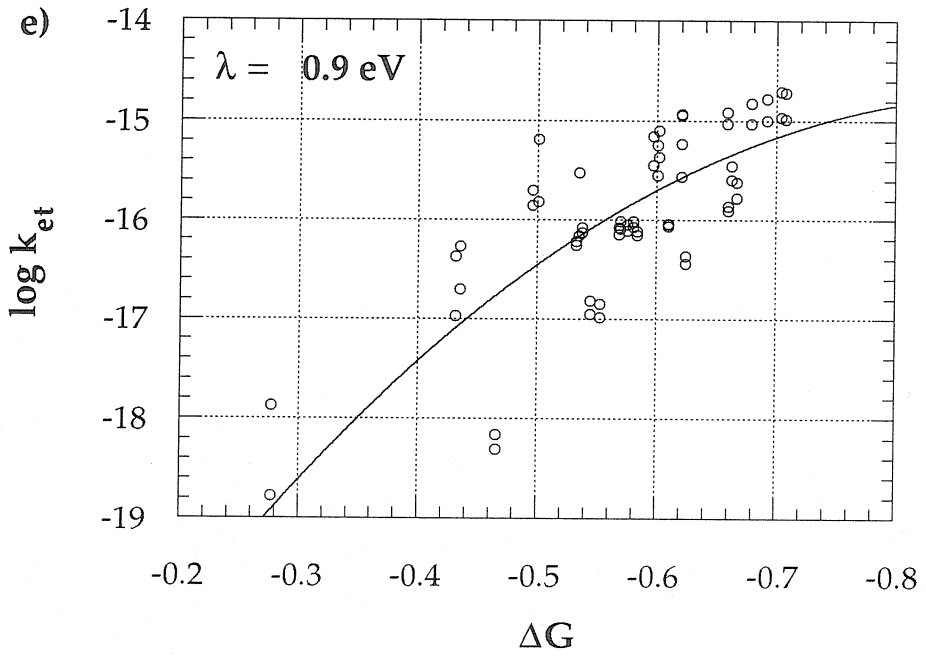
e)
λ = 0.9 eV
-14
-15
-16
-17
-18
-19
log k_et
-0.2
-0.3
-0.4
-0.5
-0.6
-0.7
-0.8
ΔG

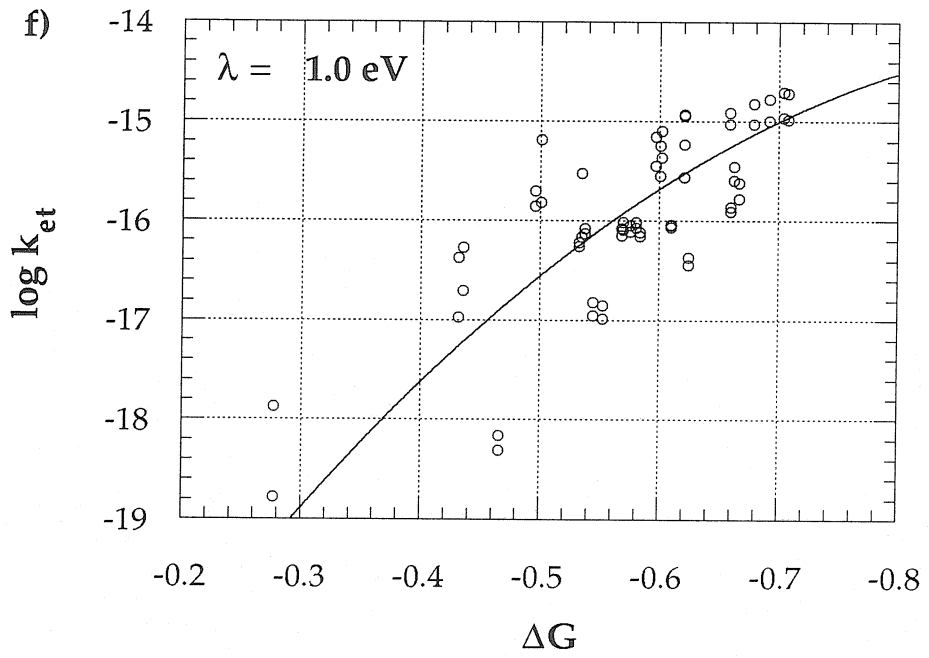
f)
λ = 1.0 eV
log k_et
-14
-15
-16
-17
-18
-19
-0.2
-0.3
-0.4
-0.5
-0.6
-0.7
-0.8
ΔG

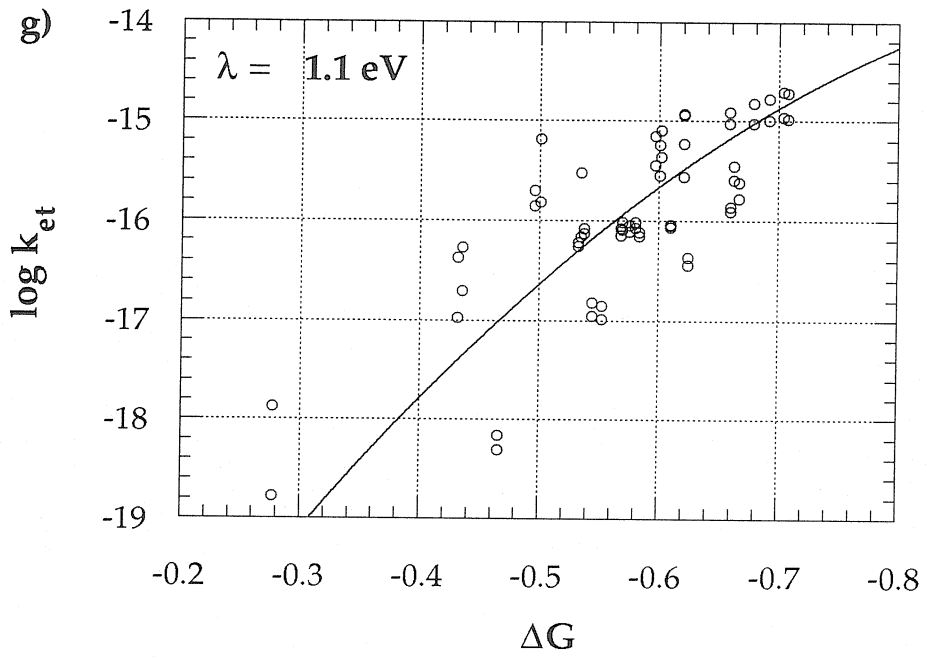
g)
λ = 1.1 eV
log k_et
-14
-15
-16
-17
-18
-19
-0.2
-0.3
-0.4
-0.5
-0.6
-0.7
-0.8
ΔG

reaction to its value at a semiconductor electrode. It does seem unlikely, however, that λ would be more than 2x greater than that in a self-exchange process. solution since the dielectrics are not that much different. More work with different redox couples needs to be done to better understand this effect.

The value of $k_{et,max}$, is to our knowledge, the first experimental estimate of the maximally exothermic rate constant for interfacial charge transfer at any semiconductor liquid junction to date. The value obtained from fitting the data (10^{-15} cm^4-s^{-1}) is higher than the theoretical value for $k_{et,max}$ quoted earlier, but given the number of unknown quantities in that estimate, the present experimental value is not unreasonable. When λ was varied from 0.7 eV to 1.1 eV, the best fit for $k_{et,max}$ varied from 10^{-16} cm^4-s^{-1} to 10^{-14} cm^4-s^{-1} (0.7 eV and 1.1 eV

respectively). A $k_{et,max}$ as high as 10^{-12} can be ruled out by examining a related system. Recently the barrier height for the n-Si/CH_3OH-dimethylferrocene-dimethylferricenium($Me_2Fc^{+/0}$) system has been determined to be 1.0 eV.[45] This, along with the fact that this n-Si/CH_3OH system is known to be bulk recombination limited[41] (i.e., not electron transfer limited) allows an upper limit to be placed on the electron transfer rate constant for this system (driving force = 1.1 eV). At an open circuit voltage of -0.680 V (a bulk limited value) and a current of 20 mA-cm^{-2}, n_s can be determined from N_d and E_{cb}, then a k_{et} can be calculated from Eq. 4. This gives the upper limit for the electron transfer rate constant for this system to be 10^{-14} cm^4 -s^{-1} at $\Delta G^{\circ\prime}$ = -1.1 eV. Assuming the electronic coupling for these two one-electron outer sphere redox couples are similar, this observation constrains the values of λ and $k_{et,max}$ to values that maintain the Marcus curve at or below this value. Fig. 8a shows the $Me_2Fc^{+/0}$ point added

Figure #8 This shows the addition of the maximum log k_{et} for the $Me_2Fc^{+/0}$ system (log $k_{et} = 10^{-14}$; $\Delta G^{\circ\prime} = 1.1$ eV) plotted with the $MV^{2+/\bullet+}$ data. a) Plot showing the best fit equation is clearly consistent with this limit. b) Plot showing log $k_{et,max} = -14$ and the best fit $\lambda = 1.0$ eV is as large as log $k_{et,max}$ can be without exceeding this $Me_2Fc^{+/0}$ limit. c) Plot showing the equation when log $k_{et,max} = -12$ and the best fit $\lambda = 1.3$ eV. This clearly is not consistent with the $MV^{2+/\bullet+}$ data.

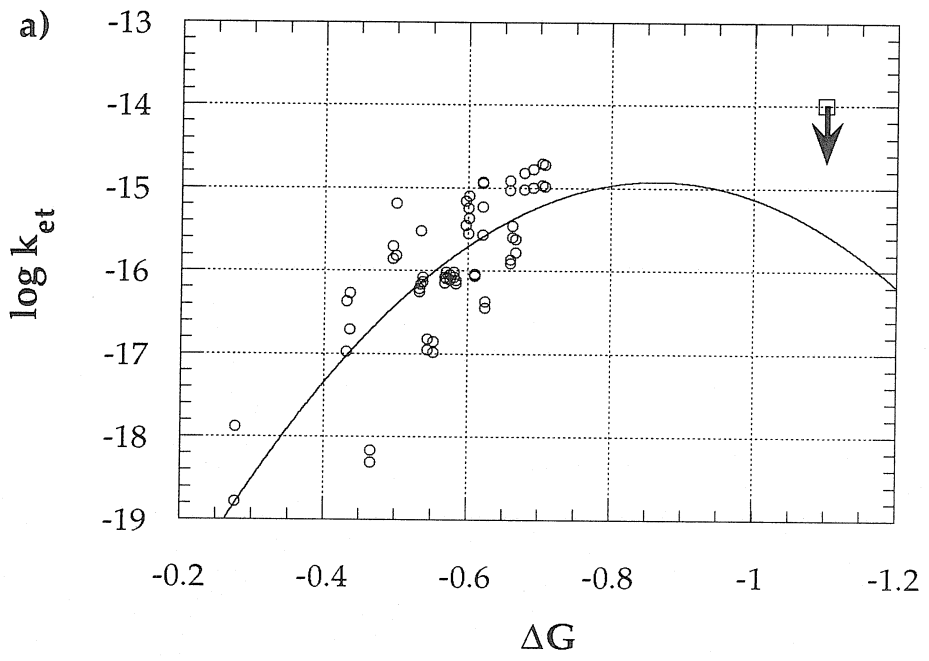
a)
-13
-14
-15
-16
-17
-18
-19
log k_{et}
-0.2
-0.4
-0.6
-0.8
-1
-1.2
ΔG

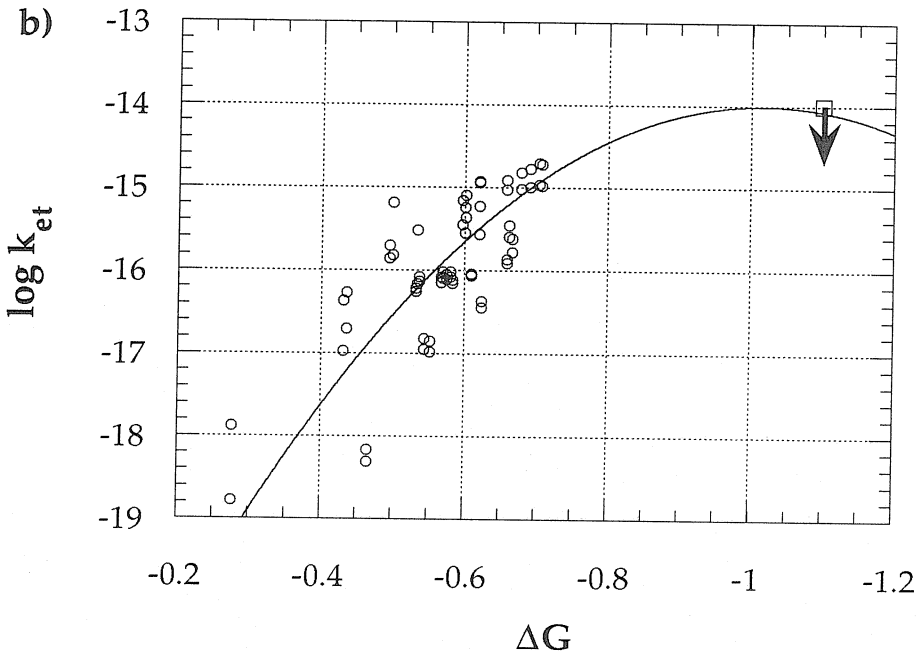
b)
-13
-14
-15
-16
-17
-18
-19
log k_{et}
-0.2
-0.4
-0.6
-0.8
-1
-1.2
ΔG

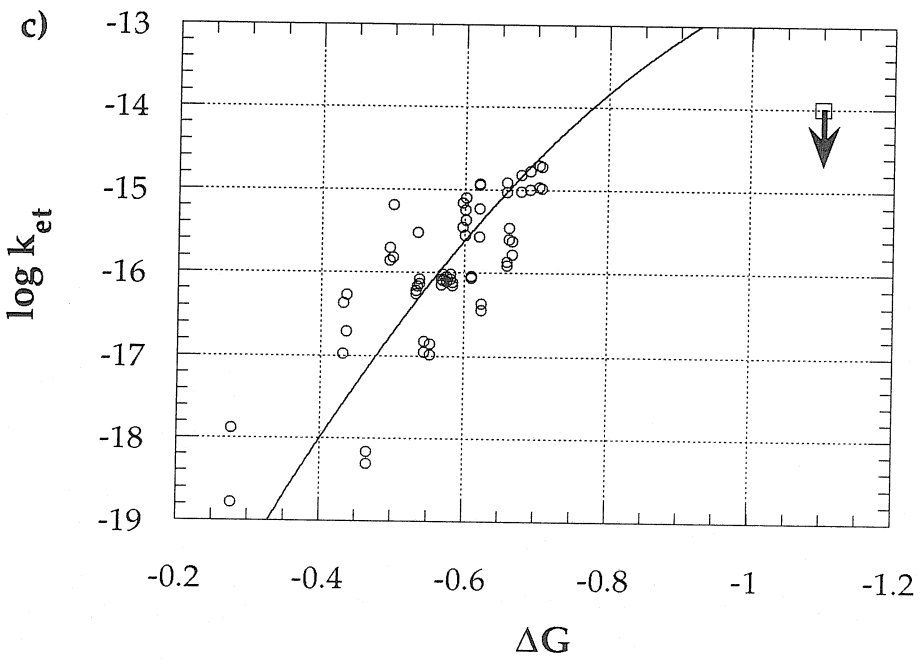
c)
-13
-14
-15
-16
-17
-18
-19
log k_{et}
-0.2
-0.4
-0.6
-0.8
-1
-1.2
ΔG

to the $MV^{2+/\bullet+}$ data and the curve defined by the best fit to the $MV^{2+/\bullet+}$ data (λ = 0.9 eV; $k_{et,max} = 10^{-15}$ cm^4-s^{-1}). These values for λ and $k_{et,max}$ give a curve well below this point and so are consistent with the present best fit interpretation of the data. By inspection, even with the flattening of the curve in the inverted region, due to tunnelling, the $k_{et,max}$ cannot rise above 10^{-14} cm^4-s^{-1}, still be consistent with the $Me_2Fc^{+/0}$ point, and fit the $MV^{2+/\bullet+}$ data (see Fig. 8b). Fig. 8c shows the fit to the $MV^{2+/\bullet+}$ data for a $k_{et,max} = 10^{-12}$ cm^4-s^{-1}, giving λ = 1.3 eV. There would need to be drastic differences between the redox couples for this value of $k_{et,max}$ to be reasonable. Thus a limit can be set of 10^{-14} cm^4-s^{-1} for the $k_{et,max}$ in this system.

Measurement of rate constants in the "inverted" region (*i.e.*, at higher $\Delta G^{\circ\prime}$) would allow a much more quantitative evaluation of the data and increase the understanding of semiconductor/liquid junctions. Unfortunately, simply choosing a redox couple with a more positive value of $E^{\circ\prime}$ does not allow exploration of this regime. Increasing the $\Delta G^{\circ\prime}$ too much, causes a different mechanism to dominate the charge flow, thus direct measurement of k_{et} is not possible. For example the $Me_2Fc^{+/0}$ system mentioned above has a more positive $E^{\circ\prime}$ and has been shown to be controlled by a bulk recombination mechanism, not direct electron transfer to solution. These non-electron transfer limited systems only allow upper limits to be placed on the rate constants and do not allow the actual rate constant to be measured. More one-electron, outer-sphere redox couples need to be explored that are about 0.2 V more positive of the $MV^{2+/\bullet+}$ used in this study to determine if k_{et} can be measured at increased driving force without another mechanism dominating the charge flow through the semiconductor/liquid junction.

Alternate explanations for the data in Fig. 6 cannot be ruled out. The assumptions needed to apply the Marcus expression for this system may not be valid. It is possible that the electronic coupling between the silicon and the acceptor in solution (κ_{el}) changes when the reaction that shifts the bandedge occurs. This would invalidate the assumption of Eq. 1 and might still give a plot such as in Fig. 6. It is possible that the adsorption of the $MV^{2+/\bullet+}$ to the surface influences the electron transfer and thus the calculated rate constant by increasing $[A]_s$ and giving an apparent k_{et} higher than its true value. Cyclic voltammetery on the HF etched sample in $MV^{2+/\bullet+}$ solution showed a peak to peak separation (E_{pp}) of ~80 mV, demonstrating that for this surface, there is no significant adsorption (an E_{pp} of zero is expected for a fully adsorbed electroactive species). If adsorption is important, this is an unusual system in that it shows a first order dependence on acceptor concentration up to at least 0.1 M. Thus the surface would still need to be in the linear region of the adsorption isotherm and not saturating.

Conclusions:

This work has demonstrated one of the first electron transfer limited semiconductor liquid junction systems, along with "ideal" M-S plots to determine the energetics of the conduction band. This has allowed the first exploration of the driving force dependence of the electron transfer rate constants. Simple Marcus relationships give a λ of 0.86 eV and a $k_{et,max}$ of 1×10^{-15} cm^4-s^{-1} for the reduction of $MV^{2+/\bullet+}$ at silicon in CH_3OH-LiCl. Limits on the value for $k_{et,max}$ of 10^{-14} cm^4-s^{-1} have been established. More work needs to be done to investigate the response of this system to different redox couples and solution conditions to determine the general behavior of

electroactive species at semiconductor electrodes and to decide if the theory needs to be adjusted to explain a $k_{et,max}$ 10^{-14} cm^4-s^{-1}.

References

(1) Lewis, N. S. *Ann. Rev. Phys. Chem.* **1991**, *42*, 543.

(2) Tan, M. X.; Laibinis, P. E.; Nguyen, S. T.; Kesselman, J. M.; Stanton, C. E.; Lewis, N. S. *Prog. Inorg. Chem.* **1994**, *41*, 21.

(3) Gerischer, H. *Faraday Discuss.* **1980**, *70*, 137.

(4) Kohl, P. A.; Harris, D. B.; Winnick, J. *J. Electrochem. Soc.* **1990**, *137*, 3315.

(5) Kohl, P. A.; Ostermayer, F. W. *Ann. Rev. Mat. Sci.* **1989**, *19*, 379.

(6) Elliott, D. J. *Integrated Circuit Fabrication Technology*; Mc-Graw Hill: New York, 1989.

(7) Unagami, T. *J. Electrochem. Soc.* **1980**, *127*, 476.

(8) Gerischer, H. *Pure & Appl. Chem.* **1980**, *52*, 2649.

(9) Nazeeruddin, M. K.; Kay, A.; Rodicio, I.; Humphry-Baker, R.; Muller, E.; Liska, P.; Vlachopoulos, N.; Gratzel, M. *J. Amer. Chem. Soc.* **1993**, *115*, 6382.

(10) O'Regan, B.; Gratzel, M. *Nature* **1991**, *353*, 737.

(11) Valchopoulos, N.; Liska, P.; Augustynski, J.; Gratzel, M. *J. Amer. Chem. Soc.* **1988**, *110*, 1216.

(12) Rosenwaks, Y.; Thacker, B. R.; Nozik, A. J.; Ellingson, R. J.; Burr, K. C.; Tang, C. L. *J. Phys. Chem.* **1994**, *98*, 2739.

(13) Rosenwaks, Y.; Thacker, B. R.; Ahrenkiel, R. K.; Nozik, A. J. *J. Phys. Chem.* **1992**, *96*, 10096.

(14) Shreve, G. A.; Lewis, N. S. *J. Electrochem. Soc.* **1995**, *142*, 112.

(15) Hafeman, D. G.; Parce, J. W.; McConnell, H. M. *Science* **1988**, *240*, 1182.

(16) de Rooij, N. F.; van de Vlekkert, H. H. In *Chemical Sensor Technology*; N. Yamazoe, Ed.; Kodansha, Ltd.: Tokyo, 1991; Vol. 3; pp 213.

(17) Finklea, H. O. *Semiconductor Electrodes*; Elsevier: New York, 1988.

(18) Gregory, R. P. F. *Photosynthesis*; Blackie & Son Ltd.: Glasgow, 1989, pp 160.

(19) Morrison, S. R. *Electrochemistry at Semiconductor and Oxidized Metal Electrodes*; Plenum: New York, 1980.

(20) Wrighton, M. S. *Interfacial Photoprocesses: Energy Conversion and Synthesis*; American Chemical Society: Washington, DC, 1980; Vol. 184, pp 1.

(21) Koval, C. A.; Howard, J. N. *Chem. Rev.* **1992**, *92*, 411.

(22) Memming, R. *Ber. Bunsenges. Phys. Chem.* **1987**, *91*, 353.

(23) Gerischer, H. In *Physical Chemistry: An Advanced Treatise*; H. Eyring; D. Henderson and W. Yost, Ed.; Academic: New York, 1970; Vol. 9A; pp 463.

(24) Horrocks, B. R.; Mirkin, M. V.; Bard, A. J. *J. Phys. Chem.* **1994**, *98*, 9106.

(25) Miller, B.; Menezes, S.; Heller, A. *J. Electrochem. Soc.* **1979**, *126*, 1483.

(26) Closs, G. L.; Calcaterra, L. T.; Green, N. J.; Penfield, K. W.; Miller, J. R. *J. Phys. Chem.* **1986**, *90*, 3673.

(27) McLendon, G. *Acc. Chem. Res.* **1988**, *21*, 160.

(28) Marcus, R. A.; Sutin, N. *Biochim. Biophys. Acta* **1985**, *811*, 265.

(29) Fox, L. S.; Kozik, M.; Winkler, J. R.; Gray, H. B. *Science* **1990**, *247*, 1069.

(30) Marcus, R. A. *J. Chem. Phys.* **1956**, *24*, 966.

(31) Marcus, R. A. *J. Chem. Phys.* **1956**, *24*, 979.

(32) Marcus, R. A. *J. Phys. Chem.* **1990**, *94*, 1050.

(33) Marcus, R. A. *J. Phys. Chem.* **1991**, *95*, 2010.

(34) Gerischer, H. *J. Electrochem. Soc.* **1966**, *113*, 1174.

(35) Gerischer, H. *J. Phys. Chem.* **1991**, *95*, 1356.

(36) Garrett, C. G. B.; Brattain, W. H. *Phys. Rev.* **1955**, *99*, 376.

(37) Bard, A. J.; Faulkner, L. R. *Electrochemical Methods: Fundamentals and Applications*; John Wiley & Sons: New York, 1980, pp 629.

(38) Rosenbluth, M. L.; Lewis, N. S. *J. Phys. Chem.* **1989**, *93*, 3735.

(39) Koval, C. A.; Olson, J. B. *J. Phys. Chem.* **1988**, *92*, 6726.

(40) Gronet, C. M.; Lewis, N. S.; Cogan, G.; Gibbons, J. *Proc. Natl. Acad. Sci., USA* **1983**, *80*, 1152.

(41) Rosenbluth, M. L.; Lewis, N. S. *J. Am. Chem. Soc.* **1986**, *108*, 4689.

(42) Thurber, W. R.; Mattis, R. L.; Liu, Y. M.; Filliben, J. J. *J. Electrochem. Soc.* **1980**, *127*, 1807.

(43) Sze, S. M. *The Physics of Semiconductor Devices;* 2nd ed.; Wiley: New York, 1981.

(44) Lewis Group, private communication, **1994**.

(45) Laibinis, P. E.; Stanton, C. E.; Lewis, N. S. *J. Phys. Chem.* **1994**, *98*, 8765.

Chapter Three

Limits on the Active Corrosion Rate of Si Surfaces in Contact with CH_3OH-Ferrocene$^{+/0}$ and CH_3OH-1,1'-Dimethylferrocene$^{+/0}$ Solutions

ABSTRACT

Although Si/CH_3OH contacts have been extensively investigated and reported to provide highly efficient photoelectrochemical energy conversion devices, a recent study using the scanning electrochemical microscope (SECM) has claimed that in CH_3OH solutions, Si surfaces in contact with 4.57 mM ferrocenium (Fc^+) actively corrode in the dark, at a rate of 75 nm-s^{-1}. This conclusion was inferred from an anomalously large feedback current in an SECM experiment. The present work describes a search for active corrosion of Si in contact with CH_3OH-ferrocene$^{+/0}$ and CH_3OH-dimethylferrocene(Me_2Fc)$^{+/0}$ solutions through the use of very sensitive electrochemical, chemical, and physical methods. For CH_3OH-1.0 M $LiClO_4$-100 mM Me_2Fc-80 mM Me_2Fc^+ solutions, an upper limit on the active corrosion rate of 6.6×10^{-6} nm-s^{-1} has been established through direct experimental measurements; thus, a 400 μm thick Si photoelectrode in contact with the CH_3OH-$Me_2Fc^{+/0}$ electrolyte would require over 1500 years to corrode completely at room temperature. An alternative explanation for the SECM data, based on the documented existence of an inversion layer at the Si/liquid contact, is presented and shown to be consistent with the available data.

I. INTRODUCTION

Semiconductor/liquid contacts formed using Si/CH_3OH junctions with 1,1'-dimethylferrocene ($Me_2Fc^{+/0}$) as the redox couple have been shown to

provide extremely efficient photoelectrochemical cells.[1-3] These Si/CH_3OH junctions are perhaps the most well-characterized semiconductor/liquid contacts to date, having been probed by a variety of chemical, electrical, electrochemical, and spectroscopic methods.[4-11] Because of the substantial body of knowledge involving the surface chemistry and materials processing characteristics of Si, Si/CH_3OH interfaces provide a nearly ideal system for developing new methodologies to investigate the behavior of solid/liquid interfaces.

Recent data obtained using the scanning electrochemical microscope (SECM) have been interpreted to indicate that Si surfaces actively corrode at a mass-transfer-limited rate in contact with CH_3OH-ferrocene ($Fc^{+/0}$) solutions.[12] In this SECM experiment, an anomalously large feedback current, compared to that expected for an insulating surface, was observed when Fc^+ was generated at an SECM tip in close proximity to a Si crystal. This excess feedback current was hypothesized to arise from reaction of Fc^+ with the Si, leading to oxidation of the Si and regeneration of Fc in the vicinity of the tip.[12]

Curiously, Si oxide formation in this open system would be expected to passivate the Si[5,13] and thus could not produce the observed sustained feedback current. It was therefore speculated that active corrosion of Si occurred in the SECM experiment, resulting in the formation of a soluble $Si(OCH_3)_4$-type moiety.[12] The reported rate constant of 0.37 cm-s^{-1} corresponds to an equivalent corrosion current density of 240 mA-cm^{-2} and to an active Si corrosion rate of 75 nm-s^{-1}.[12] As support for this hypothesis, SECM measurements of the Si surface after ~15 minutes at a smaller current showed a ~1 μm deep feature in the Si. This etch rate corresponds to a corrosion rate of 1.1 nm-s^{-1} and an equivalent corrosion current density of 3.5

mA-cm^{-2}, assuming a 4-electron decomposition stoichiometry in the oxidation of Si to soluble Si(IV).

The presence of even as little as 3.5 mA-cm^{-2} of corrosion current density at 4.6 mM Fc^+ would have serious implications for the photoelectrochemical measurements reported previously from various laboratories, including our own.[3,4] Typical photocurrent densities of Si electrodes under 1 Sun illumination are 20-30 mA-cm^{-2},[1,14] so a corrosion current-density of 3.5 mA-cm^{-2} (and certainly one of 240 mA-cm^{-2}) would cast serious doubt onto the interpretation of the previously reported current density-voltage measurements. The presence of significant, active corrosion of the Si would also complicate the interpretation of prior open circuit voltage (V_{oc}) data for the Si/CH_3OH contact. Measurements of V_{oc} have shown quantitative agreement with theoretical expectations based on the Shockley diode equation,[2,4] but if the sample is corroding significantly, V_{oc} might also reflect a mixture of the electrode potential for regenerative electrochemical processes in combination with the electrode potential for a corrosion reaction.

In contrast to the SECM results, prior studies of long term photocurrent flow through n-Si/C_2H_5OH-$Fc^{+/0}$ and n-Si/CH_3OH-$Me_2Fc^{+/0}$ systems have reported no bulk weight loss of the Si.[1,3,15] In addition, the photoelectrochemical efficiency of a 400 μm thick Si specimen in contact with a propylene carbonate-CH_3OH-$Me_2Fc^{+/0}$ electrolyte was reported to be stable during ≈1 month of illumination at short circuit,[1] which is much longer than the failure time of ~4 days that would be predicted from even the 1.1 nm-s^{-1} corrosion rate of the SECM experiment. From these results, as well as other reports, it would appear that the corrosion of Si/alcohol-ferrocene systems is insignificant on typical laboratory timescales. In view of these apparently

contradictory conclusions concerning the stability of Si electrodes, we have performed a quantitative study of the corrosion of Si at n-Si/CH_3OH-$Fc^{+/0}$ and n-Si/CH_3OH-$Me_2Fc^{+/0}$ contacts. In this series of experiments, we have reexamined with higher sensitivity the current density-voltage (J-V) data in the dark for n-Si/CH_3OH-$Me_2Fc^{+/0}$ and p-Si/CH_3OH-$Me_2Fc^{+/0}$ contacts. We have also performed weight loss experiments for Si crystals in contact with CH_3OH-$Fc^{+/0}$ and CH_3OH-$Me_2Fc^{+/0}$ solutions. In addition, we have lithographically fabricated posts of Si oxide to act as blocking layers and to provide a sensitive height reference for the presence of any corrosion features on Si in contact with CH_3OH-$Fc^{+/0}$ and CH_3OH-$Me_2Fc^{+/0}$ solutions. Stylus profilometry data were then collected on such "post-referenced" Si electrodes after ~116 days of continuous contact with methanolic solutions of ferrocenes. Analogous stability data were obtained for "post-referenced" Si photoelectrodes that were illuminated and run as electrodes in CH_3OH-based photoelectrochemical cells. We report the results of these studies below.

II. EXPERIMENTAL

Me_2Fc and Fc were obtained from Strem Chemical and were sublimed before use. $LiClO_4$, Me_2FcBF_4, and $FcBF_4$ were prepared as described previously.[3,4] Mg powder (EM Scientific) and I_2 (EM Scientific) were added to reagent grade methanol (EM Scientific) and the pure liquid was distilled under ambient pressure. All electrolytes and redox couples were then dissolved into the solvent, and any particulates were removed by filtration through a membrane filter with 1 μm diameter pores. All samples for use in corrosion measurements were stored for the duration of their exposure to the various solutions in a flush tank that was continuously purged with $N_2(g)$

and that displayed oxygen concentrations of less than 10 ppm (as monitored by fuming of diethyl zinc).

Si electrodes used in J-V experiments were prepared as described previously.[3] The electrodes were etched in 48 wt% *aq.* HF (Mallinckrodt Inc., Paris, KY), rinsed with H_2O, rinsed with methanol, blown dry in a stream of N_2(g), and then immersed into the desired solution. All exposures of Si to the test solutions were performed in the dark except where otherwise specified. J-V data were collected using a Princeton Applied Research (PAR) model 173 potentiostat, a PAR model 175 universal programmer, and a Houston Instruments model 2000 X-Y recorder. Experiments in the presence of illumination also included a PAR model 179 digital coulometer. Illumination was generated by a water-filtered ELH-type W-halogen bulb with a dichroic rear reflector. The incident light intensity was adjusted using neutral density filters to give the desired current densities at the Si photoelectrode.

X-ray photoelectron spectroscopy (XPS) was performed using an M-Probe Surface Spectrometer (Surface Science Instruments (Fisons)). The instrument was maintained at a base pressure of $5x10^{-10}$ torr. XP spectra were taken by exciting electrons with Al Kα (1486.6 eV) X-rays and collecting data with a hemispherical analyzer. Data collection and analysis of the oxide thickness were performed with the M-Probe package software, version 3.4.

The silicon oxide posts were fabricated in the Microdevice Laboratory at the NASA Jet Propulsion Laboratory (JPL), Pasadena, CA, using standard photolithography methods. A silicon dioxide layer was first grown at ≈1000°C on a 1.6 Ω-cm resistivity, (100)-oriented n-type Si wafer (Silicon Sense; Nashua, NH) using an electric furnace that contained a water-saturated oxygen atmosphere. The oxidized silicon wafers were then spin-coated with

AZ5214-E photoresist on a Headway Research spin-coater at 4500 RPM for 40 seconds. The coated wafers were then baked at 95°C for 2 minutes. A chromium-patterned quartz mask, which had been prepared prior to the Si oxide growth steps, was used to expose line patterns in the photoresist. To expose the patterns, a coated wafer and the mask were placed in a Karl Suss MJB3 mask aligner and exposed to UV light for 45 seconds. The photoresist was developed in AZ 400K developer (20% by volume in water) for 30 seconds to remove the exposed areas of the photoresist. The patterned wafers were then etched for 2 minutes in buffered 10% HF(aq) to remove the exposed oxide areas, and the wafers were rinsed in acetone to remove the photoresist. Scanning electron microscopy (SEM) and profilometery were then used to characterize the final structure, which consisted of posts 150 nm in height and 100 μm in width that were separated by a center-to-center distance of 500 μm.

For the long-term corrosion experiments, the wafer was cut into ~1 cm^2 pieces. Each piece was then marked on the back for identification, weighed on a Sartorius model 2462 scale (±0.1 mg), etched in a 9:1 by volume H_2O:buffered HF (40/20/5 vol% NH_4F/49%HF/H_2O from Transene Co. Rowley, MA) solution for 20 seconds, rinsed with H_2O, rinsed with CH_3OH, and dried under a stream of N_2(g). The height of the oxide posts was then determined by profilometry using a Sloan-Dektak model 3030 profilometer (± 1 nm). The specimens were then transferred into the N_2 flush tank and were immersed into their respective test solution. Samples were removed from the solutions at 4 days, 47 days, and 116 days after immersion, rinsed with methanol, dried under N_2(g), and weighed. Each sample was then etched with buffered HF, rinsed with H_2O, rinsed with CH_3OH, and dried under N_2(g), after which profilometry data were taken to determine the extent of etching.

III. RESULTS

A. Current Density *vs.* Voltage Data for Si/CH_3OH-$Me_2Fc^{+/0}$ Contacts

An anodic dissolution process leading to active corrosion of Si should result in the presence of a non-zero short circuit current density, and a non-zero open circuit voltage, for Si/CH_3OH-$Fc^{+/0}$/Pt cells in the dark. To investigate this possibility, J-V data have been obtained in the nearly complete absence of band-gap illumination for n-Si and p-Si surfaces in contact with the electrolytes of concern.

Figure 1 displays the J-V characteristics for a 2 Ω-cm resistivity, (100)-oriented, n-type Si sample in contact with CH_3OH-1.0 M $LiClO_4$-0.10 M Me_2Fc-0.020 M Me_2FcBF_4. The open circuit voltage was -2 mV, and the short circuit current density was $(7\pm2)\times10^{-4}$ mA-cm^{-2}. These very small non-zero V_{oc} and J_{sc} values presumably arose from effects of stray light entering the system. The limiting reverse bias current density was on the order of 0.05 mA-cm^{-2}. This value was somewhat variable from electrode to electrode and was presumably dominated by the defect density, stray illumination, and/or edge effects of the crystal/liquid contact. Nevertheless this sets an upper limit on any electrochemically active corrosion process.

Figure 2 displays the J-V characteristics for a 0.68 Ω-cm resistivity, (100)-oriented p-type Si sample in the same solutions. The J-V characteristic was nearly ohmic and to within experimental error had an intercept at the origin. This type of behavior is consistent with the low barrier height value that had been estimated previously for p-Si/CH_3OH-$Me_2Fc^{+/0}$ contacts.[16] Thus, neither the n-type nor p-type samples displayed significant open circuit voltages or short circuit current densities in the dark. Assuming a 4-electron decomposition process and a maximum corrosion current of 0.05 mA-cm^{-2},

Figure #1 Dark J-V characteristics for a 2 Ω-cm resistivity, (100)-oriented, n-type Si sample in contact with CH_3OH-1.0 M $LiClO_4$-0.10 M Me_2Fc-0.020 M Me_2FcBF_4. The open circuit voltage was -2 mV, and the short circuit current density was $(7\pm2)\times10^{-4}$ mA-cm^{-2}. The limiting reverse bias current density was on the order of 0.05 mA-cm^{-2}.

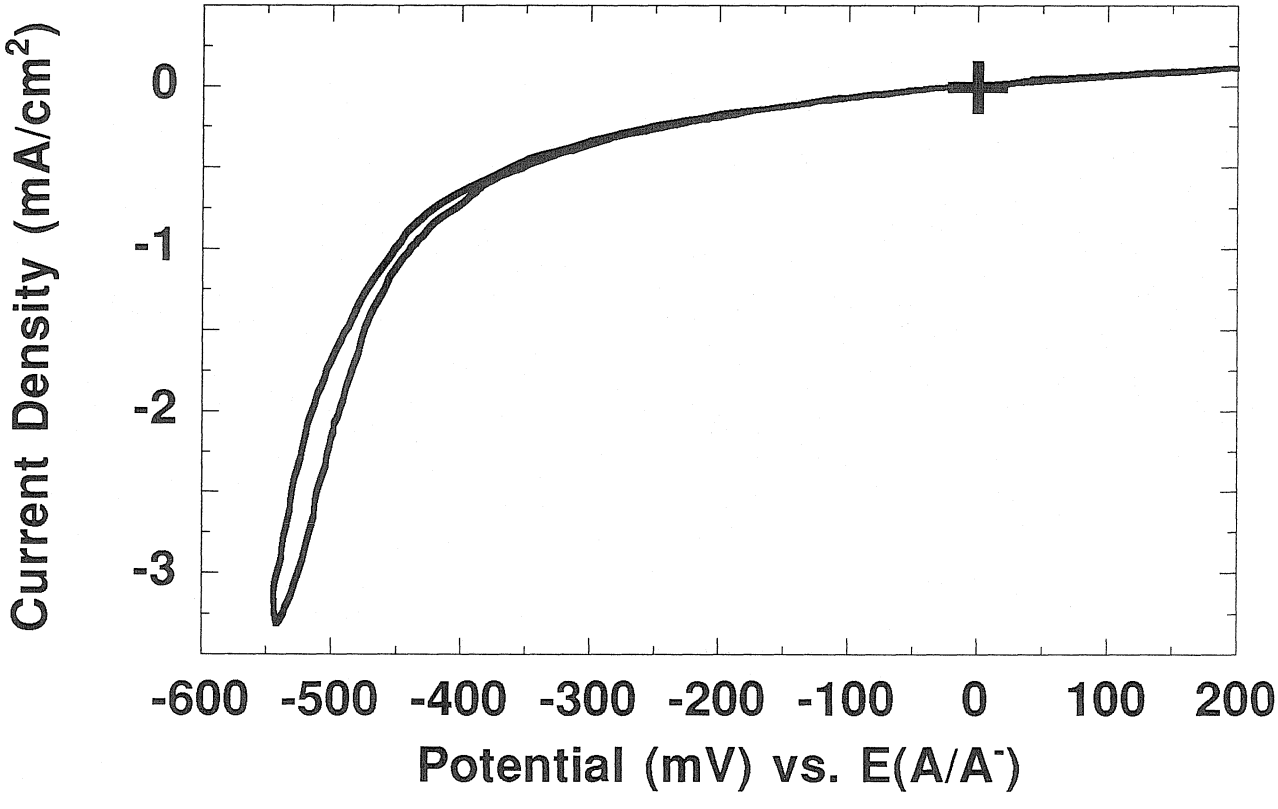
Current Density (mA/cm^2)
0
-1
-2
-3
-600
-500
-400
-300
-200
-100
0
100
200
Potential (mV) vs. E(A/A$^-$)

Figure #2 Dark J-V characteristics for a 0.68 Ω-cm resistivity, (100)-oriented p-type Si sample in contact with CH_3OH-1.0 M $LiClO_4$-0.10 M Me_2Fc-0.020 M Me_2FcBF_4. The J-V characteristic was nearly ohmic, and to within experimental error (±2 mV) had an intercept at the origin.

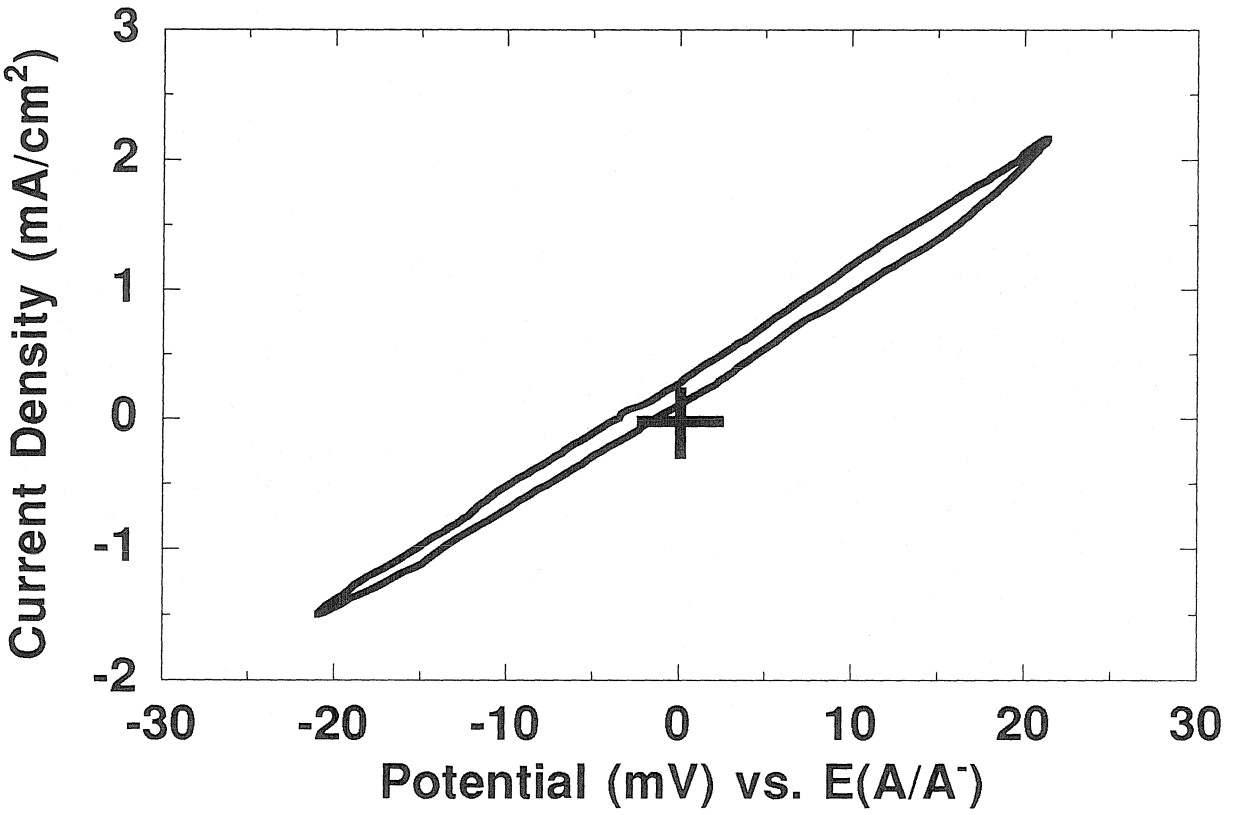
Current Density (mA/cm²)
3
2
1
0
-1
-2
-30
-20
-10
0
10
20
30
Potential (mV) vs. E(A/A⁻)

an upper limit of 0.015 nm-s^{-1} can be placed on the electrochemically detectable corrosion process of Si in these electrolytes.

B. Physical Measurements of Corrosion: Weight Loss and Profilometry Data for n-Si/CH_3OH-$Me_2Fc^{+/0}$ and n-Si/CH_3OH-$Fc^{+/0}$ Contacts in the Presence and Absence of Illumination

Another series of experiments was performed to search for any physically detectable corrosion of the Si surface. In addition to the traditional criterion of bulk weight loss of the crystal,[17] we have performed more sensitive measurements through the use of lithographically defined surface structures. These structures have allowed investigation of corrosion in the nm-thickness regime, as opposed to weight loss measurements, which generally are only accurate to thickness changes of ~1-10 μm.[18]

Figure 3 contains a scanning electron microscope photograph of a typical sample used for this study. Standard Si lithographic processing methods[19] were employed to produce a series of "posts," consisting of SiO_2, which were deposited onto the Si surface (Figure 4). SiO_2 is insoluble in CH_3OH, so under our conditions, corrosion under the posts was blocked. In addition, previous X-ray photoelectron spectroscopic (XPS) work[5] and current-density *vs.* voltage studies[1,5] have shown that Si itself does not passivate either in the dark or under illumination in contact with n-Si/CH_3OH-$Me_2Fc^{+/0}$ solutions under anaerobic conditions. Thus, if the Si were actively corroding in contact with the CH_3OH-$Me_2Fc^{+/0}$ or CH_3OH-$Fc^{+/0}$ electrolyte, sustained removal of Si through etching would occur in the regions not covered by the oxide posts (Figure 4C). After removal of these posts by etching the oxide in HF (Figure 4D), any etching of the Si from exposure to the methanolic solutions would be readily detectable through

Figure #3 A scanning electron microscope photograph of a typical "post-referenced" Si sample used for this study. The white lines are the SiO_2 posts and the dark regions indicate the underlying silicon wafer. Standard Si lithographic processing methods were employed to produce this series of SiO_2 "posts" that were 150 nm high, 100 μm wide and were separated by a 500 μm center-to-center distance on the Si wafer.

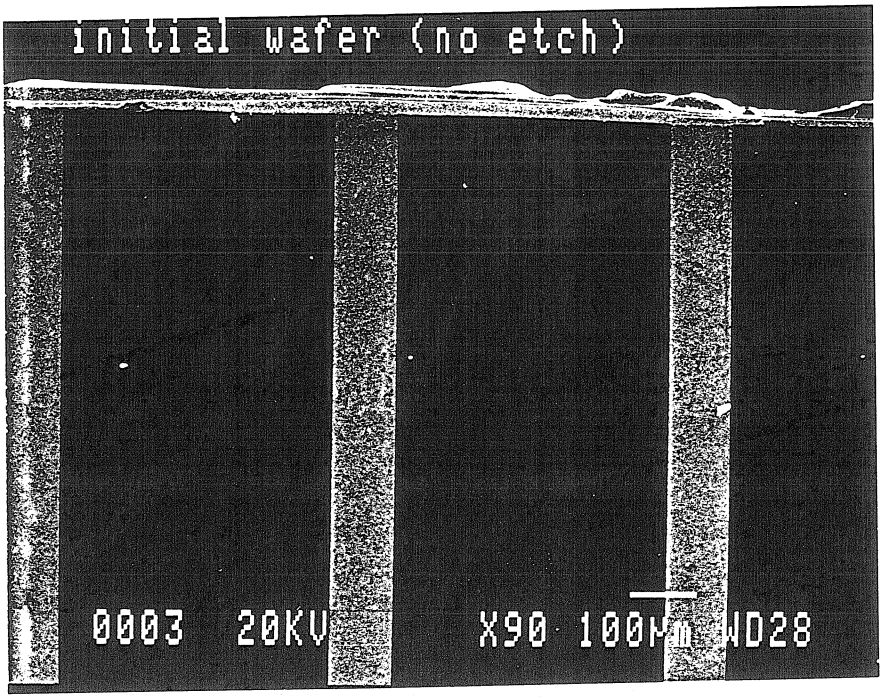
initial wafer (no etch)
0003 20KV X90 100µm WD28

Figure #4 Schematic of the fabrication procedure for the SiO_2 structures used in this study. A) The photoresist was spin-coated onto the wafer, exposed, and developed to expose areas of oxide. B) The exposed oxide was removed by etching in HF. C) Samples were exposed to methanolic solutions, with the oxide protecting the areas underneath the posts from corrosion. D) Removal of the oxide and subsequent profilometry revealed the extent of silicon etching. Note that the size of the surface features is not to scale in this schematic diagram.

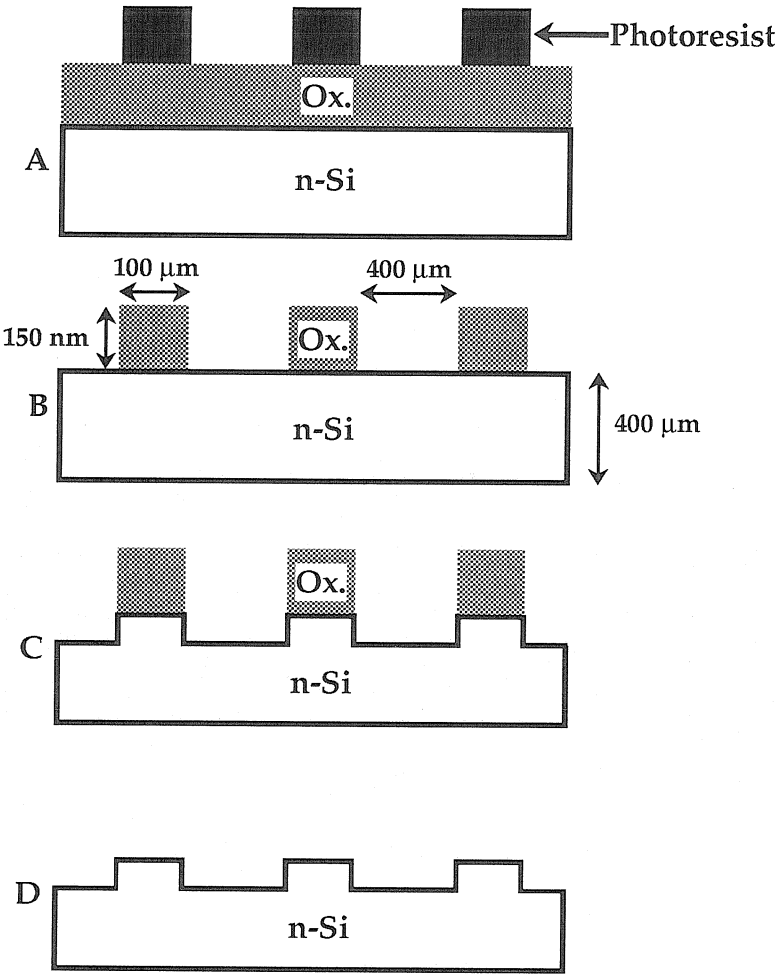
Photoresist
Ox.
A
n-Si
100 μm
400 μm
150 nm
Ox.
B
n-Si
400 μm
Ox.
C
n-Si
D
n-Si

profilometry measurements of height differences between the protected and unprotected regions of the specimen.

Initial attempts to quantify the Si corrosion rate were performed using the "post-referenced" Si specimens in a CH_3OH containing photoelectrochemical cell that had either $Me_2Fc^{+/0}$ or $Fc^{+/0}$ as the active redox couple. In one initial experiment, 380 C of photogenerated anodic charge was passed at short circuit through an n-Si/CH_3OH-1.0 M $LiClO_4$-0.20 M Me_2Fc-0.0020 M Me_2FcBF_4 contact. This amount of charge represented 130% of the total charge that would be required to entirely corrode this particular Si specimen, assuming a 4-electron/Si atom decomposition process to produce the Si(IV) oxidation state. No evidence for etching of the Si electrode was observed from profilometry measurements of these samples. The lack of height change established an upper limit on the etch rate of $< 9x10^{-5}$ nm-s^{-1}. In a separate experiment, 48 C of photocurrent was passed through an n-Si/CH_3OH-1.0 M $LiClO_4$-0.030 M Fc-0.0050 M $FcBF_4$ contact. Profilometry measurements without removal of the oxide posts showed no evidence of active corrosion. Subsequent XPS analysis of this electrode showed significant unoxidized Si still near the surface, as demonstrated by the detection of a prominent peak for substrate Si, with the bulk Si-[Si(2p)] to SiO_2-[Si (2p)] peak ratio corresponding to less than 1 nm of average oxide coverage over the entire specimen.

More sensitive corrosion experiments in the absence of illumination were then undertaken with these structures according to a strict double-blind experimental protocol. One co-worker prepared several samples that contained oxide posts, and another labelled and partitioned the samples into four groups. The sample groups were then sealed in jars in a N_2(g) flush box (O_2 concentrations <10 ppm). In this protocol, specimens were grouped as

follows: 1) three samples were established as a control group in N_2, 2) six samples were immersed in CH_3OH-1.0 M $LiClO_4$ solution, 3) six samples were immersed in CH_3OH-1.0 M $LiClO_4$-100 mM Me_2Fc-80 mM Me_2FcBF_4 solution, and 4) six samples were immersed in CH_3OH-1.0 M $LiClO_4$-30 mM Fc-80 mM $FcBF_4$. After elapsed times of 4 days, 47 days and 116 days, selected samples were removed from the solutions, rinsed with CH_3OH and dried in N_2. These samples were then prepared for analysis, and appeared identical except for an identification code that had been scribed onto the back side of the sample. A co-worker with no knowledge of the sample histories weighed the samples, etched away the oxide posts in buffered HF(aq), and then performed profilometry measurements to determine whether the samples had been etched. The data were then correlated with the sample history by simultaneous disclosure between the two parties. Sample chips generally yielded ~50 profilometry determinations of the etch pit depth for each specimen (~15 data points per scan, with scans being performed near the top, middle, and bottom of each specimen). The multiple etch pit determinations for a given specimen were used to establish a mean and standard deviation for the possible corrosion rate of the sample.

No weight change was detected (± 0.5 mg) for any sample. For the longest duration runs, this lack of weight change established an upper limit on the active corrosion rate of 1×10^{-4} nm-s^{-1}. More precise corrosion rates were obtained from the profilometry measurements. No etching was detected at 4 days, whereas at 47 days of exposure to the electrolyte pits of ~22 nm and ~45 nm were detected for n-Si/CH_3OH-$Me_2Fc^{+/0}$ and n-Si/CH_3OH-$Fc^{+/0}$ contacts, respectively. Table I summarizes the results of the profilometry measurements for the samples exposed to the various solutions for the 116 day period. A 10 nm etch pit was estimated as the detection limit

Table #1 Each entry represents the mean and standard deviation of a profilometry scan of different portions of the sample, with the number of determinations given in the adjacent column. The measurements on all samples did not change significantly after extended etching in HF, indicating that the oxide posts were completely removed and that the pit depths indicated corrosion of the silicon. Since the data did not change significantly after extended HF etching, values from all HF-etched specimens were used to calculate the etch rate in a particular solution. The mean of the mean pit depths for each scan was then used as a measure of the average corrosion rate for each piece.

Solution	Sample #	Etch time of posts by HF	# of measurements	Average pit depth across sample mean ± s (nm)
1.0 M $LiClO_4$-CH_3OH	IV	2 min	-	< 10
1.0 M $LiClO_4$-CH_3OH	VIII	2 min	-	< 10
1.0 M $LiClO_4$-CH_3OH	X	2 min	-	< 10
1.0 M $LiClO_4$-CH_3OH	II	1 min	14	72±16
80/100 mM $Me_2Fc^{+/0}$		1 min	12	67±3
		1.5 min	12	67±3
		1.5 min	12	67±3
Mean				68±2
1.0 M $LiClO_4$-CH_3OH	IX	1 min	9	70±4
80/100 mM $Me_2Fc^{+/0}$		1 min	14	66±4
		1 min	8	64±5
		1.5 min	10	68±4
		1.5 min	10	68±4
Mean				67±2
1.0 M $LiClO_4$-CH_3OH	XVII	1.5 min	10	63±2
80/100 mM $Me_2Fc^{+/0}$		1.5 min	10	67±1
		1.5 min	10	67±3
		2 min	10	66±2
		2 min	12	59±3
Mean				64±3

1.0 M $LiClO_4$-CH_3OH	I	1.5 min	10	110±3
80/30 mM $Fc^{+/0}$		1.5 min	10	112±6
		1.5 min	9	110±6
		2 min	12	111±4
		2 min	12	108±5
Mean				110±1
1.0 M $LiClO_4$-CH_3OH	VII	1.5 min	12	119±6
80/30 mM $Fc^{+/0}$		1.5 min	14	123±4
		1.5 min	10	122±6
		2 min	10	126±8
		2 min	12	119±8
Mean				122±3
1.0 M $LiClO_4$-CH_3OH	XVIII	1.5 min	10	173±3
80/30 mM $Fc^{+/0}$		1.5 min	10	188±4
		1.5 min	12	152±8
		2 min	12	178±5
		2 min	12	154±10
Mean				169±16

of our setup, based on the variation in height (from the profilometry data) of an uncorroded, HF-etched, "post-referenced" Si wafer. The data in Table I therefore established an upper limit of the corrosion rate of silicon in contact with CH_3OH-1.0 M $LiClO_4$ solutions as $1x10^{-6}$ nm-s^{-1} of Si. Assuming a constant corrosion rate over the lifetime of the wafer, these data imply that a typical 400 μm thick Si wafer would not be completely etched after >12,000 years in this electrolyte. The mean corrosion rates for n-Si/CH_3OH-$Me_2Fc^{+/0}$ contacts were $(6.8\pm0.2)x10^{-6}$ nm-s^{-1}, $(6.7\pm0.2)x10^{-6}$ nm-s^{-1}, and $(6.4\pm0.3)x10^{-6}$ nm-s^{-1} for samples II, IX, and XVII respectively. The mean corrosion rates for n-Si/CH_3OH-$Fc^{+/0}$ contacts were $(11.0\pm0.1)x10^{-6}$ nm-s^{-1}, $(12.2\pm0.3)x10^{-6}$ nm-s^{-1}, $(16.9\pm1.6)x10^{-6}$ nm-s^{-1} for samples I, VII, and XVIII respectively. Assuming a corrosion stoichiometry of 4 electrons/Si atom, the highest observed corrosion rate of $(16.9\pm1.6)x10^{-6}$ nm-s^{-1} would correspond to a corrosion current density of $5.4x10^{-11}$ mA-cm^{-2}. These data indicate that even for the most active corrosion processes detected in these experiments (sample #18), the failure of a 400 μm thick Si wafer from active corrosion would require 750 years.

IV. DISCUSSION

The data presented herein indicate that n-Si samples are extraordinarily stable in all of the electrochemical and photoelectrochemical environments evaluated. No evidence for significant corrosion was found during extended duration experiments either in the dark or under illumination. Additionally, the electrochemical data described above indicate that prior photoelectrochemical J-V measurements[1-5,10,15] are not confounded by the presence of significant corrosion currents. Using sensitive assays for etch-induced changes in the near-surface topography, direct measurements of

the corrosion rates of n-Si/CH_3OH-$Me_2Fc^{+/0}$ and n-Si/CH_3OH/$Fc^{+/0}$ contacts were only possible when high concentrations of the oxidized forms of the redox species (80 mM) were present in extended duration experiments. Even under these forcing conditions, which contained significantly higher concentrations of oxidant than that used in prior SECM experiments (80 mM Fc^+ in the corrosion measurements *vs.* 4.6 mM Fc^+ in the SECM experiments), the corrosion rates were insignificant for most applications using typical wafer thicknesses on reasonable laboratory timescales. All of the measurements reported herein were, therefore, consistent with the body of prior data which indicated that these systems offer stable, durable photoelectrochemical cells.[1-5,10,15]

Based on the experiments described above, the lifetime of an operating n-Si/CH_3OH-$Me_2Fc^{+/0}$ cell is almost certainly limited by passivation due to silicon oxide formation, as opposed to being limited by active corrosion processes of the Si electrode. Given the low values for the corrosion rate and the correspondingly long stability times inferred from the corrosion data, decomposition of the electrolyte, decomposition of the redox couple, and/or mechanical seal failure are more likely to limit the operational lifetime of an operating n-Si photoelectrochemical cell[1] than is active corrosion of the Si electrode. In this respect, the previously reported operation of a Si-based photoelectrochemical cell for over one month of continuous air-mass 1.0 simulated illumination attests to the impressive stability of semiconductor/liquid contacts in properly designed nonaqueous electrolytes.[1]

It is also possible to explain the apparently anomalous SECM feedback data in view of the data presented herein. In the SECM experiment, the tip current increased as the tip-sample distance was decreased.[12] If the substrate were an electrical conductor, increases in feedback current should be observed

as the tip/sample distance is decreased, and the observed SECM current *vs.* distance behavior would not be anomalous or indicative of corrosion processes.[20] Alternatively, if the substrate were an insulator, Fc^+ under the tip could not equilibrate with Fc in the bulk of the solution, so the feedback current should decrease as the tip sample distance is decreased. The observed increase in current as the SECM tip approached the sample, along with the assumption of a substrate that was insulating to faradaic current flow, were therefore taken to indicate an active corrosion process.[12]

Recent electrical studies, however, have shown that the n-Si/CH_3OH-$Me_2Fc^{+/0}$ and n-Si/CH_3OH-$Fc^{+/0}$ contacts are in strong inversion at equilibrium, with barrier heights of ≈1.0 eV.[21-23] Such a high barrier height at a Si/liquid contact must produce significant, mobile, minority carriers in the near-surface region of the solid, and these mobile carriers will be able to support faradaic charge flow parallel to the solid/liquid contact. In fact, the theoretically predicted current pathway parallel to the solid/liquid contact has recently been detected directly using a transconductance method, in which minority carrier current flow with a near-surface resistivity of only ~0.2 Ω-cm was detected through impedance measurements from implanted p^+ contacts in the near-surface region of an n-type Si/CH_3OH-$Fc^{+/0}$ contact.[21] In the SECM experiment, these mobile minority carriers will facilitate equilibration of any Fc^+ generated under the tip with Fc in the unperturbed portions of the electrode/liquid contact. In other words, although the n-Si/CH_3OH-$Me_2Fc^{+/0}$ interface is rectifying to current flow perpendicular to the solid/liquid contact, it is a conductor with respect to current flow parallel to the solid/liquid contact. Since current flow parallel to the surface is the important pathway for generating feedback current in the SECM experiment, the SECM data actually confirm the presence of an inversion layer at the

n-Si/CH_3OH/$Me_2Fc^{+/0}$ contact, as opposed to indicating the presence of an active corrosion process that generates an unknown, highly CH_3OH-soluble, Si(IV) species. Thus, the SECM configuration provides an experimentally convenient, though qualitative, probe for the presence of carrier inversion and is complementary to the quantitative transconductance measurements described in the recent literature[21] for investigating this aspect of the energetics of semiconductor/liquid contacts.

Without further information on the nature of the electrode surface before and after the SECM experiments and in view of the lack of significant corrosion determined herein, it is only possible to speculate about the origin of the 1 μm "pit" that was reported in the SECM studies. The presence of a corrosion "pit" was inferred from a decreased feedback current in the region of the SECM experiment after maintaining the tip at a fixed position for 15 minutes.[12] This decrease in current could also be produced by any other phenomenon that disturbs the ability to obtain electrochemical feedback in the SECM geometry. A likely explanation for the decline in tip current is oxidation of the Si surface in the region under the tip. Prior electrochemical studies have shown that silicon will form a passivating oxide under band gap illumination in alcohol solvents at low concentrations of redox donor species.[15] Under the SECM conditions, the ferrocene in the region of the tip was converted at a mass-transport-limited rate to Fc^+, depleting the Fc donor that is required to compete with oxidation of the Si. Oxide formation would increase the resistance of the Si to faradaic current flow parallel to the solid/liquid contact, and would therefore produce the observed decrease in local SECM tip current. Other explanations, such as perturbations in the steady state concentration profile of redox species in the region of the tip, also cannot be ruled out without direct information on the surface condition of

the Si specimen before and after the SECM experiment. Nevertheless, local passivation seems the most likely explanation, given the other information on the behavior of Si/CH_3OH contacts and the stability data of these contacts described herein.

In summary, the active corrosion rates of silicon in contact with CH_3OH-$Fc^{+/0}$ or CH_3OH-$Me_2Fc^{+/0}$ electrolytes are exceedingly small. These corrosion rates are sufficiently low that they do not affect prior interpretations of the J-V behavior of these contacts, and the low corrosion rates validate earlier claims concerning the stability of n-Si/CH_3OH-$Me_2Fc^{+/0}$ and n-Si/C_2H_5OH-$Fc^{+/0}$ contacts for photoelectrochemical energy conversion applications. The observation of "anomalous" feedback current in an SECM experiment of these contacts is validation of prior evidence for the presence of a conductive inversion layer in the near-surface region of these Si electrodes, and does not arise from a diffusion-limited chemical reaction with ferrocenium that produces a soluble Si(IV) species and corrodes the Si electrode.

Acknowledgments:

I would like to acknowledge the experiments and help of co-workers Kathy E. Pomykal, and Christoph D. Karp in the work reported in this chapter.

V. REFERENCES

(1) Gibbons, J. F.; Cogan, G. W.; Gronet, C. M.; Lewis, N. S. *Appl. Phys. Lett.* **1984**, *45*, 1095.

(2) Rosenbluth, M. L.; Lieber, C. M.; Lewis, N. S. *Appl. Phys. Lett.* **1984**, *45*, 423.

(3) Gronet, C. M.; Lewis, N. S.; Cogan, G.; Gibbons, J. *Proc. Natl. Acad. Sci., USA* **1983**, *80*, 1152.

(4) Rosenbluth, M. L.; Lewis, N. S. *J. Am. Chem. Soc.* **1986**, *108*, 4689.

(5) Tufts, B. J.; Kumar, A.; Bansal, A.; Lewis, N. S. *J. Phys. Chem.* **1992**, *96*, 4581.

(6) Fantini, M. C. A.; Shen, W. M.; Tomkiewicz, M.; Gambino, J. P. *J. Appl. Phys.* **1989**, *66*, 2148.

(7) Shen, W.-M.; Fantini`, M. C. A.; Tomkiewicz, M.; Gambino, J. P. *J. Appl. Phys.* **1989**, *66*, 1759.

(8) Chazalviel, J.-N. *Electrochim. Acta* **1990**, *35*, 1545.

(9) Kobayashi, H.; Chigami, A.; Takeda, N.; Tsubomura, H. *J. Electroanal. Chem.* **1990**, *287*, 239.

(10) Kobayashi, H.; Takeda, N.; Sugahara, H.; Tsubomura, H. *J. Phys. Chem.* **1991**, *95*, 813.

(11) Bruckenstein, S.; Rosamilia, J. M.; Miller, B. *J. Phys. Chem.* **1985**, *89*, 677.

(12) Horrocks, B. R.; Mirkin, M. V.; Bard, A. J. *J. Phys. Chem.* **1994**, *98*, 9106.

(13) Bocarsly, A. B.; Walton, E. G.; Wrighton, M. S. *J. Am. Chem. Soc.* **1980**, *102*, 3390.

(14) Fonash, S. J. *Solar Cell Device Physics*; Academic: New York, 1981.

(15) Legg, K. D.; Ellis, A. B.; Bolts, J. M.; Wrighton, M. S. *Proc. Natl. Acad. Sci.* **1977**, *74*, 4116.

(16) Lewis, N. S. *J. Electrochem. Soc.* **1984**, *131*, 2496.

(17) Parkinson, B. *Acc. Chem. Res.* **1984**, *17*, 431.

(18) A weight loss error of ± 0.2 mg would correspond to $\pm 9 \times 10^{-5}$ cm^{-3} of Si, implying a thickness error of ± 1 μm for a sample area of 1.0 cm^2.

(19) Wolf, S.; Tauber, R. N. *Silicon Processing for the VLSI Era*; Lattice Press: Sunset Beach, 1986.

(20) Kwak, J.; Bard, A. J. *Anal. Chem.* **1989**, *61*, 1221.

(21) Laibinis, P. E.; Stanton, C. E.; Lewis, N. S. *J. Phys. Chem.* **1994**, *98*, 8765.

(22) Kumar, A.; Lewis, N. S. *Appl. Phys. Lett.* **1990**, *57*, 2730.

(23) Farardo, A.M.; Karp, C.D.; Kenyon, C.N.; Pomykal, K.E.; Shreve, G.A.; Tan, M.X.; Lewis, N.S. *Sol. Energy Mater.* in press.

Chapter Four

An Analytical Description of the Consequences of Abandoning the Principles of Detailed Balance and Microscopic Reversibility in Semiconductor Photoelectrochemistry

ABSTRACT

Key differences between the conventional and "irreversible" models of semiconductor photoelectrochemistry are identified and discussed within the framework of experimental observations. Conceptual differences between these two models appear to lie in the treatment of interfacial charge transfer processes for photogenerated charge carriers. The conventional model utilizes detailed balance principles to obtain rate constant relationships for all interfacial charge transfer events at semiconductor/liquid contacts and uses the principle of microscopic reversibility to evaluate these rate constants for situations away from equilibrium. In contrast, the irreversible model postulates that local statistical detailed balance does not apply to charge transfer events in photoelectrolysis, and that such charge transfer events are highly irreversible, like photoemission into a vacuum. It is shown analytically that the two models predict differences in the behavior of the available free energy produced by a photoelectrochemical cell at a fixed incident light intensity. The conceptual implications of these differences are evaluated analytically and are also compared to experimental results for semiconductor/liquid junctions.

I. INTRODUCTION

Renewed interest in the photoelectrochemistry of metal oxides, for applications in waste water treatment and photochemical energy

conversion,[1-5] has focused attention on the various theoretical models for charge transfer at semiconductor/liquid interfaces. The conventional model for semiconductor/liquid contacts[6-19] has closely followed that developed in the solid state literature,[20-23] and has utilized the principles of detailed balance and microscopic reversibility to derive an analytical formalism for the behavior of semiconducting photoelectrodes. An alternative proposal suggests that the principle of detailed balance does not apply to water photoelectrolysis, and that charge transfer reactions in semiconductor photoelectrolysis processes are highly irreversible.[24-26] The purpose of this chapter is to examine analytically some of the differences between these two treatments, and to identify the experimental and conceptual consequences of these two different models.

This work addresses our understanding of the conventional, statistical model, and its applicability to semiconductor photoelectrochemistry. We have also attempted to identify the means by which the conventional model might be modified in order to formulate a conceptually different model for photoelectrochemistry that is in accord with the stated postulates of the "irreversible" model. It is our hope that by clearly re-elucidating the equations for the conventional, statistical model, and the changes required therein to formulate a distinct model for photoelectrochemistry, proponents of the "irreversible" model will be able to clarify, in an analytical treatment, what predictions the "irreversible" model makes that are different than the conventional model. This will also enable an analytical identification of how those predictions would affect the observables (*e.g.*, the voltage, current, or quantum yield) in the operation of a photoelectrochemical cell, while maintaining a physically justifiable treatment of charge transfer processes at solid/liquid interfaces.

II. THEORETICAL FRAMEWORK

A. Basic Assumptions of the Conventional Model for Photoelectrochemistry

We first consider the conventional model for photoelectrochemistry, originally described by Gerischer[11-14] and widely adopted throughout the literature.[6-19,27-35] The equations of this model have recently been re-cast into a simplified form for the purposes of elucidating basic issues in the kinetics of water photoelectrolysis.[6,7] This simplified form is expanded analytically herein, including some aspects of the minority carrier kinetics that were implicit in the prior treatment.

1. Conditions in the Dark

a. Charge Transfer Rate Constant Relationships at Equilibrium: Use of the Principle of Detailed Balance

When placed in contact with an electrolyte solution, a semiconductor of band gap energy E_g, of bulk free carrier density n_b, with a density of states in the conduction band $N_c(E)$ ($N_v(E)$ in the valence band), and with energies at the solid/liquid contact of E_{cb} for the bottom of the conduction band and E_{vb} for the top of the valence band, will undergo interfacial charge transfer until equilibrium is reached. At equilibrium, the Fermi level, E_f, in the semiconductor equals the electrochemical potential of the solution, $E(A/A^-)$. The removal of charge from a nondegenerate n-type semiconductor will produce a depletion region near the solid/liquid contact, and will produce a barrier height, $\phi_b = (1/q)(E(A/A^-) - E_{cb})$ of the junction.[8,22,23] The electric

potential gradient in the solid will result in a reduced equilibrium electron concentration, n_{so}, at the solid/liquid interface.

To describe the current flow at this interface, we will first consider electron exchange through the conduction band. Electron flow from the solid to the liquid can be characterized by an interfacial charge transfer rate constant, $k_n(E)$ (See Figure 1). This rate constant $k_n(E)$ will, in general, have a different value at every possible electron energy, E. This rate constant, with units of $cm\text{-}s^{-1}\text{-}eV^{-1}$, implicitly incorporates the dependence of the charge transfer rate at every energy on the concentration of acceptors in the solution phase.[11,27,36] The resulting "forward" cathodic electron flux, $U_{n,f}$, is obtained by integrating the charge transfer rate at each energy over all possible electron energies in the conduction band:

$$U_{n,f} = \int_{E_{cb}}^{-\infty} k_n(E) n_s(E) dE \qquad [1]$$

where $n_s(E)$ is the surface electron concentration as a function of energy.

The reverse current for this set of charge transfer processes proceeds from the solution into the empty states of the conduction band of the solid. Taking the concentration of empty states in the solid as a constant, including it and the concentration dependence of solution species into the apparent interfacial charge transfer rate constant, yields:

$$U_{n,r} = \int_{E_{cb}}^{-\infty} k_n'(E) dE \qquad [2]$$

where $k_n'(E)$ is the rate constant for the process at each electron energy (in units of $cm^{-2}\text{-}s^{-1}\text{-}eV^{-1}$) and $U_{n,r}$ is the flux corresponding to the "reverse"

Figure #1 Representation of the interfacial kinetic processes in the conduction band of a semiconductor/liquid junction. The bottom of the conduction band at the solid/liquid contact has an energy $E = E_{cb}$. Multiplication of the electron concentration, $n_s(E)$, at every energy E (four energies, E_1,E_2,E_3,E_4, are shown) by the rate constant at each energy, $k_n(E)$, yields the rate of interfacial charge transfer at each electronic energy level of the system. The rate constant $k_n(E)$ implicitly incorporates the concentration of the acceptor states at energy E. At every energy there must also be a reverse rate constant, $k_n'(E)$, representing electron flow from the electrons in the solution at energy E into the empty states in the conduction band at this energy. At equilibrium, the forward charge transfer rate must equal reverse charge transfer rate at every energy E. The rate constant ratios for these processes determine the chemically reversible equilibrium constant, K(E), at each electronic energy E of the system. Although the situation is only shown for electrons in the conduction band, a similar situation occurs for holes in the valence band. Note that energies are on the electrochemical scale, with more positive values being further from vacuum and indicating more oxidizing species.

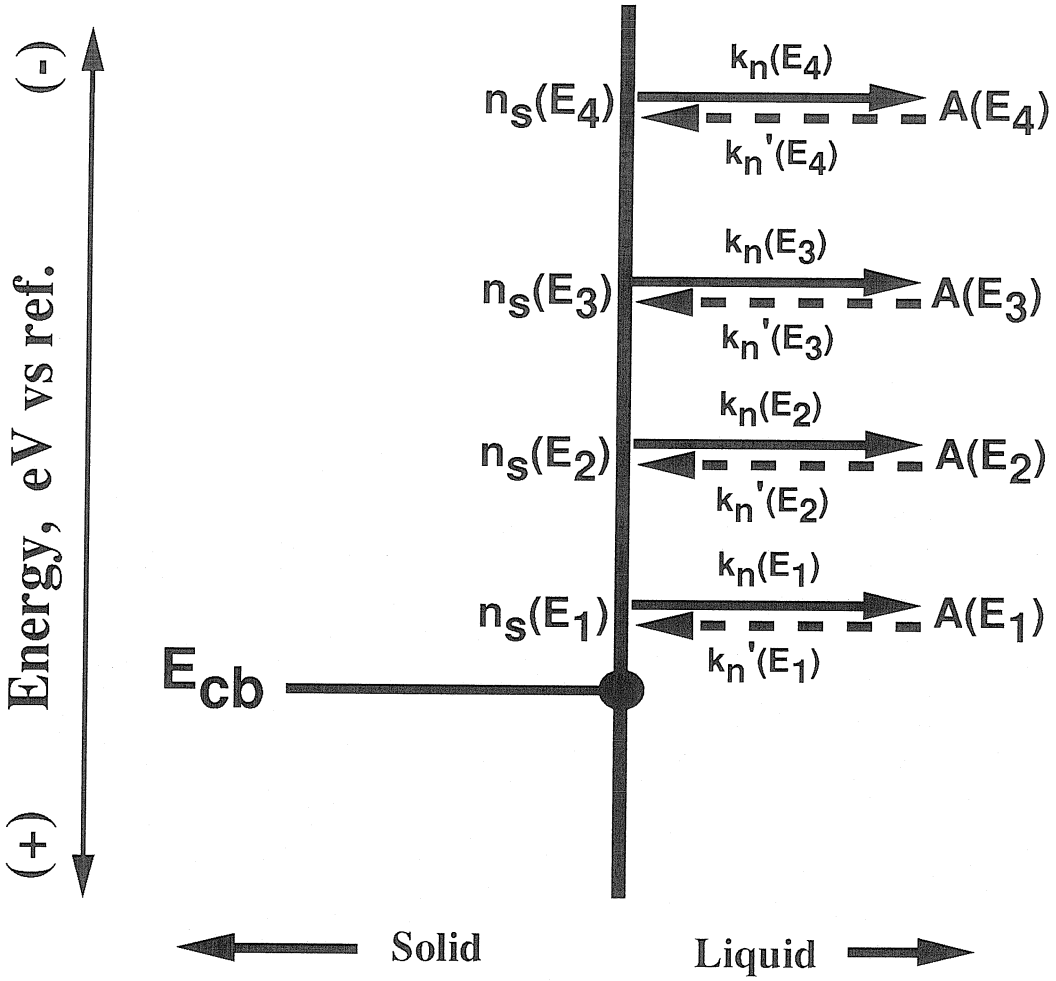
(-)
Energy, eV vs ref.
(+)
$k_n(E_4)$
$n_s(E_4)$
$A(E_4)$
$k_n'(E_4)$
$k_n(E_3)$
$n_s(E_3)$
$A(E_3)$
$k_n'(E_3)$
$k_n(E_2)$
$n_s(E_2)$
$A(E_2)$
$k_n'(E_2)$
$k_n(E_1)$
$n_s(E_1)$
$A(E_1)$
$k_n'(E_1)$
E_{cb}
Solid
Liquid

process of $U_{n,f}$. The net interfacial electron flux, $U_{n,tot}$, is thus:

$$U_{n,tot} = \int_{E_{cb}}^{-\infty} [k_n(E)n_s(E) - k_n'(E)]dE \qquad [3]$$

A similar equation can be obtained for the net hole flux across the interface through the valence band:

$$U_{p,tot} = \int_{E_{vb}}^{\infty} [k_p(E)p_s(E) - k_p'(E)]dE \qquad [4]$$

Here, $k_p(E)$ is the rate constant for hole transfer from the valence band energy E into the donor species in the solution, $p_s(E)$ is the hole concentration at the semiconductor surface at energy E, $k_p'(E)$ is the rate constant at energy E for the "reverse" process in which holes are injected from the solution species into the valence band of the solid, and $U_{p,tot}$ is the net interfacial hole flux.

At equilibrium, no net current can flow through the interface. Thus, we obtain:

$$U_{tot} = \int_{E_{vb}}^{\infty} [k_p(E)p_{so}(E) - k_p'(E)]dE - \int_{E_{cb}}^{-\infty} [k_n(E)n_{so}(E) - k_n'(E)]dE = 0 \qquad [5]$$

with $n_{so}(E)$ and $p_{so}(E)$ equal to the equilibrium electron and hole concentrations at the surface at energy E, respectively. The negative sign between the integrals arises from the sign conventions of Eqs. 3 and 4, in which a positive carrier flux of either electrons or holes designates a net flow of the appropriate carrier from the solid into the liquid.

To obtain the desired expressions for the interfacial kinetics, $k_n'(E)$ and $k_p'(E)$ must be related to other known parameters of the system. A key aspect of the conventional theory of semiconductor photoelectrochemistry is the assumption that charge transfer equilibrium will eventually be attained under any arbitrary condition of temperature, pressure, *etc.*[6-19] Within this

framework, each possible charge transfer pathway must separately have zero net flux at equilibrium, or else equilibrium could not be attained.[37] This is essentially a restatement of the principle of detailed balance.[6-11,13-19,37-39] Therefore, the charge transfer equilibration arising from current flow in the conduction band process can be treated separately from the equilibration being established due to current flow arising from the valence band, as long as both processes are included in the final equations describing the equilibrium state of the system. Thus, setting the net flux equal to zero in Eqs. 3 and 4 for every value of E yields the desired relationships between the forward and reverse charge transfer rate constants at each energy E:

$$k_n(E)\, n_{so}(E) = k_n'(E) \qquad \text{for } E_{cb} \geq E > -\infty \qquad [6]$$

and

$$k_p(E)\, p_{so}(E) = k_p'(E) \qquad \text{for } \infty < E \leq E_{vb} \qquad [7]$$

The quantities $n_{so}(E)$ and $p_{so}(E)$ are readily calculated from the Fermi distribution function if the density of states *vs.* energy in the solid is known. Thus, Eqs. 6 and 7 provide analytical expressions for the ratios $k_n(E)/k_n'(E)$ and $k_p(E)/k_p'(E)$ at every energy E of a semiconductor/liquid interface.

Although the energy dependence of the rate constants $k_n(E)$ and $k_p(E)$ have been derived originally by Gerischer[11,27,38] using the classical Marcus theory rate constant expressions for outer sphere electron transfer processes,[40,41] the specific functional form of $k_n(E)$ *vs.* E or of $k_p(E)$ *vs.* E is not needed for any of the analysis contained herein. As indicated by Eqs. 6 and 7, only the rate constant ratios $k_n(E)/k_n'(E)$ and $k_p(E)/k_p'(E)$ at each value of E are dictated by the principle of detailed balance. These ratios are thus all that

we will require to evaluate the key predictions of the conventional model for photoelectrochemistry.

b. Rate Constant Relationships For Thermalized Carriers at Equilibrium: Use of the Principle of Detailed Balance

Although the conventional model encompasses arbitrary electron and hole distributions in the solid, this model also allows a derivation of simpler rate constant expressions for the special case in which carriers are considered to be thermalized, *i.e.*, in which the electrons and holes each have an effective temperature equal to that of the surroundings. Figure 2 depicts the important energetic parameters and kinetic processes for interfacial transfer of thermalized charge carriers in a photoelectrochemical cell. For thermalized electrons, Eq. 3 simplifies to:

$$U_{n,tot} = k_n n_s - k_n' \qquad [8]$$

In other words, thermalized electrons leave the solid with an effective charge transfer rate constant k_n, and return to the solid with an effective rate constant k_n'. A similar equation can be obtained for the net flux of thermalized holes across the interface through the valence band:

$$U_{p,tot} = k_p p_s - k_p' \qquad [9]$$

This expression is the simplification of Eq. 4 for thermalized holes in the valence band.

The averaged charge transfer rate constant for thermalized electrons, k_n, is readily evaluated by considering that essentially only those carriers within $\approx$3kT of E_{cb} contribute to the charge transfer process. The thermalized electrons in the conduction band therefore exhibit a charge transfer rate

Figure #2 Representation of the four pathways for charge transfer through the semiconductor/liquid interface and the energetics for this system. The surface electrons (of total surface concentration n_s) and surface holes (of total surface concentration p_s) are assumed to be thermalized at the temperature of the lattice and thus react from the conduction bandedge energy, E_{cb}, and the valence bandedge energy, E_{vb}, respectively. The rate constant k_n is obtained from integrating the energy dependent rate constant, $k_n(E)$, over ≈3kT in energy, so that k_n represents the averaged charge transfer rate constant for most of the distribution of thermalized electrons in the conduction band of the solid. k_n' is the analogous rate constant for electron transfer from solution into the empty states of the conduction band. The hole transfer rate constant k_p is analogous to k_n, but has been averaged over ≈3kT around E_{vb} to account for the distribution of thermalized holes in the valence band. k_p' is the averaged rate constant for hole transfer from solution into the empty hole states in the valence band of the semiconductor. $E(A/A^-)$ is the electrochemical potential of the solution phase, $q\phi_b$ is the energy barrier for electron transfer into the semiconductor, and qV_n is the energy separation between the Fermi level, E_f, and the conduction bandedge in the bulk of the semiconductor.

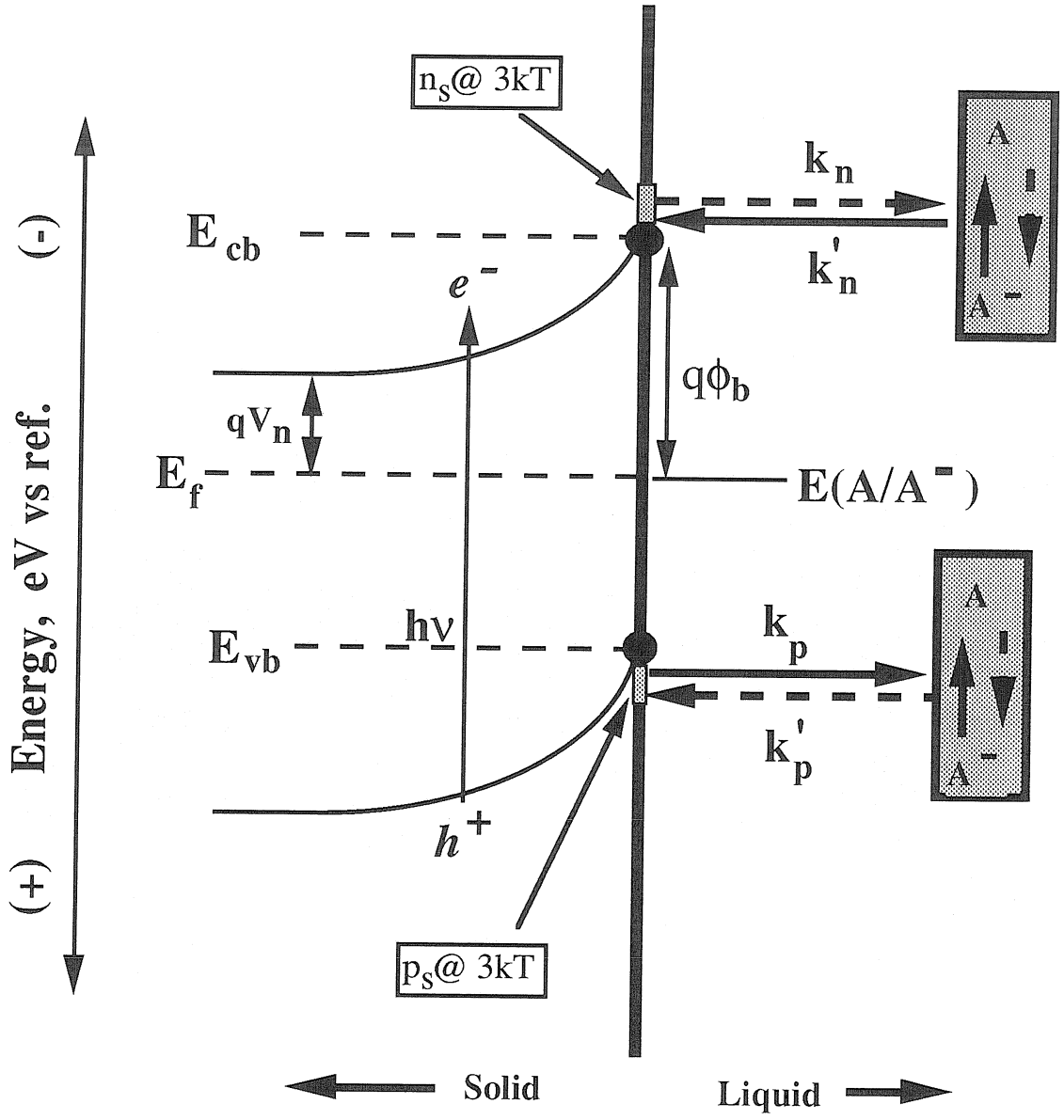
Energy, eV vs ref.
(-)
(+)
n_s@ 3kT
p_s@ 3kT
E_{cb}
E_f
E_{vb}
$E(A/A^-)$
qV_n
$q\phi_b$
$h\nu$
e^-
h^+
k_n
k'_n
k_p
k'_p
A
A^-
Solid
Liquid

constant in the framework of Eq. 1 as if they had an effective standard state energy of $E \approx E_{cb}$. For thermalized electrons in the conduction band of a nondegenerate semiconductor, the Boltzmann approximation can be used to evaluate the Fermi distribution function, *i.e.*, to evaluate n_{so} from $n_s(E)$. Thus, we obtain the well-known expression of:

$$n_{so} \approx N_c \exp[(E_{cb} - E(A/A^-))/kT]$$

for the surface electron concentration (in units of cm^{-3}), when the carriers are thermalized.

Applying detailed balance to the electron charge transfer rate constants for thermalized carriers at equilibrium therefore yields:

$$k_n n_{so} = k_n' \qquad [10]$$

The units of k_n are now $cm\text{-}s^{-1}$, because $k_n(E)$ has explicitly been integrated over the energy of the thermalized carrier distribution to obtain the effective value for the charge transfer rate constant. Thus, for thermalized electrons, the desired rate constant ratio is:

$$k_n'/k_n = N_c \exp[(E_{cb} - E(A/A^-))/kT])$$

Similar expressions can be obtained for the surface hole concentration, and for the effective hole transfer rate constant, for thermalized holes in the semiconductor valence band. The effective hole transfer rate constant for thermalized holes, k_p, is related to the equilibrium hole concentration at the surface by:

$$k_p p_{so} = k_p' \qquad [11]$$

This yields the following rate constant ratio:

$$k_p'/k_p = N_v \exp(E(A/A^-) - E_{cb} - E_g)/kT]$$

These expressions make sense because the electron transfer process through the conduction band takes place to reflect an equilibrium constant, $K_n = k_n/k_n'$, for exchange of thermalized electrons into and out of the solid. Thermalized electrons in the solid at energy E_{cb} are therefore in equilibrium with electrons from a liquid of energy $E(A/A^-)$, with a similar thermodynamic relationship for the valence band process.[6-19] Reference to the description above shows that the general expressions for an arbitrary carrier distribution, Eqs. 6 and 7, preserve this equilibrium constant relationship at every electronic energy level of the carrier distribution. The conventional model of photoelectrochemistry therefore yields simple, intuitive expressions for the charge transfer kinetics of thermalized charge carriers under equilibrium conditions, and also describes the relevant charge transfer kinetics for arbitrary electron energies of the system.

c. Charge Transfer Rate Constant Relationships Away From Equilibrium: Use of the Principles of Detailed Balance and Microscopic Reversibility

In order to obtain a description of current flow through the solid/liquid contact, the expressions derived above must be related to the charge transfer processes that occur away from thermal equilibrium. To make this linkage, the conventional model of photoelectrochemistry invokes the principle of microscopic reversibility, which states that elementary chemical transformations have the same values of their transition probabilities (*i.e.*, forward and reverse rate constants) at, and away from, equilibrium. If this

were not true, then for elementary rate processes, the equilibrium constant for an elementary chemical transformation, K, could not be related to the forward, k_f, and reverse, k_r, rate constants through the conventional expression $K = k_f/k_r$. The equivalent quantum mechanical statement is that the matrix elements for an elementary electronic transition are invariant regardless of whether equilibrium is established.[37] The principle of microscopic reversibility thus allows the rate constant ratios that have been obtained from the application of the principle of detailed balance at equilibrium to be applied to the interfacial kinetic processes that occur under non-equilibrium conditions.[21,37,42] This approach will rigorously describe the kinetics for an arbitrary distribution of electronic levels away from equilibrium provided that the correct distribution functions for reactants and products are included in the kinetic analysis.

We first treat the simple case of interfacial charge carrier flow from thermalized carrier distributions, and then generalize this approach to arbitrary carrier distributions. Since the expressions for $U_{n,tot}$ and $U_{p,tot}$ in Eqs. 8 and 9 are still valid, Eqs. 10 and 11 provide explicit expressions for k_n' in terms of k_n and k_p' in terms of k_p. Concise expressions for the net conduction and valence band fluxes are thus:

$$U_{n,tot} = k_n(n_s - n_{so}) \qquad [12]$$

$$U_{p,tot} = k_p(p_s - p_{so}) \qquad [13]$$

$$U_{tot} = k_p(p_s - p_{so}) - k_n(n_s - n_{so}) \qquad [14]$$

Eqs. 12-14 demonstrate that the rates of the interfacial charge transfer reactions for thermalized processes are driven by the surface concentration of thermalized holes and electrons even for non-equilibrium conditions.[6-19]

The derivation of expressions such as Eqs. 12-14 is not possible without explicitly or implicitly invoking the principles of detailed balance and microscopic reversibility.

The general case of a non-thermalized carrier distribution is also given explicitly by the conventional theory of photoelectrochemical charge transfer kinetics. In this situation, the more complicated expressions, Eqs. 3 and 4, obtained from detailed balance, must be used to calculate the interfacial charge carrier flow at each energy, E. Again the surface carrier excesses (now at energy E), relative to their values at equilibrium, drive the rates of charge transfer across the solid/liquid contact. Explicit integration of these expressions over energy, with the appropriate distributions of carriers in the solid, therefore provides a general, analytical approach for the interfacial kinetics for an arbitrary carrier distribution.

2. Conditions Under Illumination

We now apply the equations developed above from the conventional model of photoelectrochemistry to the specific case of a semiconductor photoelectrode under illumination. Expressions for two key observables, the light-limited photocurrent and the open circuit photovoltage, will be obtained. Specific examples for a thermalized carrier distribution are provided first, and the results are then generalized to an arbitrary charge carrier distribution.

a. Behavior of the Photocurrent

Under illumination, excess electrons and holes will be created in the semiconductor. For simplicity, we first consider the case of photogenerated, but thermalized, carriers (*i.e.* carriers in thermal equilibrium with their

respective bands). Because these photogenerated charge carriers are thermalized in the bands of the solid, such excess charge carriers must be considered, with respect to interfacial charge transfer reactions, as kinetically identical to the charge carriers that are generated from the thermal excitation. Only the concentration of carriers, n_s and p_s, can be altered by the presence of illumination. Thus, in the conventional model of photoelectrochemistry, Eqs. 12-14 also describe the current flow under illumination, except that n_s and p_s now include the photogenerated carriers as well as those generated from thermal excitation.[6-19,38,43]

An absorbed photon flux Γ_o (photons-cm^{-2}-s^{-1}) will produce excess electrons and holes (Δn_b and Δp_b) in the bulk of the semiconductor. The number of photogenerated electrons must equal the number of photogenerated holes, and both quantities are directly proportional to Γ_o. Under low level injection ($\Delta n_b << n_{b,dark}$), n_b is essentially unchanged from its value in the dark. However, Δp_b is far greater under illumination than p_b in the dark. To an excellent approximation, p_b under illumination equals Δp_b, because with n_i equal to the intrinsic carrier concentration of the semiconductor, generally $\{p_{b,dark} = (n_i^2/n_{b,dark})\} << \Delta p_b$ for any reasonable photon flux.

The net hole flux is therefore non-zero under illumination. Expressing the fraction of holes generated in the bulk that successfully cross the interface as Φ_p, and realizing that generally $\Delta p_s >> p_{so}$, the net hole flux under illumination is simply given by continuity as:[10,36]

$$U_{p,tot} \approx \Phi_p \Gamma_o \qquad [15]$$

In the conventional model of photoelectrochemistry, the minority carrier flux due to photogenerated carriers is thus directly proportional to the incident photon flux in low level injection.[6-19]

A similar conclusion is obtained for an arbitrary distribution of photogenerated charge carriers.[11,27] Continuity of carriers at the solid/liquid interface will still result in Eq. 15, so the conventional model of photoelectrochemistry predicts that the minority carrier flux is proportional to the incident photon flux in low level injection even for arbitrary energy distributions of the photogenerated carriers.

b. Behavior of the Photovoltage

It is also useful to consider the photovoltage developed by the illuminated semiconductor electrode. We again will illustrate the situation initially for thermalized carrier distributions, for which simple closed form solutions of the relevant equations are readily available. At open circuit, the net current through the interface must be zero. Therefore, the surface electron concentration under illumination will increase until $U_{n,tot} = U_{p,tot}$, so that $U_{tot} = 0$. In low level injection n_b is essentially unchanged from its value in the dark, so Eq. 12 still suffices to describe $U_{n,tot}$. Thus, at open circuit:[6,7,10,36]

$$U_{tot} = \Phi_p \Gamma_o - k_n(n_s - n_{so}) = 0 \qquad [16]$$

Writing the voltage developed by illumination as $(AkT/q)\ln(n_s/n_{so})$, where A = the ideality factor, and combining this with Eq. 16, leads to the desired expression for the open circuit voltage, V_{oc}:

$$V_{oc} = (AkT/q)\ln\{\Phi_p \Gamma_o/(k_n n_{so}) + 1\} \qquad [17]$$

The open circuit voltage thus starts at zero and increases logarithmically with light intensity (when $[\Phi_p \Gamma_o/(k_n n_{so})] >> 1$), in the framework of the conventional model of photoelectrochemistry.[6-19]

For an arbitrary distribution of photogenerated carriers, simple closed form solutions for the photovoltage cannot be readily obtained. The entropy of the photogenerated carriers, as well as their internal energy distribution, must be accounted for in order to properly describe the free energy produced by the photoelectrode under these circumstances. In the specific situation where all of the recombination occurs through interfacial charge transfer across the solid/liquid contact, the required quantities can be evaluated from the generalized detailed balance and microscopic reversibility constraints in Eqs. 3 and 4. These equations will yield values for the carrier concentrations, $n_s(E)$ and $p_s(E)$, which then can be related to the photovoltage of the system. An analytical evaluation of this situation, however, is beyond the scope of this work, and is not necessary to contrast the conventional model with predictions of the irreversible photoelectrolysis model.

B. Basic Assumptions of The Irreversible Photoelectrolysis Model

The irreversible photoelectrochemical model has recently been advanced as still being a viable photoelectrochemical model that is different than the conventional model.[26] This alternative model for photoelectrochemistry states that local statistical detailed balance is not maintained in photoelectrolysis reactions at semiconductor electrodes,[24] that thermalized, but photochemically generated carriers react formally from the bandedge energies,[26] and that such charge transfer reactions are highly irreversible, like photoemission into a vacuum.[25,26] In this section, we examine analytically these postulates of the irreversible photoelectrolysis

model. In section C, we then describe the consequences of the assumptions of the irreversible model and analyze the predictions of both the irreversible and conventional models with respect to certain key experimental observations.

As published in the literature,[24-26] no analytical equations have been presented or derived for the irreversible model. Thus we will attempt to modify the equations above in a fashion which reflects the postulates of the irreversible model. To do this, we must consider what "irreversible" charge transfer kinetics implies. The conventional model, using chemically reversible kinetic rate constant ratios evaluated from the principles of detailed balance and microscopic reversibility, analytically describes photocurrent flow under a variety of non-equilibrium conditions. These include both low quantum yield and high quantum yield processes away from equilibrium, *i.e.*, all situations for which $n_s(E) \neq n_{so}(E)$ and/or $p_s(E) \neq p_{so}(E)$ for any energy E (*vide supra*). So "irreversible" cannot simply refer to situations away from equilibrium (*i.e.*, $U_{n,tot} > 0$ and/or $U_{p,tot} > 0$), because if this were the case, and if the rate constant ratios $k_n(E)/k_n'(E)$ and $k_p(E)/k_p'(E)$ were the same at every energy E as those of the conventional model, there would be no distinct "irreversible" model to evaluate. Similarly, the conventional model analytically describes the charge carrier kinetics for arbitrary carrier distributions, so "irreversible" cannot refer merely to specific (*i.e.*, thermal *vs.* non-thermal) carrier distributions, while preserving the rate constant ratios $k_n(E)/k_n'(E)$ and $k_p(E)/k_p'(E)$ given by the principles of detailed balance and microscopic reversibility. Arbitrary magnitudes of the interfacial charge transfer rate constant ratios are included analytically into the conventional theory (for various energies E and/or various barrier heights at the semiconductor/liquid contact), so the

"irreversible" model cannot differ from the conventional theory merely by reference to specific situations with large, but chemically reversible, rate constant ratios [$k_n(E)/k_n'(E)$ and/or $k_p(E)/k_p'(E)$] at a given energy E. Thus, for there to be a distinct "irreversible" model to evaluate, "irreversible charge transfer kinetics" must imply that the *charge transfer rate constant ratios*, $k_n(E)/k_n'(E)$ and/or $k_p(E)/k_p'(E)$, are different for some energy E than the rate constant ratios obtained at this same energy from the application of the principles of detailed balance and microscopic reversibility. Otherwise, the models are the same in all essential features and there is no "irreversible" model to evaluate.

The irreversible model is not specific as to whether equilibrium is generally attained in the dark in a photoelectrochemical cell. We will assume that this model allows that equilibrium is always reached in the dark for a photoelectrochemical cell, since all available experimental data indicate that this is the case.[8,9,32,44-51] Therefore, within our analysis of the irreversible photoelectrochemical model, it must be the case that Eqs. 8 and 9 still hold, *i.e.*, that detailed balance still applies to carriers generated thermally in the dark, in order to allow equilibrium to be reached.

Because the basic rate constant expressions for interfacial charge transfer in the dark are apparently no different in either model, the key questions must revolve around the forward and reverse rate constants for photogenerated carriers. For purposes of notational clarity, quantities that are relevant to the situation in the irreversible photoelectrolysis model under illumination will be designated through the use of asterisk superscripts. As described above, for the irreversible model to be different from the conventional model, the inequality

$$n_s(E)\,[k_n^*(E)/k_n^{*\prime}(E)] \neq n_s(E)\,[k_n(E)/k_n'(E)] \quad \text{and/or}$$
$$p_s(E)\,[k_p^*(E)/k_p^{*\prime}(E)] \neq p_s(E)\,[k_p(E)/k_p'(E)]$$

must hold for some value of energy E in the photogenerated carrier distribution. Therefore, since the conventional model applies to an arbitrary carrier distribution, it must be the case that:

$$[k_n^*(E)/k_n^{*\prime}(E)] \neq [k_n(E)/k_n'(E)] \quad \text{and/or}$$
$$[k_p^*(E)/k_p^{*\prime}(E)] \neq [k_p(E)/k_p'(E)]$$

Furthermore, the hypothesis that charge transfer reactions proceed irreversibly from the solid to the liquid must imply that:

$$[k_n^*(E)/k_n^{*\prime}(E)] > [k_n(E)/k_n'(E)] \quad \text{and/or}$$
$$[k_p^*(E)/k_p^{*\prime}(E)] > [k_p(E)/k_p'(E)]$$

Thus, to obtain a distinct "irreversible" model, the rate constant ratios at a given energy must be larger than the values of $k_n(E)/k_n'(E)$ and $k_p(E)/k_p'(E)$ that are obtained for the thermally generated carriers at energy E, *i.e.*, different from those given by the equilibrium constant expressions derived for thermally generated carriers (Eqs. 6 and 7) using the principle of detailed balance.

The irreversible photoelectrolysis model has been applied to thermalized carrier distributions, and states that photogenerated, thermalized charge carriers are treated kinetically as if they arise from the bandedge energies.[26] Since this is precisely the situation described for all types of thermalized charge carriers in Eqs. 8 and 9 of the conventional model, the rate constants for transfer of photogenerated carriers across the solid/liquid

interface in the irreversible model are identical to those expressed in Eqs. 8 and 9. Thus, for the simpler case of thermalized carrier distributions,

$$k_n^* = k_n \qquad \text{and} \qquad k_p^* = k_p$$

Therefore, for thermalized carriers, the irreversible model can only fundamentally differ from the conventional model because

$$k_n^{*\prime} << k_n' \qquad \text{and/or} \qquad k_p^{*\prime} << k_p'$$

Otherwise, the models for thermalized carrier distributions would be identical in all essential forms and there would be no irreversible model to evaluate in this scenario. As described below, a similar statement can be formulated for the general case of an arbitrary carrier distribution.

C. Differences Between the Models

Adopting the assumptions of the irreversible photoelectrolysis model as stated in the literature, within the framework described above, has several important consequences both theoretically and experimentally. We will first discuss differences between the two models formulated above with regard to a threshold for photocurrent, and then we will discuss differences in the behavior of the photovoltage. We will discuss possible differences for thermalized carriers first, and will then generalize these to arbitrary carrier distributions. Finally, several other important aspects of the irreversible photoelectrolysis model, that follow directly from its unique stated hypotheses, will be examined.

1. Behavior of the Photocurrent

The behavior of the photocurrent *vs.* light intensity in photoelectrolysis systems has been one of the key experimental points of focus in both the conventional and irreversible photoelectrolysis models.[6,7,24-26] In fact, the use of a photocurrent threshold had been proposed as a primary method for experimentally distinguishing between these two models.[24] The theoretical behavior of the photocurrent within the two models is therefore of importance both historically and conceptually.

The conventional model of photoelectrochemistry predicts a linear dependence of the minority carrier photocurrent (in our examples, the hole photocurrent) on the incident photon flux under low level injection conditions.[6-19] This arises simply because the minority carrier flux will be linearly related to the flux of photogenerated carriers, as expressed in Eq. 15. Even if there are non-linear recombination regimes in which the linearity between Γ_o and $U_{p,tot}$ is destroyed, the conventional model *never* predicts a regime in which no net minority carrier photocurrent is expected, except at the unique value of $\Gamma_o = 0$.[6-19] The conventional, statistical model therefore predicts no threshold in photocurrent as a function of light intensity. This conclusion was clearly described in a recent theoretical and experimental treatment of photoelectrolysis with $SrTiO_3$ and TiO_2 electrodes.[6,7] Although the irreversible photoelectrochemical model also predicts no photocurrent threshold, it is clear that the photocurrent behavior of photoelectrochemical cells can be satisfactorily explained by the conventional model.[6-19,52]

2. Behavior of the Photovoltage

Although the models do not predict differences in photocurrent *vs.* light intensity behavior, they do predict differences in photovoltage behavior. We again discuss the simpler case of thermalized carriers first, and then generalize to arbitrary carrier distributions.

a. Thermalized Carrier Distributions

In the irreversible photoelectrolysis model, the reverse reaction rate constants for molecules created from photogenerated, thermalized carriers, $k_n^{*'}$ and $k_p^{*'}$, are apparently different than the reverse reaction rate constants for molecules created from thermally generated carriers, k_n' and k_p'. These reverse rate constants determine, in essence, the photovoltage of the system under illumination. Thus, if the photogenerated carriers are undergoing irreversible charge transfer reactions, the free energy produced by the photoelectrode will be greater than if the molecules created by the photogenerated carriers were capable of undergoing reversible charge transfer reactions. In the limit of near total irreversibility, as postulated in the irreversible model ("photoemission into a vacuum"),[24-26] the photogenerated carriers would be capable of providing essentially an infinite source of photoproducts, thus sustaining a free energy output approximating that of the semiconductor band gap even at arbitrarily low light intensities. This arises because the photoproducts are assumed not to undergo significant back reactions in the irreversible photoelectrolysis model.

In contrast, the conventional model of photoelectrochemistry predicts a logarithmic dependence of the available free energy from a photoelectrode as a function of the incident light intensity (Eq. 17).[6-19] Thus, as pointed out

previously,[6,7] the free energy *vs.* light intensity behavior, as opposed to the photocurrent *vs.* light intensity behavior, is the quantity of interest that should differentiate between the two theories. An exhaustive review of the literature indicates that the predictions of the conventional model for photoelectrochemistry with respect to the logarithmic behavior of the free energy on incident photon flux (with an asymptotic behavior at low light intensities to the equilibrium condition) are fully consistent with experimental observations on regenerative cells, and are also consistent with recent studies of the behavior of water photoelectrolysis cells.[6-19,27-30,32-34,44-51,53,54] To our knowledge, there is no report of a stable photoelectrochemical cell whose available free energy rises rapidly to the band gap energy at extremely low photon fluxes. Thus, we are aware of no experimental support for the irreversible charge transfer model of photoelectrochemistry.

It is also useful to examine conceptually the consequences of the treatment of the rate constants within the two different approaches. To be specific in the discussion below, we will assume that the irreversibility arises from a thermalized electron transfer process, *i.e.*, $k_n^{*\prime} << k_n'$, although similar conclusions apply if the irreversibility arises from the thermalized hole transfer process (*i.e.*, if $k_p^{*\prime} << k_p'$). The assumption that $k_n^{*\prime} << k_n'$ is equivalent to stating that molecules which have been reduced by photogenerated, thermalized electrons react differently than those molecules that have been reduced by thermally generated electrons. The irreversible photoelectrolysis model explicitly states that the two types of electrons in the semiconductor are kinetically treated the same (*i.e.*, both types of carriers react formally from the bandedge energy),[26] so the difference in the back reaction rate constants can *only* arise from differences among the molecules in the

solution. This amounts to labeling the molecules according to whether they were formed by a photogenerated carrier or a thermally generated one.[55]

A similar conclusion is reached even if the irreversibility is postulated to arise from differences in reaction rates between thermalized photocarriers and thermally generated carriers, *i.e.*, $k_n^* \neq k_n$ and/or $k_p^* \neq k_p$. This occurs because detailed balance requires that equilibrium is reached in the dark for each separate photon energy in the thermal blackbody distribution that is characteristic of that particular temperature of the system. Thus, at an arbitrary temperature, some fraction of the thermal excitation arises from photons of an arbitrary energy, E_{phot}, and carriers created by photons of this energy must be in equilibrium with the molecules in the solution at the given temperature. If the irreversibility in the model does not arise from the products, *i.e.*, if $k_n^{*'} = k_n'$ and $k_p^{*'} = k_p'$, then it must be the case that $k_n^* >> k_n$ and/or $k_p^* >> k_p$; otherwise, the models are again identical and reversibility is attained according to the principles of detailed balance and microscopic reversibility. Again focusing on the electron transfer process for specificity, the assumption $k_n^* >> k_n$ amounts to labeling the electrons in the semiconductor according to their source, and requires distinguishing thermalized, photogenerated electrons that are created by energy E_{phot} in the thermal bath from those created by photons of energy E_{phot} due to deliberate, additional illumination of the solid/liquid contact.

b. Arbitrary Carrier Distributions

This analysis can be readily extended to photogenerated, non-thermalized "hot" carriers, *i.e.*, to an arbitrary carrier distribution. The quantities in the basic equations above are simply extended to be explicit functions of energy and momentum (and electric field strength, if desired). If

equilibrium in the dark is assumed, detailed balance implies that $k_n(E,\vec{p})$ $n_{so}(E,\vec{p}) = k_n'(E,\vec{p})$ for all possible electron energies, E, and all possible electron momenta, $\vec{p}$; otherwise, it would be possible to conceive of situations in the thermal bath in which equilibrium in the dark at the solid/liquid contact would not be attained. If irreversible behavior of photogenerated carriers is postulated for carriers of any specific value of E and/or $\vec{p}$, this implies that $k_n(E,\vec{p})/k_n'(E,\vec{p}) \neq k_n^*(E,\vec{p})/k_n^{*'}(E,\vec{p})$ for some value of $(E,\vec{p})$. This again amounts to labeling either the electrons, or the reagents formed from this specific class of electrons, according to their source. Thus, the arguments presented above, while referenced specifically to thermalized carriers, apply equally rigorously to an arbitrary carrier distribution.

D. Behavior of Photogenerated Minority Carriers Under Non-Equilibrium Conditions

The treatment described above of the conventional model also provides insight into some experimental data claimed to support hot carrier transfer at semiconductor/liquid contacts.[56-58] The observation of photocurrent for reduction of acceptors with standard electrochemical potentials, $E^{o'}(A/A^-)$, more negative than E_{cb} for photocathodes has been interpreted as evidence for "hot," non-thermalized carrier injection at the solid/liquid interface.[56-58] This aspect of photoelectrochemical behavior also can be consistently explained within the conventional framework of photoelectrochemistry using thermalized carrier distributions having the temperature of the semiconductor lattice.

In the conventional model of photoelectrochemistry, Eq. 13 describes the kinetics expected for interfacial charge transfer of thermalized minority

carriers. We use holes as minority carriers, and photoanodes as electrodes, to be consistent with the equations used in the treatment above. Although k_p is a function of $E_{vb} - E^{o'}$ (*i.e.*, of the driving force for thermalized interfacial charge transfer), k_p does not vanish to 0 when $E^{o'} \geq E_{vb}$. Within the conventional theoretical framework, hole transfer from photogenerated carriers is still expected for species with formal electrochemical potentials more positive than E_{vb}, because p_s under illumination is generally much larger than p_s in the dark. In particular, the Marcus-Gerischer relationship predicts that

$$k_p = \sigma v \delta (kT/\pi\lambda)^{1/2} \exp\{-[(E_{vb} - E^{o'} - \lambda)]^2/(4\lambda kT)\}[A^-] \qquad [18]$$

where σ is the cross section for minority carrier capture, v is the thermal velocity, δ is the effective reaction distance, and λ is the reorganization energy for the reagents in the charge transfer process.[9,18,19,32,36,39] Although this particular relationship has not been fully verified experimentally for semiconductor electrodes at present,[36] it is consistent with expectations of a finite, and possibly large, rate constant for charge transfer even when $E^{o'} > E_{vb}$ for an n-type semiconductor.

The analysis of minority carrier photocurrent densities then becomes a quantitative issue, because the observed magnitude of the minority carrier photocurrent must be compared quantitatively to that predicted from a thermalized carrier distribution using Eq. 13. For small values of k_p, p_s will simply increase in the light until continuity is re-established at steady state.[36] The excess minority carriers can then react by transferring charge across the interface in order to generate current, or the carriers can recombine to generate heat. This situation has been analytically described recently and will not be reviewed further here.[36] However, it is clear that a finite interfacial

photocurrent is expected under these conditions even in the absence of hot carrier effects.

An additional feature of concern with most of the experiments to date is that they have been analyzed only in the absence of significant concentrations of minority carrier donors (majority carrier acceptors) in the electrolyte, *i.e.*, only with the reduced form of the redox pair, A/A^-, when an n-type semiconductor is considered, and with the oxidized form of A/A^- when a p-type semiconductor is considered.[56-58] In the absence of minority carrier donors in the solution, k_p' will be artificially low, because k_p' implicitly contains the concentration of reagent in the solution. Thus, in a stirred solution with only minority carrier acceptor reagents present in the electrolyte, a significant minority carrier based photocurrent density can be expected for most values of $E^{o'}$ relative to E_{vb}. These expectations, with appropriate notational changes, apply equally rigorously to experiments at photocathodes. We therefore conclude that a conventional model of photoelectrolysis, with a purely thermalized minority carrier distribution, may suffice to explain many of the photocurrent density-voltage experiments presented in the literature as evidence for so-called "supra bandedge reactions".[56-58] In general, additional quantitative analysis, including explicit values of the thermalized minority carrier charge transfer rate constants and adsorption isotherms for the molecular reagents, would be required to demonstrate the presence of "hot" carrier injection processes using only the steady-state current-voltage properties of a photoelectrode as the experimental observable. One such approach has been recently described by Koval and co-workers, who have used photocathodes with a low dopant density to provide information on the thermalized carrier charge transfer rates, and then complemented these results with an investigation of the steady-state

current-voltage properties of highly doped photocathodes in contact with the same electrolyte.[59] The equations presented herein provide a simple framework from which to address these issues, as well as those of photoelectrolysis reactions,[6,7] in an analytical fashion.

III. CONCLUSIONS

A simplified, conventional model of photoelectrochemistry has been presented which captures the essence of many important aspects of the statistical theory of semiconductor electrochemistry. Key conceptual differences between this model and the irreversible charge transfer model for photoelectrochemistry as presently stated in the literature appear to lie in the treatment of the rate constant ratios for interfacial charge carrier kinetics. The conventional model utilizes detailed balance and microscopic reversibility principles to obtain rate constant relationships for all carriers both at, and away from, equilibrium. To be a distinct theory from the conventional model of photoelectrochemistry, the irreversible model must postulate different rate constant ratios at a given energy from the rate constant ratios obtained using the principles of detailed balance and microscopic reversibility. Thus, in the irreversible theory, photogenerated carriers at some energy E must produce different interfacial kinetic processes than do thermally generated charge carriers of the same energy. An analytical formulation of the irreversible charge transfer model, derived from the details published in the literature, results in several predictions that are neither well-founded nor supported by experimental observations. In contrast, the conventional model for photoelectrochemistry is in accord with all available data on these systems, including regenerative photoelectrochemical cells and photoelectrolysis systems. In addition, the conventional kinetic treatment, with thermalized

carrier distributions, can qualitatively explain a class of experimental data that has been taken previously to indicate conclusively the presence of non-thermalized hot carrier transfer at semiconductor/liquid contacts. Distinguishing between the presence of thermalized and "hot" carriers from measurements of the steady-state photocurrent-voltage properties of semiconductor/liquid contacts therefore requires a quantitative analysis of the interfacial charge transfer rate constants expected for the junction of concern.

IV. REFERENCES

1. M. Muneer, S. Das, V. B. Manilal and A. Haridas, *J. Photchem. Photobiol. A: Chem.*, **63**, 107 (1992).
2. C. S. Turchi and D. F. Ollis, *J. Catal.*, **122**, 178 (1990).
3. R. W. Matthews and S. R. McEvoy, *J. Photochem. Photobiol. A: Chem.*, **64**, 231 (1992).
4. B. O'Regan and M. Grätzel, *Nature*, **353**, 737 (1991).
5. P. V. Kamat and N. M. Dimitrijevic, *Solar Energy*, **44**, 83 (1990).
6. A. Kumar, P. G. Santangelo and N. S. Lewis, *J. Phys. Chem.*, **96**, 834 (1992).
7. J. M. Kesselman, A. Kumar and N. S. Lewis, in "The First International Conference of TiO_2 Photocatalytic Purification and Treatment of Water and Air," D. Ollis, Elsevier, London, Ontario, Canada (1992).
8. *Semiconductor Electrodes*; **55**, H. O. Finklea, Elsevier, New York (1988).
9. S. R. Morrison, "Electrochemistry at Semiconductor and Oxidized Metal Electrodes," Plenum, New York (1980).
10. S. J. Fonash, "Solar Cell Device Physics," Academic, New York (1981).
11. H. Gerischer, *Z. Phys. Chem.*, **26**, 223 (1960).
12. H. Gerischer and I. Mattes, *Z. Phys. Chem.*, **49**, 112 (1966).
13. H. Gerischer, in "Physical Chemistry: An Advanced Treatise," p. 463, Academic, New York (1970).
14. H. Gerischer, *J. Electroanal. Chem.*, **58**, 263 (1975).
15. R. Memming, *Philips Tech. J.*, **38**, 160 (1978).
16. R. Memming, in "Topics in Surface Chemistry," p. 1, Plenum Press, New York (1978).
17. R. Memming, in "Electroanalytical Chemistry," p. 1, Marcel Dekker, Inc., New York (1979).
18. R. Memming, in "Photoelectrochemistry, Photocatalysis and Photoreactors: Fundamentals and Developments," p. 107, D. Reidel Pub. Co., Hingham, Mass (1985).
19. R. Memming, *Ber. Bunsenges. Phys. Chem.*, **91**, 353 (1987).
20. W. Shockley and W. T. Read, *Phys. Rev.*, **87**, 835 (1952).
21. W. Shockley and H. J. Queisser, *J. Appl. Phys.*, **32**, 510 (1961).
22. S. M. Sze, "The Physics of Semiconductor Devices," 2nd Ed., Wiley, New York (1981).

23. E. H. Rhoderick and R. H. Williams, "Metal-Semiconductor Contacts," 2nd Ed., Oxford University Press, New York (1988).
24. A. J. Nozik, *Ann. Rev. Phys. Chem.*, **29**, 189 (1978).
25. F. Williams and A. J. Nozik, *Nature*, **271**, 137 (1978).
26. B. A. Gregg and A. J. Nozik, *J. Phys. Chem.*, **97**, 13441 (1993).
27. H. Gerischer, *Adv. Electrochem. Electrochem. Engr.*, **1**, 139 (1961).
28. F. Willig, R. Eichengerger, N. S. Sundaresan and B. A. Parkinson, *J. Am. Chem. Soc.*, **112**, 2702 (1990).
29. M. Evenor, D. Huppert and S. Gottesfeld, *This Journal*, **133**, 296 (1986).
30. H. Tributsch, *Structure and Bonding*, **49**, 127 (1982).
31. H. Tributsch, in "Mod. Aspects. Electrochem.," p. 303, Plenum Press, New York (1986).
32. C. A. Koval and J. N. Howard, *Chem. Rev.*, **92**, 411 (1992).
33. J. Reichman, *Appl. Phys. Lett.*, **36**, 574 (1980).
34. J. Li and L. M. Peter, *J. Electroanal. Chem.*, **193**, 27 (1985).
35. H. Gerischer and A. Heller, *J. Phys. Chem.*, **95**, 5261 (1991).
36. N. S. Lewis, *Ann. Rev. Phys. Chem.*, **42**, 543 (1991).
37. J. S. Blakemore, "Semiconductor Statistics," Dover Publications, Inc., New York (1987).
38. H. Gerischer, *This Journal*, **113**, 1174 (1966).
39. H. Gerischer, *Adv. Electrochem. Electrochem. Eng.*, **4**, 249 (1966).
40. R. A. Marcus, *J. Chem. Phys.*, **24**, 966 (1956).
41. R. A. Marcus, *J. Chem. Phys.*, **24**, 979 (1956).
42. This implicitly assumes the validity of the (generally applicable) condition that the relevant nuclear configurations at each individual electronic energy of the system are identical for processes that produce the reactants and products at this energy either at, or away from, equilibrium.
43. Note that the rate constants for interfacial charge transfer of thermalized charge carriers, given explicitly by the Marcus/Gerischer formalism, treat both thermally generated and thermalized, photogenerated carriers as if they formally transfer across the interface from the bandedge energies. For example, $k_n = \sigma v \delta (kT/\pi\lambda)^{1/2} \exp\{-[(E_{cb} - E^{o'} - \lambda)]^2/(4\lambda kT)\}[A^-]$, with σ the reactant cross section, v the thermal velocity, δ the effective reaction distance, and λ the reorganization energy for the process. The specific energy dependence of k_n and k_p is

not required for any of our discussion, and is not dictated from detailed balance principles, so it is not discussed at length in this chapter. Note, however, that the conventional model does *not* formally treat either thermally or photogenerated carriers as if they arose from "quasi-Fermi levels," and the interfacial charge transfer rate constants in this model are *not* functions of the quasi-Fermi level positions, in contrast to the assertions presented recently.[26]

44. B. A. Parkinson, *J. Chem. Ed.*, **60**, 338 (1983).
45. B. Parkinson, *Acc. Chem. Res.*, **17**, 431 (1984).
46. K. Rajeshwar, *J. Appl. Electrochem.*, **15**, 1 (1985).
47. K. Rajeshwar, P. Singh and J. DuBow, *Electrochimica Acta.*, **23**, 1117 (1978).
48. A. J. Bard, *Science*, **207**, 139 (1980).
49. A. Heller, *Acc. Chem. Res.*, **14**, 154 (1981).
50. M. S. Wrighton, *J. Chem. Ed.*, **60**, 877 (1983).
51. M. A. Fox, in "Photocatalysis: Fundamentals and Applications," John Wiley & Sons, New York (1989).
52. Note that a recent critique of reference 6 has misrepresented the conclusions of that work, and has erroneously stated that Kumar *et al.*[6] concluded that the absence of a photocurrent threshold indicated that the irreversible model was not applicable to the system under study.[26] In actuality, the conclusions of Kumar *et al.*[6] were: 1) the conventional model does not predict a photocurrent threshold [contrary to an earlier analysis];[24] 2) a photocurrent threshold was not observed experimentally in the systems studied; 3) the conventional model was fully consistent with the available data on all photoelectrochemical cells and photoelectrolysis cells; 4) there was therefore no need for an alternative model for photoelectrochemistry.[6] At present, it seems that there is a consensus on point #1, because a reevaluation[26] of the statistical model concurs with Kumar *et al.*[6,7] that the earlier analysis,[24] which deduced that the conventional theory predicted a threshold in photocurrent, was erroneous.
53. H. Tributsch, in "Photocatalysis and Environment: Trends and Applications," p. 297, Kluwer Academic Publishers, Dordrecht (1988).

54. L. M. Peter, in "Electrochemistry," p. 66, Royal Society of Chemistry, London (1984).

55. In the specific case of TiO_2, for which irreversibility has been postulated in photoelectrolysis reactions,[24,25] the accepted value for the conduction bandedge is very close to the formal potential for $H_2(aq)/H_2O$ under standard conditions.[8] Thus, detailed balance yields an equilibrium constant $K_n \approx 1$ for thermalized electrons in the conduction band of TiO_2 reacting to form $H_2(aq)$ under standard conditions. This is in agreement with the experimental observations on the system.[6,8] The irreversible photoelectrolysis model, however, hypothesizes that $K_n >> 1$ under illumination while maintaining, by stated assumption, the same forward rate constant for photogenerated, thermalized carriers as for thermally generated carriers.[25,26] Thus, within this framework, the H_2 molecules at the TiO_2/H_2O contact must react with the TiO_2 surface at different rates depending on their source of formation from either thermally generated, or photogenerated, thermalized electrons. If the irreversibility were postulated to arise from the hole transfer process, a similar conclusion would apply to the O_2 molecules formed in the solution. A similar conclusion would also be obtained if any interfacial charge transfer rate constant ratio, at any energy, were modified from that given by the principles of detailed balance and microscopic reversibility. Note that although the form of the carrier distribution in the solid cannot be readily determined from steady-state photocurrent-voltage data,[6] the conclusions derived herein are independent of whether the photoreactions occur from thermalized or "hot" carrier distributions.

56. A. J. Nozik and F. Williams, *Nature*, **312**, 21 (1984).

57. G. Cooper, A. J. Turner, B. A. Parkinson and J. A. Nozik, *J. Appl. Phys.*, **54**, 6463 (1983).

58. J. A. Turner and A. J. Nozik, *Appl. Phys. Lett.*, **41**, 101 (1982).

59. C. A. Koval and R. Torres, *J. Am. Chem. Soc.*, **115**, 8368 (1993).